UCRL-51486

STAGE III DISLOCATION PINNING IN SILVER RESULTING FROM GAMMA IRRADIATION

Richard A. Van Konynenburg
(Ph.D. Thesis)

November 14, 1973

Prepared for U.S. Atomic Energy Commission under contract No. W-7405-Eng-48

LAWRENCE
LIVERMORE
LABORATORY

University of California/Livermore

"Reference to a company or product name does not imply approval or recommendation of the product by the University of California or the U.S. Atomic Energy Commission to the exclusion of others that may be suitable."

Printed in the United States of America
Available from
National Technical Information Service
U. S. Department of Commerce
5285 Port Royal Road
Springfield, Virginia 22151
Price: Printed Copy $___*; Microfiche $0.95

*Pages	NTIS Selling Price
1-50	$4.00
51-150	$5.45
151-325	$7.60
326-500	$10.60
501-1000	$13.60

TID-4500, UC-25
Materials

LAWRENCE LIVERMORE LABORATORY
University of California, Livermore, California, 94550

UCRL-51486

STAGE III DISLOCATION PINNING IN SILVER RESULTING FROM GAMMA IRRADIATION

Richard A. Van Konynenburg
(Ph. D. Thesis)

MS. date: November 14, 1973

Contents

STAGE III DISLOCATION PINNING IN SILVER RESULTING FROM GAMMA IRRADIATION

Abstract

The objectives of this work were to test the validity of the vibrating string dislocation model in silver, to determine in which annealing stage long-range migration first occurs, to measure the migration energy and identify the defect responsible for observed annealing, to investigate the possibility of dislocation pipe diffusion, and to obtain an estimate of the efficiency of dislocations in trapping point defects. A brief summary of the history of research in the fields of radiation damage, point defects, and pertinent dislocation effects is presented. Relevant results from theory and previous experiments are discussed. Apparatus capable of continuously measuring changes in the elastic modulus and internal friction during gamma irradiation over the temperature range from <4 K to well above room temperature is described. A novel hollow-cylinder sample geometry permits use of a source strength of only 1 Ci. Survey experiments over a wide temperature range and isothermal irradiations above room temperature are discussed. The results are explained in terms of the Koehler-Granato-Lücke vibrating string dislocation model and the Thompson-Buck-Huntington-Barnes defect-dislocation interaction model. Consistent results are obtained under the assumptions of wide dislocation splitting and the presence of two dislocation components. Long-range migration appears to occur first in Stage I in silver. The activation energy for the observed Stage III annealing is about 0.48 eV. The responsible defect is most likely the single interstitial atom. Pipe diffusion is necessary to explain the results. The trapping efficiency of dislocations could not be determined because of the presence of more than one dislocation component.

I. Introduction

Throughout past centuries, the development of civilization has been closely associated with mankind's use of materials. This fact, of course, often has been used in estimating the period and degree of advancement of past cultures from their archeological remains.

In modern times, having reached the limits of capability of materials found to be native to the environment or created more-or-less by happenstance, man has turned to development of new ones. In so doing, he has found that progress depends to an increasing degree on his depth of understanding of the structure of matter and of processes occurring in materials on the atomic scale. This is particularly true when a combination of particular properties is required as, for example, in the wall of a nuclear fusion reactor where thermal, mechanical, nuclear, and chemical requirements are tightly circumscribed.

Recently, expanding technology and its consequent accelerated use of natural resources has brought about increased concern about their depletion. Development of means of reprocessing and reuse of materials as well as extraction of ever more dilute concentrations of them will, no doubt, draw upon our understanding of atomic structure and processes to a greater degree than has been the case heretofore.

This thesis study was undertaken with the intent of contributing to development of this understanding. The particular topic chosen, dislocation pinning in silver resulting from gamma irradiation, is relevant, since it deals with defects on an atomic scale in a metal: defects that determine many of its properties, among them being the all-important mechanical ones. In addition, it examines the basic processes of radiation damage, a phenomenon of great technological importance in the nuclear age.

Part II deals with the history of relevant topics in solid-state physics. Part III discusses the current objectives and outlines the experimental approach, and Part IV treats the application of theory and previous experimental results to the present study. Part V describes the experimental apparatus, while Part VI relates the survey experiments. Part VII covers the quantitative experiments, and conclusions are given in Part VIII.

II. General History of Fields Having a Bearing on the Present Study

Three principal topics shared among solid-state physics, solid-state chemistry, and metallurgy apply to this study, namely, radiation damage, point defects, and dislocations. Each has received considerable attention and is discussed in detail elsewhere as referenced. The main events in the history of each of these topics will be summarized here, to provide a setting for description of the present work.

In examining these three areas of study, one finds that they are closely interrelated. None of them, of course, is completely understood, and progress in one area has often necessitated making assumptions about the others. Radiation damage will be considered first.

A. RADIATION DAMAGE

Radioactivity was discovered by Becquerel in 1896. In the years following his discovery, interest turned toward the study of penetration of matter by radiation. The early work concerned itself with the "stopping power" of materials for the radiation rather than with the concomitant effects on the materials themselves. This work led to the elucidation of the primary interaction processes between radiation and matter. For the present work, the most important of these are the photoelectric effect, explained by Einstein in 1905, the Compton effect (1923), and Rutherford scattering (1911).

The first serious interest in the lasting effects of radiation on matter arose during the Second World War, when Spedding and Teller pointed out in 1942 that "the presence of high radiation flux might cause changes in the mechanical properties of reactor materials."[1] Subsequent calculations by Wigner showed that energetic neutrons would be able to displace a significant number of atoms from their normal lattice sites. These predictions led to studies of reactor and cyclotron radiation damage, primarily for applied purposes.

After the war, there was a lull in the work until the early 1950's, when several groups began systematic studies directed toward development of basic understanding of the radiation-damage process, in addition to the continuing applied work in nuclear reactor development. The field came to include the effects of the heavy charged particles such as protons, deuterons, alphas, heavy ions, and fission fragments, in addition to those of fast electrons, fast and thermal neutrons, and gamma rays, in all types of solids. Most recently, interest has arisen in the effects of radiation damage in aerospace equipment and high-energy accelerators. Efforts in the field have been directed toward determining the threshold energy for atomic displacement, the nature of the

interatomic collision mechanisms (including replacement collisions, focusing,[2] and channeling), the magnitude of energy-loss mechanisms, and the number and physical arrangement of displaced atoms.

The current situation in the radiation-damage field is that the primary interaction mechanisms between radiation and matter are understood, but a complete understanding of behavior after the primary interactions is still to be developed. Specifically, it is known how much energy a flux of a given type of radiation of a known energy will deposit in a given volume of a solid; and it can be estimated how much of this energy will be used in producing Frenkel pairs, but the number and physical arrangement of the pairs cannot be predicted with much certainty, particularly in the case of heavy particle damage.

In the case of metals, the field of radiation damage merges naturally into the field of point defects, since they are the only surviving vestiges after a very short time has elapsed. The next subsection will review the history of point-defect studies. Further details of the history of radiation damage may be found in the review articles by Kinchin and Pease[3] and by Seitz and Koehler[4] and in the book by Billington and Crawford.[5] A recent book in the radiation-damage field was written by Thompson.[6]

B. POINT-DEFECT STUDIES

The regular shapes of solid crystals were first explained in 1665 by Robert Hooke, who proposed that they were due to the regular packing of small spherical particles.[7] A similar explanation was made by Haüy in 1784.[8] In 1848, Bravais showed that there are 14 possible space lattices in which particles can be arranged in a regular manner.[9] In 1912, von Laue correctly predicted that x rays would be diffracted by a regular arrangement of atoms. The concept of the perfect crystal lattice, with each atom having an identical environment in terms of the number and arrangement of neighboring atoms, was thus firmly established.

In the early years of the twentieth century, the perfect lattice concept led to the explanation of several properties of crystals, including their specific heat and their cohesive energy. However, there were some properties that could not be explained in terms of the perfect lattice. These included behavior under stress, crystal growth and recrystallization, diffusive properties, optical and dielectric properties of insulators, photoconductivity, and some aspects of electrical and thermal conductivity.[10]

In 1926, Frenkel[11] published the first quantitative theory dealing with lattice defects, based on a suggestion by Joffe[12] in 1923. To explain the electrical conductivity of ionic solids, Joffe had proposed the existence of ions located in interstitial positions. Migration of these ions would serve as the conduction mechanism. Frenkel calculated the equilibrium concentration of

atoms that would be found in such positions, giving rise to an equal number of vacant sites. He showed that such defects would always be present at any temperature above absolute zero, and this provided the basis for the theory of point defects in solids. The combination consisting of one interstitial atom and its associated vacancy has come to be called the Frenkel defect (or Frenkel pair).

In 1930, Wagner and Schottky[13] examined all the possible types of point defects for a binary ionic solid, finding three independent types. These included the Frenkel defect on either sublattice, simultaneously occurring vacancies on both sublattices (sometimes called the Schottky defect), and the isolated interstitial. By invoking point defects, some of the properties left unexplained by the perfect lattice concept could now be understood.

The point defects were characterized by the energies required for their formation and migration. The first calculation of these energies for point defects in metals was made by Huntington and Seitz for copper in 1942.[14] They found that the formation energy for an interstitial in copper is much greater than that for a vacancy, whereas the migration energies are reversed in relative magnitude. Later calculations confirmed these findings. The migration of point defects was modeled on a computer by Vineyard in 1957,[15] using a statistical mechanical approach. Several other computer models have since been used.

Experimental studies of point defects have been difficult to interpret unequivocally because of the frequent inability to conclusively identify the defects responsible for an observed process in a single type of experiment. However, it has become clear that the behavior of a specific point defect depends only on its individual identity and not on its mode of creation. For this reason, defects can be created by a variety of methods and the results compared, giving more information than can be obtained with a single type of experiment. The usual procedure in studying point defects has been to create them by thermal activation at equilibrium or by the nonequilibrium methods of quenching, cold working, or irradiation, and to observe their subsequent behavior by one or more of several methods. Among these are measurements of electrical resistivity, elastic modulus, internal friction, stored energy, lattice parameter and macroscopic length, hardness, magnetic after-effect, positron annihilation, and anomalous transmission and diffuse scattering of x rays. Observations have also been made with the electron and field-ion microscopes.

In early work, experimenters found that, as they created defects and annealed samples through a range of temperatures, they observed fairly distinct "recovery stages"[16] distinguished by the activation energies for the annealing processes and hence by the approximate temperatures at which they occurred. These stages were labeled, and controversy soon arose over the

identity of the particular defect responsible for each stage. This disagreement has continued until now, with various conflicting models being proposed and modified as new experimental and theoretical results became available. In an effort to resolve this dispute, point-defect experiments mainly have attempted to determine the following information:

1. Type and configuration of defects present
2. Formation energy
3. Formation mechanism
4. Migration energy
5. Migration mechanism
6. Binding energy between defects
7. Disappearance mechanism.

One of the most powerful techniques for studying point defects involves their interaction with line defects, more commonly called dislocations. The next section will examine the history of dislocation theory, including interactions with point defects and effects on internal friction and modulus defect. Further discussion of point defects can be found in Damask and Dienes.[17]

C. DISLOCATIONS, POINT-DEFECT INTERACTIONS, INTERNAL FRICTION, AND MODULUS DEFECT

Among the properties of solids that could not be explained by the perfect lattice concept was their behavior under stress. It was shown by Frenkel (1926) that the strength of a perfect crystal would be much greater than that observed for real solids.[18] In response to this, several workers[19] in the 1920's and 1930's proposed dislocations and successfully explained the discrepancy. It was later seen that dislocations also account for the presence of slip bands, anomalously high x-ray reflection intensity and angular spread, and the observed growth of crystals at low solution supersaturation.

Bragg (1940) demonstrated the presence of dislocations in bubble rafts.[20] Dislocations have since been observed by crystal growth steps, etching, precipitation, electron microscopy, x-ray diffraction, and field ion emission.

Mott and Nabarro[21] first considered the blocking of dislocation motion by small strained regions, and Cottrell[22] calculated the interaction energies between small spherical defects and dislocations.

Zener[23] explained the basis for much of the observed internal friction in metals, but Read[24] first pointed out the contribution of dislocations to the internal friction. Koehler[25] suggested that dislocations in a periodic stress field behave like vibrating strings; and Granato and Lücke[26] solved the vibrating string equation in convenient form, explaining the observed amplitude-dependent internal friction in terms of dislocation breakaway from pinning points. Thompson and Holmes,[27,28] and Dieckamp and Sosin[29] observed the

pronounced effects of irradiation on inelastic properties. Work by Stern and Granato[30] and Thompson and Paré[31] in the MHz region verified the maximum in the decrement as a function of frequency as predicted by the vibrating string model.

Current efforts in this field have been directed toward quantitative tests of the vibrating string model, employing controlled amounts of basic radiation defects, as in the work of Thompson et al.,[32-34] and controlled dislocation parameters, as in the recent work of Paré and Guberman.[35] A review article in this field has been written by Thompson and Paré.[36]

III. Objectives and Description of this Work

The objectives established at the beginning of this work were as follows:

1. To test the validity of the vibrating string dislocation model in silver.
2. To determine in which annealing stage long-range migration first occurs in silver.
3. To determine the migration energy of whatever annealing process is observed, in order to identify the defect responsible.
4. To investigate the possibility of dislocation pipe diffusion.
5. To obtain an estimate of the efficiency of dislocations in trapping point defects.

To accomplish these objectives, it was decided to employ the technique pioneered by Thompson et al.[32-34] in their studies of copper. A description of the experimental approach is as follows: Point defects were created in the metal by gamma irradiation; their behavior was studied by monitoring the internal friction and the elastic modulus of a specimen that was driven in mechanical vibration; the temperature was controlled in order to study its effects on the kinetics of the processes taking place; and the damage was annealed out in situ after each experiment so as not to disturb the dislocation structure.

Silver was chosen as the material to be studied in the present work because of the possibility of preparing highly pure, well-characterized, single-crystal specimens and because of the availability of results from previous work that promised to aid in understanding our own results.

Gamma radiation was chosen for its convenience and its ability to create a nearly uniform concentration of relatively simple defects over a fairly thick sample. By the use of a cylindrical geometry, with the source placed inside the hollow specimen, it was possible to do experiments with a relatively small and inexpensive facility. The defects created should be of the most basic type, since the energy that can be transferred to an atom by gamma irradiation is limited by momentum considerations. The specimens could be thick enough to withstand the necessary handling without recrystallizing in subsequent anneals.

Internal friction and elastic modulus measurements were selected because of their sensitivity to low defect concentrations. This property enabled us to ensure that complications due to interaction between the radiation-produced defects would not arise.

IV. Theory and Previous Results that Apply to the Present Study

In the interpretation of an experiment of this type, one must consider three particular aspects of the fields whose history was outlined above: specifically, the creation of point defects by gamma irradiation, their behavior during annealing, and their interaction with dislocations, giving rise to changes in the internal friction and the elastic modulus. This section will review the current state of the theory that deals with these three areas.

A. GENERAL SUMMARY OF APPLICABLE THEORY

It may be helpful to consider a general overview of the results predicted by theory and supported by past experiments before discussing the theory in detail. Later sections will amplify the statements made here.

First of all, one begins with a single crystal of pure silver in a well-annealed state. There is a certain density and arrangement of dislocation lines and small concentrations of vacancies and interstitial atoms present. The irradiation is begun, and the gamma rays penetrate the sample. Some of them interact with electrons via the Compton and photoelectric effects. A portion of these recoil electrons interact in turn with silver atoms by Rutherford scattering. Some of the atoms are knocked out of their normal lattice positions. If they have enough energy, they in turn can displace others. A portion of the displaced atoms will spontaneously move back into their original lattice sites. At sufficiently low temperatures, the rest of these defects will be "frozen into" the lattice, leaving one Frenkel pair for each surviving displacement.

If the temperature is now raised, or if the irradiation is carried out at sufficiently high temperature, the interstitials and vacancies can migrate through the crystal by a random-walk diffusion process. If there are positions or configurations of lower energy available, the defects will tend to collect in them. One such lower-energy position is the region near dislocation lines. The free energy will therefore be lowered if point defects can move to preferred sites in closer proximity to dislocation lines. This places a bias on the otherwise random diffusion, such that the concentration of defects near dislocation lines increases. Furthermore, a recent theory[33] (to be discussed in Section IV.D) predicts that an equilibrium is set up between defects in the lattice, those on dislocation lines, and those at "nodes" on dislocation lines.

If an alternating stress is now applied to the specimen by some means, the dislocations will tend to move back and forth in a direction that tends to relieve the applied stress. If the frequency of the applied stress is large

compared to the frequency associated with the jumping of the point defects, they will be unable to follow it and will impede the motion of the dislocation lines.

Since the motion of the dislocation lines constitutes an additional strain over and above the elastic strain, and since this strain has components both in and out of phase with the applied stress, the motion contributes to both the elastic modulus and, particularly, to the internal friction. If both of these are monitored, it is possible to observe arrival of defect pinning points at dislocation lines and thus to gain information about the migration of these defects.

B. CREATION OF POINT DEFECTS BY GAMMA IRRADIATION

It has been known for many years that the dominant mode of energy loss for gamma rays of energy less than a few MeV passing through matter is due to interaction with electrons.[37] This results primarily in ionization and excitation of other electrons. In the case of metals, because of their high electron mobility, these processes do not result in permanent changes in structure, but only produce heat.[17] In 1955, Dugdale[38] first showed that gamma irradiation can also produce measurable atomic displacement effects in metals. This technique was developed by Thompson and Holmes[39] and by others[40] into a precise means of studying point defects in metals through their effects on the Young's modulus and, later, the internal friction. In this section we will examine the advantages and disadvantages of gamma irradiation for defect studies, describe the mechanisms of defect production, and estimate the rate of atomic displacement for ^{60}Co gamma rays in silver.

Advantages and Disadvantages

In comparison with creation of defects by other methods such as heating and quenching, cold working, and irradiation with neutrons or charged particles, gamma irradiation offers several advantages for point-defect studies:

a. The defects produced are isolated, randomly distributed Frenkel pairs. The reason for this will be seen later. The result is that one is not troubled by having to interpret the effects of large damage cascades, contamination by injected impurities, or transmutations (the photonuclear threshold for silver[41] is over 5 MeV).

b. The dislocation structure can be maintained more-or-less undisturbed during several experiments on the same sample.

c. Thick samples can be used without seriously sacrificing defect uniformity because of the high penetration of gamma rays. (The relaxation length for ^{60}Co gamma rays in silver is about 18 mm.) This

enables one to use more robust samples and avoids significant defect-surface interactions.

d. The experimental facility can be relatively small and independent, since no reactor or accelerator is needed, once a gamma-ray source has been produced.

The disadvantages of the use of gamma rays are the relatively low cross section for defect production, the inability to vary the energy (except by changing sources), and the phenomenon of gamma heating. The low defect-production cross section can be counteracted by use of an efficient geometry and a source with high specific activity. Combining these practices with measurement of dislocation pinning results in readily observable effects. The inability to vary energy is balanced by the fortuitous availability of ^{60}Co, which emits gamma rays of nearly the optimum energy for production of individual defects. Gamma heating is compensated by using an efficient heat-exchange medium around the sample and reducing the gamma dose rate to the lowest value consistent with reasonable duration of experiments.

Mechanisms of Defect Production

For defect production in pure silver by ^{60}Co gamma rays (1.173 and 1.332 MeV), two primary interaction mechanisms are important: the Compton effect and the photoelectric effect. Although the photoelectric cross section in this case is less than 1/30 of the Compton cross section (0.28 barns versus 8.9 barns),[42] the recoiling electrons thereby created are more energetic on the average and hence make a significant contribution to atomic displacements[43] (about 40%, as will be seen below). The photoelectric contribution becomes more important as the atomic number increases.

As Einstein pointed out, in the photoelectric process the incoming photon delivers all its energy to an electron, which then recoils with a kinetic energy equal to the photon energy less the initial binding energy of the electron:

$$T_{PE} = h\nu - B_e. \qquad \text{(IV-B-1)}$$

Approximately 80% of the interactions occur with the K-shell electrons because of the requirement of momentum conservation.[44] The K-shell binding energy in a silver atom is approximately 28.8 keV. For ^{60}Co, with gamma-ray energies of 1.173 and 1.332 MeV, the majority of photoelectrons thus have energies of 1.144 and 1.303 MeV. Consequently, in this case the photoelectron energies are almost equal to the gamma-ray energies.

In the Compton effect, the gamma ray, of energy $h\nu$, is scattered rather than absorbed, and it retains an amount of energy that depends on the scattering angle. Since the photon scattering angle may range from 0° to 180°, the

energy transferred to the recoil electron has a range of possible values. For a given electron recoil angle ϕ (measured from the forward gamma-ray direction), the electron kinetic energy is given by[45]

$$T_c = h\nu \frac{2\alpha \cos^2 \phi}{(1+\alpha)^2 - \alpha^2 \cos^2 \phi}, \qquad \text{(IV-B-2)}$$

where α is equal to $h\nu/m_e c^2$, m_e is the rest mass of the electron, and c is the velocity of light. For the present case, this results in a spectrum of electron recoil energies ranging from 0 to 1.118 MeV. The average energy of the Compton recoil electrons is about half the maximum value for this gamma-ray energy range, or 0.56 MeV.[46] A comparison between this value and the energies of the photoelectrons accounts for the somewhat unexpected significance of the latter in creating defects.

The result of the Compton and photoelectric processes is thus the production of fast electrons whose energy is of the same order as that of the gamma rays producing them. The range of these electrons is less than 1/2 mm in silver. When these are completely absorbed, about 95% of the electron energy goes into ionization and excitation of other electrons. This energy is shared with the lattice, and results in the phenomenon of gamma heating. The remaining 5% is dissipated in encounters with nuclei. Almost all of it goes into bremsstrahlung, due to deceleration of the electrons.[47] Only a very small part (about 0.0001%) of the energy is used in displacing atoms. This will be demonstrated in the following subsection.

Atomic displacements occur via relativistic Rutherford scattering when the energetic electrons encounter nuclei at sufficiently small values of the impact parameter.[48] It is of interest to know the maximum amount of kinetic energy which can be transferred by an electron of energy 1.303 MeV to a silver nucleus. This can be calculated from the equation[49]

$$E_m = \frac{2T\left(T + 2 m_e c^2\right)}{Mc^2} \qquad \text{(IV-B-3)}$$

where T is the electron energy and M is the mass of the silver nucleus. The result of this calculation is $E_m = 59.9$ eV. The reason for this small energy transfer is the great disparity in masses between the electron and the silver nucleus.

Since this energy is small compared to the binding energy between the nucleus and the great majority of its orbital electrons, the entire atom recoils as a unit. If it has sufficient kinetic energy, it is displaced from its lattice site. The required energy is called the threshold displacement energy, E_d,

and has been the object of considerable study.[50] E_d is normally measured by the use of electron bombardment over a range of energies, during which the change in a property such as electrical resistivity is monitored. In principle, the value of E_d would be chosen as the point where the first change in the measured parameter occurs. In practice, because of limitations on experimental sensitivity, lack of a priori knowledge of the shape of the curve of property change versus transferred energy, atomic vibrations, annealing, initial imperfections in the sample, and the presence of more than one isotope, the determination of E_d is somewhat approximate. In addition, E_d is dependent on crystallographic direction, since it is easier to displace an atom in some directions than in others because of the arrangement of neighboring atoms. Finally, the probability of displacement is not exactly represented by a step function that changes from 0 to 1 at E_d, but should rather be depicted by a smooth curve. In spite of these complications, there have been to our knowledge two experimental determinations of E_d for silver. Lucasson and Walker[51] assigned an effective value of 28 eV, while Roberts et al.[52] measured a zero-defect production value of 24 ± 1 eV. Since polycrystalline samples were used, the first value represents a type of average over various crystallographic directions, whereas the second probably represents the value for the easiest displacement direction. This may account for the difference in values.

At this stage of discussion, the important point is that, with a maximum energy transfer of 59.9 eV and a threshold displacement energy of 24-28 eV, it is clear that no more than two displacements will be created from a single electron-scattering event. In addition, less than one electron in 10 (at 1 MeV) causes any displacement at all in silver.[53] For these reasons the damage caused by ^{60}Co gamma rays in silver is expected to consist primarily of simple, isolated Frenkel pairs, with an occasional event creating two pairs in close proximity to each other.

Rate of Atomic Displacement

The rate of displacements per unit volume produced by a gamma-ray flux density Φ acting on a total number of atoms per unit volume N_a is given by

$$\frac{dN_d}{dt} = N_a \Phi \sigma_D, \qquad \text{(IV-B-4)}$$

where σ_D is the displacement cross section. This cross section was calculated by Oen and Holmes[53] for several elements. Their method will be described briefly, and the displacement rate for the present case will be estimated from their results.

The Oen and Holmes method involved several steps:

1. The spectrum of recoil electrons was calculated, using the Klein-Nishina cross section in the case of Compton scattering the Hulme's numerical results for photoelectric absorption.
2. The average number of displaced atoms produced by a recoil electron over its entire range as a function of initial energy was calculated, using the results of M Kinley and Feshbach. For high-Z elements a numerical evaluation of the Mott series, which describes relativistic Rutherford scattering, was used. The energy loss of the electrons was calculated, using a formula from Bethé and Ashkin. A step function displacement threshold energy was assumed.
3. These results were integrated together to obtain the total atomic displacement cross section.

The displacement cross section resulting from photoelectric events can be taken from Fig. 1 in the Oen and Holmes paper. In this figure the displacement cross section is shown as a function of atomic number for three values of the gamma-ray energy. A sharp displacement threshold of 25 eV is used, which is a reasonable value for silver, since it falls between the two measured values. By interpolation, a value of about 0.02 barns is obtained. The displacement cross section due to Compton events was not calculated by these workers for silver (Z = 47). Therefore, it has been obtained by linear interpolation from the results given for Z = 40 and Z = 50, which should be accurate to one significant figure. The value is about 0.03 barns for a gamma-ray energy of 1.253 MeV, the average of the ^{60}Co gamma ray energies. The total atomic displacement cross section is therefore about 0.05 barns. It can thus be seen that the photoelectric events account for about 40% of the displacements in silver.

The displacement rate is then obtained from Eq. (IV-B-4). N_a for silver is equal to 5.86×10^{22} atoms/cm^3, and the average flux density in the sample is given by $\phi = 3.56 \times 10^9 Q/(cm^2\text{-sec})$, where Q is the source activity in curies. This equation takes account of the fact that two gamma rays per disintegration are emitted by ^{60}Co. Since the experiments used a source of activity 0.962 Ci (at the midpoint of the 34.8°C irradiation), the average gamma-ray flux density is $3.42 \times 10^9/(cm^2\text{-sec})$, which is equivalent to a dose rate of 7.4×10^3 R/hr, and produces about 1×10^7 displacements/(cm^3-sec).

Uniformity of Irradiation

To make most efficient use of the gamma rays in this work, a coaxial cylindrical geometry was chosen; i.e., the silver crystal was grown in the shape of a hollow cylinder, and the gamma-ray source was made in the form of a wand and inserted inside the crystal. This made it possible to do

satisfactory experiments with a source of about 1 Ci, compared to source strengths three or four orders of magnitude larger used by other experimenters. The penalty paid with such a geometry is a sacrifice of irradiation uniformity over the volume of the sample. It is important to obtain an estimate of the nonuniformity. There are four considerations that have a bearing:

1. The gamma-ray flux density falls off approximately as 1/r in the sample, in common with any system having cylindrical geometry. The value of 1/r varies from 3.15 cm^{-1} to 2.10 cm^{-1} across the thickness of the sample and is the dominant factor controlling uniformity.
2. The gamma-ray flux density further decreases with increasing radius because of absorption in the sample. Since the half-thickness in this case is 12.8 mm, while the sample thickness is 1.59 mm, this factor is not as significant as the first.
3. The gamma-ray flux density decreases near the ends of the sample relative to the center plane because of the finite length of the source. If the source were of the same length as the sample, this factor would amount to one-half. In the geometry actually used, the source was extended beyond the sample for 0.95 cm at top and bottom in order to reduce this factor.
4. The electron flux density, which results from the primary interactions of the gamma rays, varies with depth in the sample because of the electron "build-up effect" that arises from the small but finite electron range. This effect would be present even if the gamma-ray flux density were constant, but is particularly significant in this geometry because all the gamma rays traverse the sample radially outward. (Scattered radiation is neglected.) Thus, there is no compensation due to gamma rays flowing in different directions. In addition, comparing the thickness of the sample (1.59 mm) to the electron range (a few tenths of a millimeter, depending on energy) indicates that a significant portion of the sample volume may lie within one electron range of the source. This is the region in which the build-up occurs.

A hand calculation was performed to evaluate the electron-flux density as a function of radius at the center plane and at one end plane of the sample. In this calculation the source was divided into 10 segments, and the contributions to electron flux density due to gamma rays from each segment were evaluated and summed. The calculation took account of the inverse square loss and sample attenuation losses in gamma-ray flux density. It also took account of electron absorption in the sample. Self-absorption of gamma rays in the source was neglected, which tends to exaggerate the calculated nonuniformity.

It was assumed that the Compton and photoelectrons are scattered exactly in the initial direction of travel of the gamma rays creating them, but with an energy distribution predicted by the differential cross sections. In the case of Compton recoils, this approximation is justified on the basis that, for a 1.332 MeV gamma ray (the higher energy of the two), the greatest angle that can occur between the electron and the initial gamma-ray direction and still give an electron energy of at least 0.72 MeV (the minimum amount necessary to produce a displaced atom in a subsequent zero impact parameter collision) is about 25°. The Klein-Nishina differential cross section is such that the average angle will be considerably smaller than this, and the shape of the atomic displacement cross section as a function of energy makes the small-angle cases even more important.

In the photoelectric case, experiments[54] have shown that the distribution of angles for 1.33 MeV gamma rays is sharply peaked at about 24°. In view of these facts, and the small distances of travel involved, the straight-on approximation is considered to be valid for present purposes.

The electrons were assumed to be linearly absorbed with a range of 0.036 cm, which is the weighted average for the Compton recoils having sufficient energy to cause displacements and for the photoelectrons. Since the electrons will be unable to create displacements after their energy has dropped below about 0.72 MeV, use of this range will again exaggerate the calculated nonuniformity of defect production.

The effects of secondary scattering of gamma rays in the silver were neglected. This is justified on the basis that the relaxation length is 18 mm for the gamma rays in silver, whereas the sample thickness is 1.59 mm.

The results of the calculation showed that, within 90% of the sample volume, the electron flux density is within ±25% of the mean value. The end effects amounted to less than 5%. The displacement uniformity should be at least as high as the electron-flux density uniformity. If the defect production rate were proportional to the electron-flux density, it would have the same degree of uniformity. This would be true if the spectrum of electrons were everywhere the same except for a constant multiplier independent of energy. This in turn is true except in the region lying inside the first electron range, where the assumption gives an underestimate of defect production, tending to exaggerate the calculated nonuniformity.

In view of the above considerations, it is considered conservative to state that the atomic-displacement production rate is uniform to within ±25% of the average value, over 90% of the sample volume.

C. MORPHOLOGY OF POINT DEFECTS

When a Frenkel pair is formed by interaction between an energetic electron and an atom in the sample, the surviving interstitial may or may not be the atom which originally occupied the surviving vacancy, because of the possibility of replacement collisions. The distance separating the vacancy and interstitial after the displacement process is finished may be only a few lattice parameters or it may be many. As pointed out by Sosin and Bauer,[55] the work of Roberts et al.[56] indicates that the average separation distance is very insensitive to the electron energy in silver.

It is of interest to know the morphology of vacancies and interstitials. This question is simpler in the case of the vacancy. It is generally agreed that the vacancy occupies a single lattice position and involves some relaxation of the neighboring atoms. The interstitial, on the other hand, conceivably could have several distinctly different configurations. These are discussed by Corbett.[57] The existence of several possibilities has fueled the debate over interpretation of annealing stages for many years. The principal issue has been whether there is only one more-or-less stable configuration of the interstitial or whether there are two. These points of view have come to be known as the "one-interstitial model" and the "two-interstitial model." More will be said about these models in the next section.

Calculations[58] indicate that the stablest form of the interstitial in face-centered cubic metals is the "split ⟨100⟩" or "⟨100⟩ dumbbell" configuration. In this form a lattice site is shared by two atoms whose interatomic axis is parallel to a ⟨100⟩ direction, and there is some relaxation by neighboring atoms. Some workers believe that another form is also at least metastable. The most frequently espoused candidates are the "crowdion" and the "split ⟨111⟩" configurations. The crowdion, first proposed by Paneth[59] for the bcc structure, consists of an extra atom crowded into a close-packed ⟨110⟩ row of atoms in the fcc structure with relaxation extending for several lattice spacings along the row. The split ⟨111⟩ form is analogous to the split ⟨100⟩ interstitial, but is aligned parallel to a ⟨111⟩ direction. It is difficult to rule out or decide between these configurations by calculation, and different workers have not obtained the same results. It is hoped that new experimental techniques will shed light on the question.

D. MIGRATION OF POINT DEFECTS THROUGH THE CRYSTAL LATTICE

Mechanism

As was mentioned in the previous section, when a Frenkel pair is formed, the distance separating the vacancy and interstitial may have a range

of values. If the spacing is sufficiently small, the Frenkel pair will be mechanically unstable and will collapse (annihilate) under the driving force of its own stress field. This process requires no thermal excitation and consequently will occur even at very low temperatures. It is therefore difficult to distinguish these "very close pairs" from atoms that never leave their lattice sites at all.[60]

Frenkel pairs located somewhat farther apart will require some thermal activation to come together and annihilate, but will do so in a very small number of jumps. They are termed "close pairs."[61] At increased separations between the vacancy and interstitial, the situation changes from pairs that are still "aware" of each other's presence through their stress fields to those that are not. In the latter case, if the separation between different Frenkel pairs is still large compared to the separation between the partners in a single pair, "correlated" annihilation will occur. Otherwise, free migration will occur to other defects, such as dislocations. In the present work, it is this last process that gives rise to observed changes in the Young's modulus and the internal friction, as will be seen.

The process of migration of point defects in solids takes place by a succession of discrete atomic jumps.[62] In the case of vacancy diffusion, the mechanism is that of successive jumps by neighboring atoms into the vacant site. When an atom jumps into a vacancy, the vacancy can be considered to have jumped in the opposite direction.

The mechanism for self-interstitial migration (as differentiated from migration of foreign atoms located in interstitial sites) is not agreed upon. It may involve direct jumping of an atom from one interstitial site to another, or it may consist of an interstitial atom taking the place of one of the lattice atoms, pushing it into an interstice (interstitialcy mechanism). A third possibility is the motion of a crowdion along its axis. In any case, the atomic jumps involve motion between two positions that are separated by an energy barrier.

Mathematical Representation

There are three approaches toward mathematically representing the defect migration process: these methods may be called the microscopic, the macroscopic, and the chemical rate-equation approaches. Each has advantages; and all three are valid, provided the proper conditions are met. We will give a brief discussion of each technique and point out its particular advantages for the present work.

The microscopic approach considers the motion of individual atoms as a "random walk" process.[63] For a cubic crystal structure, the defect is considered to be equally likely to jump a fixed distance λ in any of several symmetrically distributed directions. Using this assumption, it can be shown that,

after a total of n such jumps, the rms (root-mean-square) value of the distance of the defect from its initial site is given by

$$\sqrt{\overline{R^2}} = \sqrt{n}\,\lambda, \qquad \text{(IV-D-1)}$$

If the rate of jumping is represented by Γ (so that $n = \Gamma t$), it can be seen that the rms distance through which the defect moves is proportional to the square root of the time.

In the macroscopic approach, the migration process is represented by Fick's laws of diffusion[64]:

$$\mathbf{J} = -D\,\nabla c \qquad \text{(IV-D-2)}$$

and

$$\frac{\partial c}{\partial t} = \nabla\cdot(D\,\nabla c), \qquad \text{(IV-D-3)}$$

where $\mathbf{J}$ is the flux of diffusing defects, D is the diffusion coefficient, and c is the concentration of defects. These equations are solved using the geometry and boundary conditions appropriate to the problem at hand.

The equivalence of these two approaches was shown by Einstein, who related them by the equation

$$D = \frac{1}{6}\lambda^2\,\Gamma \qquad \text{(IV-D-4)}$$

for the three-dimensional case.[65] In the case of crowdion migration, the factor $\frac{1}{6}$ is replaced by $\frac{1}{2}$, because the diffusion is in only one dimension. The advantages of the random-walk approach are that it is physically the most fundamental, and it allows atomic quantities such as vibration frequencies and jump lengths to be examined. The Fick's law approach, on the other hand, is more closely related to what can be measured in a macroscopic experiment; namely, the diffusion coefficient, D. Therefore, it permits comparison to the results of tracer diffusion experiments, for example.

The chemical rate-equation approach describes the process in terms of the average concentration of defects. In this way, geometrical parameters are kept out of the equations. This approach is mathematically the most tractable when several processes occur simultaneously. It is equivalent to the others, provided the experimental conditions are such that short-term transients are unimportant.[66]

Temperature Dependence

The diffusion coefficients for many solid-state diffusion processes have been observed to follow the Arrhenius equation, within experimental uncertainty:

$$D = D_o e^{-Q/kT}. \qquad \text{(IV-D-5)}$$

In this equation, Q is a constant value of energy, k is Boltzmann's constant, T is the absolute temperature, and D_o is called the "pre-exponential factor." This behavior suggests analysis by absolute reaction-rate theory, which, combined with Eq. (IV-D-4), yields the expression[62]

$$D = \frac{1}{6}\lambda^2 \nu_o e^{\Delta S/k} e^{-\Delta H/kT} = \frac{1}{6}\lambda^2 \nu_o e^{\Delta S/k} e^{-\Delta E/kT} e^{-P\Delta V/kT} \qquad \text{(IV-D-6)}$$

for the case of three-dimensional migration, in which λ is the jump length, ν_o is the attempt frequency, ΔS is the activation entropy, ΔH is the activation enthalpy, ΔE is the activation energy, P is the pressure and ΔV is the activation volume. It can be seen that $Q = \Delta H$ and $D_o = \frac{1}{6}\lambda^2 \nu_o e^{\Delta S/k}$. At low values of P, the last exponential shown can be neglected in comparison to the ΔE term, so that $\Delta H \approx \Delta E$.

In this equation, the attempt frequency ν_o may be viewed as the frequency with which the defect assaults the energy barrier separating it from the adjacent site. Its value is expected to be comparable to that of the Debye frequency, 10^{12}-10^{13} sec^{-1}. The term ΔE represents the height of the energy barrier, which has been observed to range between about 0.1 eV and 1 eV for various defects in silver. The term ΔV corresponds to the increase in crystal volume associated with the process of the defect moving between one site and another. The value is expected to be a fraction of one atomic volume. The term ΔS has been interpreted as the entropy change that results from modification of the vibrational frequencies of the lattice-defect system when the defect moves to the saddle point configuration between two equilibrium positions.[67]

Of the parameters appearing in Eq. (IV-D-6), the one that is most readily measured is the activation energy for migration, ΔE. Since different defects can be expected to have different values of ΔE, this parameter has come to be used as a means of identification of the particular defect responsible for an observed process.

Annealing Stages[68]

As was discussed in Section II-B, when early experimenters monitored the resistivity annealing of a metal sample that has been irradiated or

cold-worked at a low temperature, they found that recovery of the initial resistivity occurred in a series of more-or-less distinct stages: these were labeled Stages I to V and were observed in several metals. Experiments with higher resolution revealed that Stage I was actually made up of several substages. Efforts were begun to identify the defect process that accounted for each stage. Controversy soon arose over this assignment and has persisted until the present.

Annealing Models

At the present time there are two primary models for the recovery process: the one-interstitial model and the conversion-two-interstitial model. There are several points of agreement between them[69]: 1) some of Stage I is attributed to close pair annihilation; 2) some long-range motion occurs in Stage I; 3) interstitials can interact with impurities to be retained in the lattice; 4) interstitials can interact with each other to be retained in the lattice; 5) some form of interstitial defect persists until Stage III; and 6) Stage V is due to recrystallization. The main area of disagreement surrounds the issue of whether there are one or two forms of the interstitial that are at least metastable. The one-interstitial model as outlined by Corbett[69] makes the following assignments:

Stage I. Close-pair recombination and free migration of the interstitial take place, during which the interstitial can annihilate, undergo trapping at various impurity or physical trapping sites, or agglomerate.

II. The interstitial is released from traps or undergoes rearrangement-type annealing. Possibly divacancy recovery also occurs. The interstitial moves to progressively deeper and deeper traps.

III. The interstitial is released from the deepest trap in the lattice; and/or vacancy migration takes place, which cleans up the lattice.

IV. Trapped vacancies are released where they occur.

V. Recrystallization takes place.

The conversion-two-interstitial model[70] holds that there is a low-temperature metastable form of the interstitial which converts, either thermally or by interaction with other defects, to a more stable form that does not migrate until higher temperatures are reached. This model makes the following assignments:

Stage I. Close pairs and free migration of the low temperature form of interstitial (crowdion or ⟨111⟩ type).

II. Same as one-interstitial model.

III. Migration of the high-temperature form of interstitial (⟨100⟩ dumbbell).

IV. Migration of vacancies.

V. Recrystallization.

The reasoning behind these models is discussed in the Proceedings of the 1968 Jülich Conference.[71] In the present experiment, only the processes that result in long-range migration of a point defect to a dislocation can be observed, since the defect concentrations are too low to observe significant reorientation of defects in the bulk. In addition, the concentrations are sufficiently low that interstitial-interstitial and vacancy-vacancy interactions can be safely ignored.

E. STRESS FIELDS SURROUNDING DISLOCATIONS

It is in order here to define dislocations and to discuss the properties that affect their interactions with point defects as a prelude to reviewing the interactions themselves. Details can be found in Hirth and Lothe.[72]

A dislocation, as contrasted with point defects, is a one-dimensional or line defect. It exists in two fundamental forms and, in general, is a combination of them. If one considers a perfect crystal extending to infinity in all directions, the edge dislocation can be visualized as an extra half-plane of atoms having been inserted into the crystal. The edge of the extra half-plane is then called the dislocation line. Apart from elastic strains, the crystal will still appear to be perfect at all points except near the dislocation line, where there will be distortions in the lattice in order to accommodate the extra half-plane. The Burgers vector of the dislocation is defined as the vector representing the error of closure of a rectangular circuit (called the Burgers circuit) that links the dislocation line, the opposite sides of which consist of equal numbers of lattice parameters. The edge dislocation is then characterized by its dislocation line and its Burgers vector, which is typically one lattice parameter in length and is perpendicular to the line.

The screw dislocation can be pictured as a helical ramp running through the crystal with the dislocation line defined as the axis of the ramp. The Burgers vector in this case lies parallel to the line.

As mentioned above, in the general case, a dislocation consists of both edge and screw components, in that the Burgers vector and the dislocation line intersect at an angle whose absolute value lies between 0° and 90°.

In fcc (face-centered cubic) materials such as silver, dislocations have been observed to split into two partial dislocations. The effect of a partial dislocation is to create a region where the atoms do not lie in an fcc arrangement, but rather a hexagonal close-packed structure. This region is termed a stacking fault and is bounded on both sides by a partial dislocation. Such a structure can occur in fcc metals when the misfit energy due to the incorrect stacking is balanced by the decrease in the elastic energy of the split dislocations compared to that of a complete (or perfect) dislocation. The width of the stacking fault is thus governed by this balance. Silver is known to have a low

stacking fault energy,[73] and is thus expected to have wide stacking faults compared to the other fcc metals.

Dislocations would not be present at all if the crystal were in a state of thermodynamic equilibrium. However, as a practical matter, it is difficult to obtain crystals without them since they form spontaneously when a crystal is grown from the melt and multiply when even small stresses are subsequently applied to the crystal. Well-annealed fcc metals typically contain 10^6 or more dislocation lines per square centimeter, although concentrations of 10^2 have been achieved.[74]

The distortions in the lattice around dislocation lines give rise to a stress field whose form depends on the dislocation type. The stress field of a screw dislocation, according to linear elasticity theory, is purely shear:

$$\sigma_{\theta z} = \frac{\mu b}{2\pi r}, \qquad \text{(IV-E-1)}$$

where $\sigma_{\theta z}$ is the stress in the direction parallel to the dislocation line on a plane containing the line, μ is the shear modulus, b is the Burgers vector, and r is the distance from the dislocation line to the point in question.

The stress field of an edge dislocation, in the same approximation, is given by the following equations:

$$\sigma_{rr} = \sigma_{\theta\theta} = \frac{\mu b \sin\theta}{2\pi(1-\nu)r} \qquad \text{(IV-E-2)}$$

$$\sigma_{r\theta} = \frac{\mu b \cos\theta}{2\pi(1-\nu)r} \qquad \text{(IV-E-3)}$$

$$\sigma_{zz} = \frac{\mu b \nu \sin\theta}{\pi(1-\nu)r}, \qquad \text{(IV-E-4)}$$

where θ is measured from a plane perpendicular to the extra half-plane of atoms and ν is Poisson's ratio. Note that the edge dislocation has both shear and hydrostatic components and that there is an angular dependence that changes the sign of the stresses from one side of the dislocation to the other.

F. INTERACTION OF POINT DEFECTS WITH DISLOCATIONS

As was pointed out in Section IV-A, a crystal containing dislocations and point defects can achieve a configuration having lower free energy if the point defects are located in close proximity to and in proper angular relation with the dislocations. This fact results in the preferential diffusion of point defects to dislocations and gives rise to a binding energy between them.

Several possible sources of interaction have been identified. Reviews are given by Bullough and Newman[75] and by Nabarro.[76] Those that are relevant for vacancies and self-interstitials in simple metals include the first-order size interaction,[77] the second-order size interaction,[78] the inhomogeneity interaction,[79] and interactions related to changes in the vibrational modes of the crystal.[80] In addition, there is the possibility of shear-stress interactions with point defects that do not have the full symmetry of the lattice (e.g., split interstitials) and interactions resulting from elastic anisotropy, which gives a dilatational component to the stress field of a screw dislocation.

The first-order size interaction is considered to be the most important. It arises from the fact that the point defect tends to cause a local compression or dilatation, and this interacts with the hydrostatic component of the stress field around a dislocation. Since a screw dislocation has no hydrostatic component in the linear isotropic theory, this interaction should be significant only for edge dislocations. The effect of this interaction is to attract vacancies to the more crowded side of the edge dislocation slip plane and to attract interstitials to the less crowded side. This is expected to be the longest-range interaction, since the potential is proportional to $1/r$, where r is the distance between the dislocation and the point defect.

The second-order size interaction results from a consideration of the interplay of the nonlinear (third order) elastic properties of the crystal and the dilatation of the point defect. It is a shorter-range effect, the potential being proportional to $1/r^2$. It becomes particularly significant in the case of a screw dislocation, since the first-order interaction is absent.

The inhomogeneity interaction, also proportional to $1/r^2$, results from the fact that the effective elastic constants of the point defect are different from those of the surrounding matrix. If the point defect is effectively softer than the matrix, as in the case of a vacancy, it will tend to move to regions of higher stress around all dislocations, so as to reduce the elastic energy stored in the small volume it can occupy. By the same token, interstitials, being "harder," will be repelled from regions of high stress. The inhomogeneity interaction may be dominant for vacancies in metals where vacancy dilatation is small.

The vibrational mode interaction arises from the increase in entropy of the crystal when a vacancy is inserted. The presence of a vacancy lowers the frequency of the vibrational modes of the 12 nearest-neighbor atoms. According to Nabarro,[76] it is not clear whether this effect will tend to move vacancies to dilated regions or compressed regions, but he presents an argument favoring the latter.

There is little information about the size of the binding energies resulting from these various interactions. Thompson et al.[33] obtained a value of 0.35 to 0.51 eV for the binding energy of interstitials to dislocations in copper.

Also, these workers obtained an additional energy of 0.68 eV for the binding energy of interstitials to nodes on dislocation lines. Because of the similarity of silver and copper, one might expect comparable values in the present work.

G. DISLOCATION PIPE DIFFUSION

We have seen that point defects are able to migrate through the crystal lattice and that they are preferentially attracted to dislocation lines. The next question to be considered is whether or not they remain more-or-less stationary once they arrive on dislocations. There is abundant evidence that silver atoms are able to migrate much faster along dislocation lines than through the bulk lattice.[81] The self-diffusion energy associated with this process is 0.78 to 0.85 eV as measured in tracer experiments,[82] as compared with 1.76 eV for monovacancy bulk diffusion.[83] Love[84] presented a theory of dislocation pipe diffusion that proposes that the enhanced diffusion takes place by migration of interstitials in the core of the dislocation. In this theory the activation energy for self-diffusion is given by the sum of the formation and migration energies of the interstitial on the dislocation.

In the present work, interstitials are formed by the nonequilibrium process of irradiation. Therefore, if pipe diffusion is observed, it should exhibit an activation energy which includes only the migration energy of the interstitial on the dislocation line. The value should therefore be considerably less than 0.78-0.85 eV if this theory applies. In copper, Thompson et al. obtained a value of 0.42 eV.[33]

H. INTERNAL FRICTION AND MODULUS DEFECT

The properties measured in the present work are the internal friction and the modulus defect. It is well to define them here and give a brief discussion of their history before exploring the effects of dislocation pinning in the next section.

It was pointed out by Robert Hooke, in 1678, that the deformation of a body is proportional to the force applied to it.[85] This came to be known as Hooke's law and served as the basis for development of the classical theory of elasticity. On the atomic level, this law requires that the atoms of a solid lie in parabolic potential wells and maintain their positions relative to each other during deformation. In real materials, these conditions are not completely satisfied, but are sufficiently true for many purposes.

The deviations from Hooke's law are of two types. One type results from the violation of the first condition, and is expressed by the third- and higher-order elastic constants. This deviation results in anharmonic effects such as thermal expansion, a contribution to the specific heat, and

phonon-phonon interactions.[86] The other type of deviation results from violation of the second condition and results in nonelastic effects, of which one category is called anelasticity. According to Zener, anelasticity is "the property of a solid in virtue of which stress and strain are not uniquely related in the preplastic range."[23] More specifically, anelasticity necessitates the inclusion of time derivatives in the stress-strain equation, and manifests itself in such phenomena as elastic aftereffect, stress relaxation at a constant strain, variation of modulus with frequency of measurement, internal friction, and modulus defect. We are concerned here with the last two phenomena.

Internal friction (also called damping or damping capacity) results in the conversion of mechanical energy to heat in a solid in the preplastic range. It causes the decay of vibrations in a solid even when there is no loss of energy to the environment. The modulus defect of a solid is the fractional difference between the observed modulus of elasticity and the purely elastic modulus. Both of these effects can be caused by changes in the relative positions of atoms in the solid as the applied stress is varied.

The internal friction and modulus defect can be understood quantitatively by a formulation that Nowick[87] called the generalized Maxwell approach: Consider a body that is placed under a periodic stress $\sigma_1 e^{i\omega t}$. The body will undergo a strain having two components: the elastic strain and the nonelastic strain. The elastic strain is given by $\epsilon' = \epsilon'_1 e^{i\omega t}$. Note that this is in phase with the applied stress. If the atoms kept their relative positions and changed only their separation distances, this is the only strain that would occur, and Hooke's law would be satisfied (at least insofar as nonelastic effects are concerned).

The nonelastic strain is given by $\epsilon'' = (\epsilon''_1 - i\,\epsilon''_2)e^{i\omega t}$. Note that there are both in-phase and 90°-lagging components. The total strain is therefore given by

$$\epsilon = \epsilon' + \epsilon'' = [(\epsilon'_1 + \epsilon''_1) - i\epsilon''_2]\, e^{i\omega t} \equiv (\epsilon_1 - i\,\epsilon_2)e^{i\omega t}. \qquad \text{(IV-H-1)}$$

The internal friction is defined as the tangent of the angle between the stress vector and the total strain vector:

$$\tan\phi = \frac{\epsilon_2}{\epsilon_1} = \frac{\epsilon''_2}{\epsilon''_1 + \epsilon'_1} \cong \frac{\epsilon''_2}{\epsilon'_1}. \qquad \text{(IV-H-2)}$$

In general, $\epsilon'' \ll \epsilon'$, so that $\tan\phi$ is small, and can be approximated well by ϕ. The phase angle ϕ is therefore a measure of the internal friction and is equal, for low values of internal friction, to the out-of-phase strain divided by the purely elastic in-phase strain.

For a bar sample vibrating in an extensional mode, the purely elastic Young's modulus is given by Hooke's law:

$$E = \frac{\sigma_1}{\epsilon_1'}. \tag{IV-H-3}$$

The dynamic modulus is given by the applied stress divided by the total in-phase strain:

$$E' = \frac{\sigma_1}{\epsilon_1} = \frac{\sigma_1}{\epsilon_1' + \epsilon_1''}. \tag{IV-H-4}$$

The modulus defect is then defined as $(E - E')/E'$ and is referred to as $\Delta E/E$:

$$\frac{\Delta E}{E} = \frac{E - E'}{E'} = \frac{\epsilon_1''}{\epsilon_1'}. \tag{IV-H-5}$$

The modulus defect is therefore equal to the additional in-phase strain due to nonelastic processes divided by the purely elastic in-phase strain. The relationship between the modulus defect and the internal friction can thus be clearly seen. They are different aspects of the same fundamental process.

There are several ways of measuring internal friction.[23] One method is to drive a vibrating sample in forced oscillation. The driving frequency is swept slowly through the resonant frequency of the sample, and the vibration amplitude is monitored. The width of the resulting resonance peak is then a measure of the internal friction. Specifically, if Δf is the frequency interval between half-maximum amplitude on the low-frequency side of the resonance and half maximum on the high-frequency side, it can be shown that, for small values of $\tan \phi$,

$$\tan \phi \cong \frac{\Delta f}{\sqrt{3}\, f}, \tag{IV-H-6}$$

where f is the resonant frequency.

A second method is to drive the sample at constant amplitude at its resonant frequency. The fractional energy dissipated per cycle is then a measure of the internal friction. Specifically, for small values of $\tan \phi$,

$$\tan \phi \cong \frac{1}{2\pi} \frac{\Delta W}{W}, \tag{IV-H-7}$$

where ΔW is the energy lost per cycle (and therefore equal to the energy that must be added per cycle) and W is the total vibrational energy stored in the sample.

A third method is to observe the decay of amplitude of a sample placed in free vibration. The logarithmic decrement (Δ) is then defined as the natural logarithm of the ratio of successive amplitudes. For small values of tan ϕ,

$$\tan \phi \cong \frac{\Delta}{\pi}. \tag{IV-H-8}$$

A convenient way of measuring Δ is to observe the number of cycles (N) required for the amplitude to drop to $1/e$ of its initial value. Then

$$\Delta = \frac{1}{N}. \tag{IV-H-9}$$

In pulsed ultrasonic experiments it is possible to measure the attenuation of a sound wave as it passes through the sample. If the stress-wave attenuation is expressed by $\sigma = \sigma_o \exp[-\alpha x]$, then the internal friction is given by[88]

$$\tan \phi = \frac{v\alpha}{\pi f}, \tag{IV-H-10}$$

where v is the measured velocity, α is the attenuation factor, and x is distance measured in the sample. Another means of describing internal friction is in terms of the quality- or Q-factor of a resonant system. In this nomenclature,

$$\tan \phi \cong 1/Q. \tag{IV-H-11}$$

The first three measures of internal friction are equivalent if the damping is independent of strain amplitude. The ultrasonic technique is normally carried out at a higher frequency than the others, so the frequency dependence of the damping must be taken into account in comparing values obtained in this way with the others.

The modulus defect is generally measured by monitoring the change in resonant frequency due to nonelastic processes. The resonant frequency is linked to the modulus by an equation of the form

$$f \propto \sqrt{E}, \tag{IV-H-12}$$

so that

$$\frac{\Delta E}{E} \cong 2\frac{\Delta f}{f} \tag{IV-H-13}$$

for small values of $\frac{\Delta E}{E}$.

Four principal types of internal friction have been observed in metals[76]: the Bordoni peak at low temperatures, an amplitude-dependent and an amplitude-independent contribution around room temperature, and a large damping at higher temperatures. In addition, various relaxation peaks due to point-defect effects have been studied. In pure metals, the contributions around room temperature are believed to be due mainly to motion of dislocations, as was first suggested by Read.[89]

In the next section, it will be seen that the modulus defect can be quantitatively related to the internal friction when their common underlying mechanism is understood. This provides a powerful way of testing theories against experiment.

1. THE VIBRATING-STRING DISLOCATION MODEL OF KOEHLER, GRANATO, AND LÜCKE

In 1950, Koehler[25] suggested that a dislocation moving under the influence of an oscillating applied shear stress could be represented by the equation of motion

$$A\frac{\partial^2 y}{\partial t^2} + F\frac{\partial y}{\partial t} - C\frac{\partial^2 y}{\partial x^2} = \sigma_o b \cos \omega t, \qquad \text{(IV-1-1)}$$

where

A is the effective mass per unit length of dislocation and is equal to $\pi\rho b^2$, where ρ is the density of the material and b is the length of the Burgers vector

y is the displacement of an element of the line from its equilibrium position

t is the time

B is the damping coefficient, such that the term in B gives the damping force per unit length

C is equal to $2\mu b^2/\pi(1 - \nu)$, where μ is the shear modulus and ν is Poisson's ratio, such that the term in C gives the force per unit length due to the line tension on a curved dislocation

σ_o is the maximum value of the resolved shear stress and

ω is the frequency of the applied stress.

Since this equation also describes the forced vibration of a stretched string under the influence of viscous damping, this representation of dislocation motion has come to be called the vebrating-string dislocation model. Thompson and Paré[36] reviewed the model, and their discussion will be followed here.

The basic assumption of this model is that dislocations are free to move everywhere along their lengths except at certain fixed pinning points, which might be impurity atoms, lattice defects, jogs, or nodes in the dislocation network. Each free length bows out under the influence of the applied stress. The viscous damping force dissipates energy, giving rise to internal friction. The additional strain caused by dislocation motion gives rise to a modulus defect.

The boundary conditions for this equation are established by the pinning points. A dislocation loop length ℓ is assumed, with pinning points at each e id such that $y = 0$ at $x = -\frac{\ell}{2}$ and at $x = +\frac{\ell}{2}$, if the origin is located at the center of the loop.

The net work done by the applied stress during one cycle of oscillation is given by

$$W_\ell = \int_{-\frac{\ell}{2}}^{-\frac{\ell}{2}} dx \int_0^{\frac{2\pi}{\omega}} \sigma_o b \cos \omega t \, \frac{\partial y(x,t)}{\partial t} \, dt. \qquad \text{(IV-I-2)}$$

The logarithmic decrement is equal to one-half the energy dissipated per cycle per unit volume divided by the vibrational energy per unit volume $\left(= \sigma_o^2/2\mu\right)$:

$$\Delta = \frac{N_\ell W_\ell}{\sigma_o^2/\mu}. \qquad \text{(IV-I-3)}$$

N_ℓ is the nu ber of loops per unit volume. These equations express the internal friction as a function of the motion of the dislocation line. The modulus defect can be obtained from a calculation of the in-phase component of the dislocation shear strain:

$$\epsilon''_{1\ell} = b \int_{-\frac{\ell}{2}}^{+\frac{\ell}{2}} y\left(x, \frac{2\pi}{\omega}\right) dx. \qquad \text{(IV-I-4)}$$

This equation expresses the contribution of one loop of length ℓ per unit volume. The total strain is the sum of the elastic strain and the in-phase dislocation contribution. For N_ℓ loops per unit volume,

$$\frac{\sigma_o}{\mu_m} = \frac{\sigma_o}{\mu} + N_\ell \epsilon''_{1\ell}, \tag{IV-I-5}$$

where μ_m is the shear modulus with moving dislocations, and μ is the modulus without dislocation strain. The modulus defect is than given by

$$\frac{\mu - \mu_m}{\mu_m} = \frac{N_\ell \epsilon''_{1\ell}}{\sigma_o/\mu} = \frac{\Delta E}{E}. \tag{IV-I-6}$$

It is to be expected that the dislocation loops will not all have the same length. To take account of this, a loop-length distribution function $N(\ell)$ is defined such that $N(\ell)d\ell$ is the number of loops per unit volume having a length between ℓ and $\ell + d\ell$. The decrement and modulus defect then are given by

$$\Delta = \frac{\int_0^\infty w_\ell N(\ell)\, d\ell}{\sigma_o^2/\mu} \tag{IV-I-7}$$

and

$$\frac{\Delta E}{E} = \frac{\int_0^\infty \epsilon''_{1\ell} N(\ell)\, d\ell}{\sigma_o/\mu}. \tag{IV-I-8}$$

The most widely used loop-length distribution function is the exponential, which represents random uncorrelated pinning point placement:

$$N(\ell) = \frac{\Lambda}{\ell_o^2} \exp(-\ell/\ell_o) \tag{IV-I-9}$$

where Λ is the dislocation density and ℓ_o is the average loop length. This function was given first by Koehler.[25] Another often-used distribution function is the delta function, which represents loops that are all of the same length.

Several approaches have been made toward solution of the vibrating-string equation for dislocation pinning. Koehler obtained an approximate solution valid in the kilohertz range. Weertman[90] obtained a solution in closed form, but it was extremely complex and difficult to interpret. Granato and Lücke[88] obtained a Fourier series solution and found that the first term is a good approximation at frequencies low compared to $0.7C/B\ell_o^2$. They also

developed a breakaway model for amplitude-dependent internal friction. Oen, Holmes, and Robinson[91] noted that the experimental measurements of Thompson and Paré[92] indicated that the motion of dislocations was damping-limited in the MHz region. This led them to drop the inertia term from the equation and obtain closed solutions for the over-damped case. Thompson and Paré[36] give the following explicit equations for the low-frequency case, using the exponential distribution:

$$\Delta = \frac{\pi \Lambda \ell_o^4 \mu b^2 B\omega}{C^2} \qquad \text{(IV-I-10)}$$

and

$$\frac{\Delta E}{E} = \frac{\Lambda \ell_o^2 \mu b^2}{2C}. \qquad \text{(IV-I-11)}$$

One important result of this model is that the decrement is proportional to the fourth power of the average loop length, while the modulus defect is proportional to the second power. In irradiation experiments, it is possible to change the average loop length without changing Λ or B. In such experiments, the average loop length at a time t is given by

$$\ell_o(t) = \frac{\ell_{oo}}{1 + n(t)}, \qquad \text{(IV-I-12)}$$

where ℓ_{oo} is the original average loop length and $n(t)$ is the average number of pinning points added to a loop at time t. This assumes that the loop-length distribution function is initially exponential and maintains its exponential character as pinning points are added. Thompson and Holmes[27] showed that this is true if the pinning points are added in a random, uncorrelated manner.

It is thus seen that, if the contributions to the internal friction and modulus defect from pinnable dislocations can be separated from any other contributions that might be present in an experiment, it should be possible to calculate the number of pinning points on the dislocations as a function of time. This separation is normally performed by irradiation to a high enough dose to achieve complete pinning. The vibrating-string model can then be checked by comparison of the pinning point number obtained from the decrement change to that obtained from the modulus defect data.

The second important prediction at low frequencies is that the decrement should be proportional to the frequency of the applied stress. This is also subject to experimental verification, although it is more difficult in practice.

At frequencies high compared to $0.7C/B\ell_o^2$, the model predicts that the damping should be given by $\Delta = \pi \mu b^2 \Lambda / B\omega$, and the modulus defect should be

proportional to the -3/2 power of the frequency. These frequency-dependence predictions are subject to experimental verification. By measuring Λ with etch-pit counting, it also has been possible to obtain a value of B for comparison with theoretical estimates that have been given by Nabarro,[93] Brailsford,[94] and Leibfried.[95]

Since this model was conceived, many experiments have been performed to test its predictions. Most have been conducted on high-purity, well-annealed copper. These studies have been summarized by Thompson and Paré,[36] and more recently by Paré and Guberman.[96] The latter authors state:

> ...the string model has, in pure annealed copper, been verified with respect to frequency dependence, loop length dependence, and absolute magnitude of the damping in the high-frequency (MHz) range and data have been obtained which show the predicted loop length dependence of both the damping and modulus defect in the low-frequency (kHz) range.

Nevertheless, there remain some gaps in experimental confirmation, and discrepancies have also appeared. For example, the absolute magnitude of the damping coefficient was determined by Paré and Guberman[96] and found to be much greater than that determined from experiments in the MHz region. The frequency dependence in the low-frequency range has been studied, but the results are in conflict with the model below 20-25 kHz in copper.[97-99] In many experiments, the pinning-point numbers predicted by the damping and modulus-defect data have been substantially different, causing experimenters to invoke the existence of two or more types of dislocations with different values of Λ, ℓ_{oo}, B, C, and point-defect interaction energies.[100] In some cases, irradiation has caused the damping to increase rather than decrease.[97,101-103]

J. THE DEFECT-DISLOCATION INTERACTION MODEL OF THOMPSON, BUCK, HUNTINGTON, AND BARNES

As we have seen, the Koehler-Granato-Lücke vibrating-string dislocation model provides an explanation of the internal friction and modulus defect that result from dislocation motion. It accounts for changes in these properties as point defects interact with dislocations to shorten their free-loop length. It does not, however, attempt to treat the kinetics of the migration of the point defects, nor does it deal with the mechanism of the interactions or the possibility of pipe diffusion along dislocation lines.

In 1967, Thompson, Buck, Barnes, and Huntington (TBBH) reported the results of experiments involving several isothermal gamma-ray irradiations

of a copper crystal during which the internal friction and modulus defect were monitored.[32] They applied the vibrating-string model and obtained consistent results for the internal friction and modulus defect, verifying the model's predictions with respect to loop length dependence. It was noted that earlier crystals had not always given these results, presumably because of the presence of a second dislocation component.

The calculated number of pinning points in these experiments plotted as a function of time exhibited an initial transient, whose length depended on the temperature, and a linear portion whose slope increased with temperature in an Arrhenius fashion. The intercept of the linear portion projected back to zero time went from positive to negative as the temperature was increased from one run to another.

To interpret these data, the above-named authors proposed a model[33,34] that we shall call the TBHB model, after the initials of their names. This model hypothesizes the following series of events: A gamma ray penetrates the crystal volume and creates a Frenkel pair via a Compton electron process. If the defects do not annihilate each other, they are free to diffuse by a random walk to a dislocation segment. Once on a segment, a defect is free to pipe diffuse along it and possibly collide with a nodal point trap. It may be retained there or be emitted back to the dislocation and from there possibly back to the lattice. The nodal points can include existing jogs, vacancy clusters, interstitial platelets, impurity atoms, and true dislocation nodes. This scheme leads to the following set of coupled rate equations:

$$\frac{dn_L}{dt} = -\frac{n_L}{\tau_{LE}} + \frac{1}{\tau_{DL}} \int_{-\ell_o/2}^{+\ell_o/2} \eta(x,t)dx + \phi \qquad \text{(IV-J-1)}$$

$$\frac{\partial \eta(x,t)}{\partial t} = D \frac{\partial^2 \eta(x,t)}{\partial x^2} + \frac{n_L}{\ell_o \tau_{LE}} - \frac{\eta(x,t)}{\tau_{DL}} \qquad \text{(IV-J-2)}$$

$$\frac{\partial n_N}{\partial t} = \frac{-D\ \partial \eta(x,t)}{\partial x} \Bigg|_{x=\pm\ell_o/2} = \frac{a\eta}{\tau_{DU}} \Bigg|_{x=\pm\ell_o/2} - \frac{n_N}{\tau_{ND}} \qquad \text{(IV-J-3)}$$

and

$$2n_N + \int_{-\ell_o/2}^{+\ell_o/2} \eta(x,t)dx + n_L = \phi t. \qquad \text{(IV-J-4)}$$

The symbols in these equations are defined as follows:

n_L is the number of defects in the lattice

n_N is the number of defects in nodal points

$\eta(x,t)$ is the linear concentration of defects along the dislocation line

n_D is the total number of defects on a dislocation of length ℓ_o, and is given by

$$n_D = \int_{-\ell_o/2}^{+\ell_o/2} \eta(x,t)dx.$$

This is the experimentally observed pinning-point number.

τ_{LE} is the relaxation time for diffusion of the defects from the lattice to the dislocation line

τ_{DL} is the relaxation time for emission of the defects from the dislocation back to the lattice

τ_{DU} is the relaxation time characteristic of the unit jump process along the dislocation

τ_{ND} is the relaxation time for emission of the defects from the nodal point trap back to the dislocation.

These relaxation times all exhibit Arrhenius behavior.

D is the diffusion coefficient for the defect on the dislocation, and is given by

$$D = a^2/2\tau_{DU}, \qquad \text{(IV-J-5)}$$

where a is the appropriate lattice parameter.

ϕ describes the rate of defect production by the gamma irradiation, and is given by

$$\phi = (\ell_o/\Lambda)\, N_A \Phi \sigma_D, \qquad \text{(IV-J-6)}$$

where:

ℓ_o is the length of the dislocation segment which bounds the cellular volume to which the model is applied,

Λ is the dislocation density (number of dislocations/cm^2)

N_A is the number of atoms/cm^3

Φ is the gamma-ray flux, and

σ_D is the cross section for atomic displacements by gamma rays.

The relaxation time τ_{LE} is related to the unit jump time in the lattice τ_{LU} by the equation

$$\tau_{LE} \cong \left(\frac{\ell_o^2}{a^2}\right) \tau_{LU}, \qquad \text{(IV-J-7)}$$

and τ_{LU} is related to the bulk diffusion coefficient D_B by the equation

$$D_B = \frac{a^2}{\tau_{LU}}. \qquad \text{(IV-J-8)}$$

To solve these equations, the above-named authors replaced the coupling terms

$$\frac{1}{\tau_{DL}} \int_{-\ell_o/2}^{+\ell_o/2} \eta(x,t)\, dx \qquad \text{and} \qquad \eta(x,t)/\tau_{DL}$$

by average values, and applied a Green's function procedure. After applying the appropriate boundary conditions, they arrived at the following solution for n_D:

$$n_D(t) = (\phi - A)\, g_o \{t - \tau_{LE} [1 - \exp(-t/\tau_{LE})]\}$$

$$+ \frac{8(\phi - A)\ell_o^2}{\pi^4 D} (1 - g_o) \sum_{n=1,n\ \text{odd}}^{\infty} \frac{(-1)^{(n-1)/2}}{n^4}$$

$$\times \left[1 + \frac{\tau_n}{\tau_{LE} - \tau_n} \exp(-t/\tau_n) - \frac{\tau_{LE}}{\tau_{LE} - \tau_n} \exp(-t/\tau_{LE})\right], \qquad \text{(IV-J-9)}$$

where A is a constant (for a fixed temperature) given by

$$A = \phi g_o \frac{\tau_{LE}}{\tau_{DL} + g_o \tau_{LE}}, \qquad \text{(IV-J-10)}$$

g_o is given by

$$g_o = \left(1 + \frac{2a}{\ell_o} \frac{\tau_{ND}}{\tau_{DU}} + \frac{\tau_{LE}}{\tau_{DL}}\right)^{-1}, \qquad \text{(IV-J-11)}$$

and τ_n is given by

$$\tau_n = \left(\frac{2\ell_o^2}{\pi^2 a^2 n^2}\right) \quad \tau_{DU} = \frac{\ell_0^2}{\pi^2 n^2 D}. \qquad \text{(IV-J-12)}$$

By comparison of the predicted $n_D(t)$ to the data, they were able to eliminate some terms from the equation, resulting in the final equations

$$n_L(t) = \frac{\phi \ell_o}{2a} \frac{\tau_{DU}}{\tau_{ND}} \frac{\tau_{LE}}{\tau_{DL}} t + \phi \tau_{LE} [1 - \exp(-t/\tau_{LE})], \qquad \text{(IV-J-13)}$$

$$n_D(t) = \frac{\phi \ell_o}{2a} \frac{\tau_{DU}}{\tau_{ND}} \left\{ t + \left(\frac{32\ell_o}{\pi^4 a} \tau_{ND} - \tau_{LE}\right) [1 - \exp(-t/\tau_{LE})] \right\}, \qquad \text{(IV-J-14)}$$

and

$$n_N(t) = \frac{1}{2} [\phi t - n_L(t) - n_D(t)]. \qquad \text{(IV-J-15)}$$

The equation for $n_D(t)$ gives the behavior observed in their experiments: a temperature-dependent transient, a linear portion at long times whose slope has an Arrhenius temperature dependence, and an intercept that changes from positive to negative as the temperature is raised.

An important feature of the TBHB results was that the efficiency of dislocations for trapping defects was 100%, within the uncertainties involved. These authors showed that their proposed model was unique, assuming the basic correctness of a trapping (or climb) model, and that all of its features were required by experimental results. Three experimental results were particularly telling: the temperature-dependent slope, the temperature-dependent intercept, and the persistence of pinning effects for an indefinite time after irradiation had stopped. Using this model, they obtained an excellent fit to the data.

Thompson, Buck, Huntington, and Barnes obtained an activation energy for τ_{LE} of 0.64 eV, and they interpreted this as indicating that the migrating defect was the self-interstitial. The activation energy for pipeline diffusion was 0.42 eV, as mentioned before, and the energy associated with reemission of a defect from a node back to the dislocation line was 1.10 eV. The node binding energy was then computed to be 0.68 eV. The activation energy for reemission from the dislocation line to the lattice was estimated at 1.0 to 1.15 eV.

K. THE DEFECT DRAGGING MODEL OF SIMPSON AND SOSIN, AND THE DEFECT MIGRATION MODEL OF SIMPSON, SOSIN, AND JOHNSON

In addition to the models described in Sections I and J above, a few others have been proposed to account for the interaction of radiation-produced defects and dislocations. The most highly developed of these is the defect dragging model of Simpson and Sosin[104] (SS), coupled with the migration model of Simpson, Sosin, and Johnson[103] (SSJ).

The SS dragging model proposes that, at sufficiently low frequencies (below a few kHz in Cu), the point defects no longer act as rigid pinning points, but are dragged a small amount by the dislocation lines and thereby dissipate energy. In this theory, the dislocation loop length is presumed to remain constant, with a value fixed by the initial distance between nodal points. As point defects are added to the dislocation line, the damping coefficient (B in the KGL theory) increases.

Under certain conditions of loop length, frequency, damping coefficient and line tension, this model predicts an initial increase in the decrement when pinning points are added to the dislocations. As more pinners are added and the dislocation motion is increasingly restricted, the damping reaches a maximum value and decreases thereafter. At high defect densities the SS dragging model predicts that the modulus defect should decrease at a faster rate than the decrement. It also predicts that the damping should be proportional to ω^{-1} at low frequencies, and would become proportional to ω^{+1}, as predicted by the KGL model, only at high frequencies.

Using this model as the counterpart of the KGL model, Simpson, Sosin, and Johnson then used a somewhat simpler defect migration model to serve in place of the TBHB model. The chief differences between the SSJ and the TBHB models are that the former does not allow reemission of point defects from the nodes to the dislocation lines, and the time-scale of the experiment is assumed to be short compared to the lattice diffusion transient time. The SSJ model prediction can be derived from the solution of the TBHB model by assuming $t \ll \tau_{LE}$, $t \cong \tau_1$, and $\tau_{ND} \to \infty$. The result is

$$n_D = \frac{\phi\tau_1}{\tau_{LE}} \{t - \tau_1 [1 - \exp(-t/\tau_1)]\} \qquad (IV\text{-}K\text{-}1)$$

in the notation of Section J. With this solution, the intercept extrapolated back from the linear portion of the curve is negative definite, whereas it can be either negative or positive in the TBHB model. The slope has an Arrhenius temperature dependence, but its value is established by a balance between lattice diffusion and pipe diffusion rather than by a balance between pipe diffusion and node reemission. The transient is due to pipe diffusion rather than lattice diffusion.

Simpson, Sosin, and Johnson were able to obtain good agreement with experiments in Cu at a frequency of about 500 Hz, using their dragging and migration models together. By comparison with experiment, they concluded that the modulus defect and decrement (in the absence of peaking) were both proportional to $(1 + n_D)^{-1}$. They found that the presence or absence of peaking in the decrement depended strongly on prior annealing treatment.

V. Experimental Apparatus

A. REQUIREMENTS

The success of an experiment to measure internal friction and modulus changes caused by irradiation depends on the satisfaction of certain rather strict requirements, to wit:

1. Handling of the sample must be eliminated. Since the dislocation structure can be changed by application of very small stresses, it is desirable to irradiate and do all measurements and anneals without moving the sample.
2. Temperature must be controlled. Since the motion of point defects is a thermally activated process, it is very sensitive to temperature. It is desirable to measure and control the temperature to high precision. The required temperature range is wide, since some changes may occur near liquid helium temperature (4.2K), while the need for annealing to stabilize the dislocation structure requires temperatures of several hundred degrees C.
3. High vacuum or a very pure inert atmosphere must be maintained, since the internal friction of silver has been shown to be extremely sensitive to oxygen concentration.[105]
4. The measuring apparatus must not change its characteristics under irradiation or temperature variation.
5. It should be possible to turn the radiation flux on and off at will. Adequate shielding should be provided for protection of personnel. The flux must be sufficient to give readily observable changes in reasonable times. It should be uniform over the sample.
6. The frequency of the applied stress will depend on the experimental configuration used. If vibration at resonance is to be used, the frequency will depend on the size of the sample.
7. From the operator's point of view, the more nearly automatic the apparatus can be made, the better. Continuous monitoring of temperature, internal friction, and modulus, with automatic control of temperature changes and all extraneous variables, is desirable.

B. DESIGN AND GENERAL DESCRIPTION

The design of the apparatus used in this work is very similar to that described by Thompson and Glass.[106] The major differences are in the method of driving the sample, control of the phase of the driving signal, and the geometry of the sample and radiation source. The essentials of the design

are shown in Figs. 1 through 4. A general description will be given here, and details will be covered in the following sections.

The silver crystal sample is in the form of a hollow cylinder (Fig. 1). It is mounted with four small pins at its center plane and is thus free to vibrate in a longitudinal mode, which is of wavelength equal to twice the sample length. There are three rod-shaped ^{60}Co sources, each attached to the end of a Teflon wand. Each source can be inserted inside the sample and can be raised to decrease the irradiation or moved to a storage area by the use of a traveling shield assembly (Fig. 4).

The sample is mounted inside a cryostat-furnace for temperature variation and control (Fig. 2). A vacuum system consisting of mechanical and oil-diffusion pumps capable of 10 μPa is attached. A helium purification train consisting of a charcoal cold trap and a titanium furnace is used to purify helium for use as a heat-exchange gas.

The sample can be set into vibration by means of an electrostatic drive, and the motion is measured by an FM detection system (Fig. 3). Both are accomplished by a single hollow electrode whose position is controlled at less than 25 micrometers from the top of the sample (Fig. 1). This combination was first used by Cabaret[107] and later developed by Bordoni.[108]

Measurement of the decrement is made either by observing the decay of free vibrations, the width of the resonance curve in forced vibration, or the drive voltage required for a constant amplitude of vibration at resonance.

The unique features of this apparatus are its wide temperature range (less than 4°K to about 1000°K), its irradiation efficiency [an average flux of about 3.6×10^{11} gamma/(cm^2-sec) from a 100 Ci source in a sample of 2.5 cm^3 volume], and its automated operation. Most importantly, all operations take place without moving the sample.

C. SAMPLE FABRICATION

The samples for this experiment had to satisfy several requirements:

1. Their purity had to be as high as possible, since dislocation pinning is very sensitive to impurity concentration.
2. They had to be single crystals, to ensure a single resonant frequency throughout several annealing operations.
3. They had to be oriented properly, to avoid coupling to flexural vibration modes when the sample was driven.
4. They had to be hollow, to allow insertion of the radioactive source.
5. They had to have flat, parallel ends, to ensure that the driving force and vibration would be purely axial.

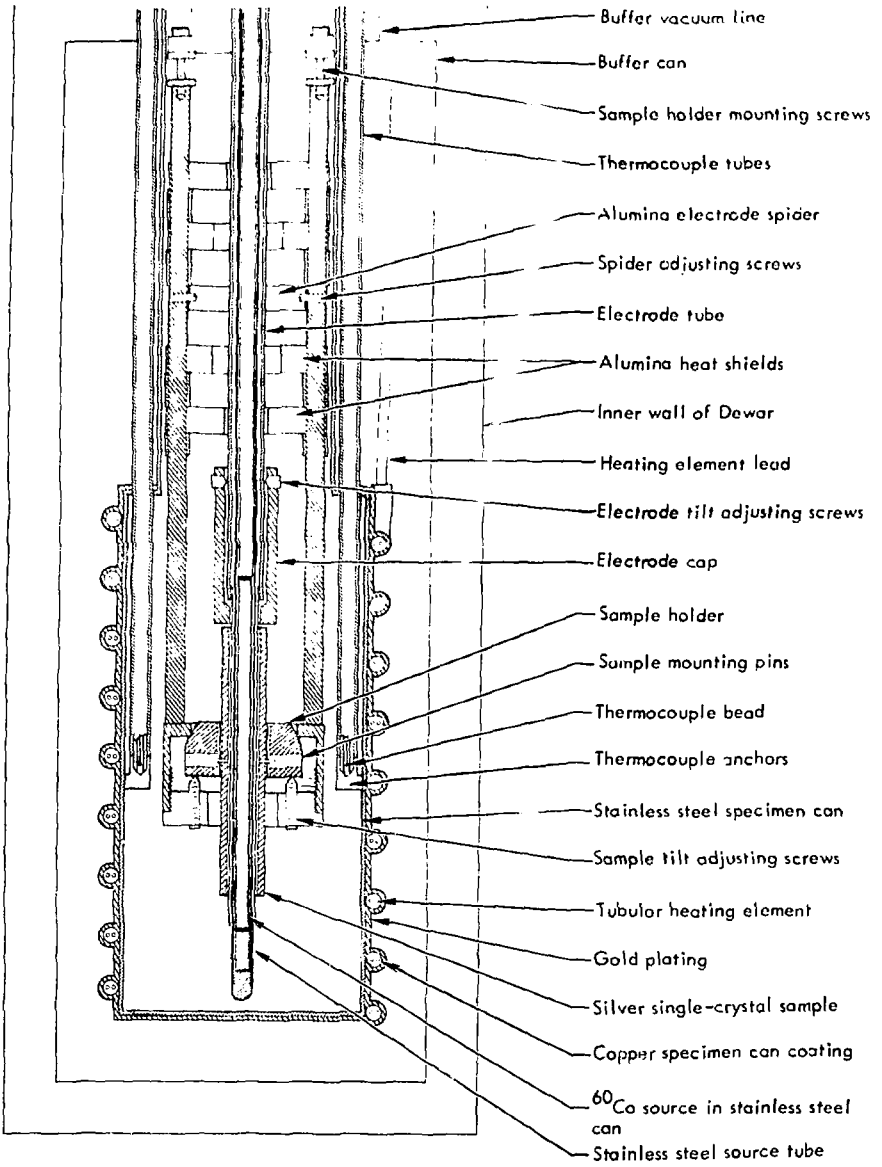

Fig. 1. Details of sample chamber.

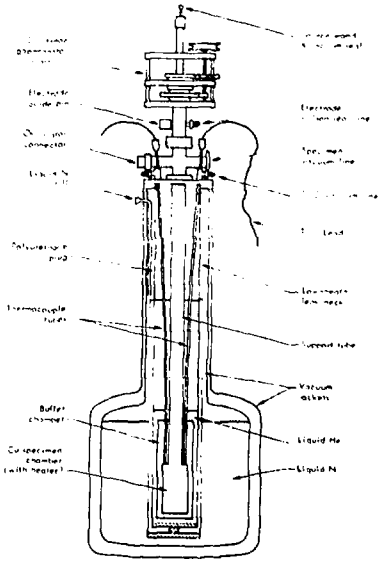

Fig. 2. Irradiation cryostat-furnace.

6. They had to be of convenient size to fit into the available double Dewar with its newly-designed cryostat assembly, and rigid enough to preclude severe deformation in normal handling.
7. They had to have some provision for mounting to the holder at the central nodal plane, with low damping losses.

These requirements were satisfied in the following way: The starting material was 99.9999% pure silver obtained from Cominco Products, Inc. (Lot HPM 3701). This material was cut to size with a jeweler's saw. It was etched in 50% reagent grade nitric acid and washed with reagent grade methanol or acetone prior to each melting.

It was decided to make the samples 9.525 mm in diameter and about 63 mm long, with a 6.35-mm-diameter axial hole for insertion of the source. The split molds used are shown in Fig. 5. They were obtained from Ultra Carbon Corporation, who fabricated them from ultra-high-purity graphite and guaranteed them to have less than 50 ppm total impurities after fabrication.

An induction furnace with an oil-diffusion-pump vacuum system was used for all melting. Melting was done either in a vacuum of 0.13 mPa or in helium gas that was purified by passage through a liquid nitrogen cold trap. The physical arrangement was as follows: The mold was placed on a stand fabricated from fused quartz so that it was vertical and located above the metal housing of the vacuum system. It was then surrounded by a fused quartz envelope in the shape of a large, inverted test tube, with about 15 mm minimum clearange between the envelope and the mold. This was attached to

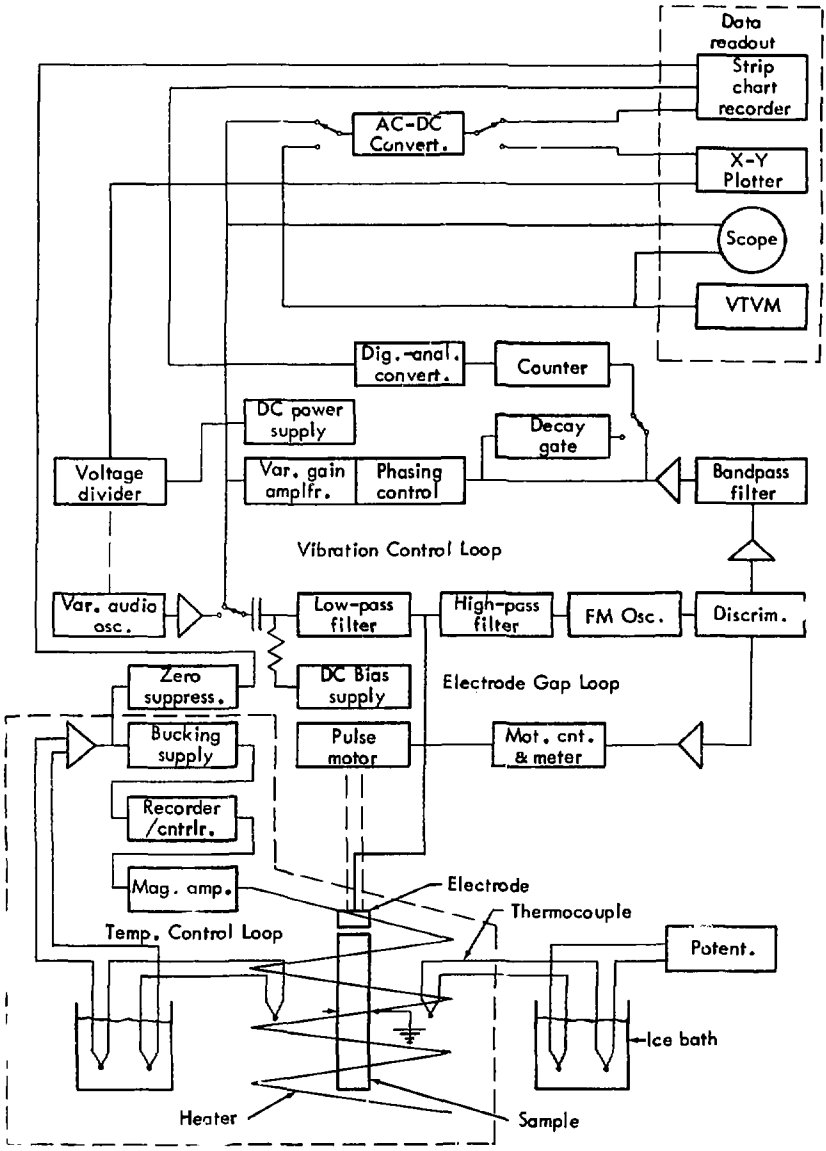

Fig. 3. Electronic system.

Fig. 4. Source transfer mechanism.

the vacuum system housing by means of a graded seal and a metal flange fitted with an O-ring. An induction coil was fabricated to surround (and clear) the envelope, and was mounted to a vertical variable speed motor drive mechanism. The induction coil was energized by a Lepel radio-frequency power unit via a flexible water-cooled coaxial cable.

The molds were first baked out at 1200°C for several hours in high vacuum using this system. The process for growing a crystal was then as follows: A hollow silver billet of the proper size was cast in the casting mold (Fig. 5, left). The silver was melted in a vacuum and 100 kPa of helium was then added to push it into the mold. The mold was cooled slowly by raising the induction coil at a rate of about 200 mm/hr to eliminate porosity. The mold was then removed from the furnace and disassembled. At this stage, the hollow billet was firmly attached to the graphite rod from the center of the mold because of differential thermal contraction. The two were placed in a stainless steel jig

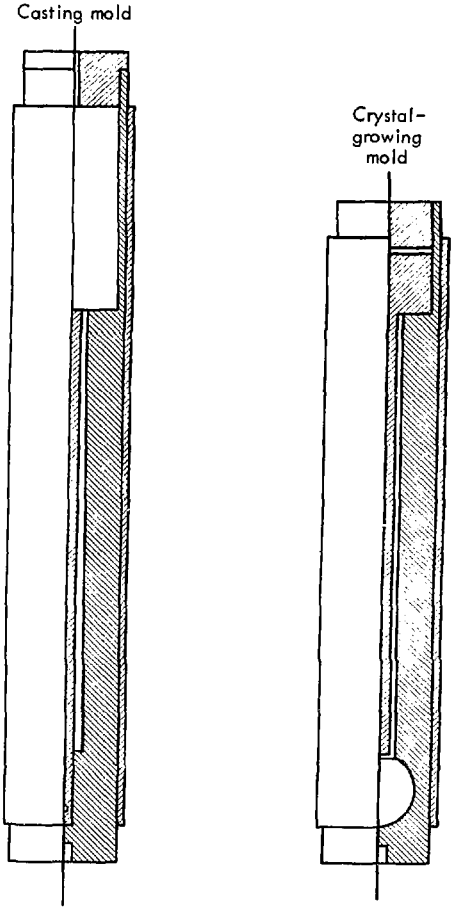

Fig. 5. Molds.

incorporating a Wilson seal and heated in another vacuum furnace to about 700°C at 10^{-6} Torr, at which temperature it was possible to pull the rod out of the billet by careful hand pressure. The billet was then cooled and removed from the furnace, and the excess material cut off with a Servomet spark machine. The polycrystalline billet was stored under clean conditions.

Next, a spherical single crystal 25.4 mm in diameter was grown in the crystal growing mold (Fig. 5, right). This was accomplished by heating the entire mold to about 1100°C and raising the induction coil at the rate of 5 mm/hr. (This is known as the modified Bridgman crystal growing technique.) Several attempts were required to produce a seed that revealed no striations upon etching. The extra stub was then removed with the Servomet spark machine set to range 6. The etched sphere showed spots corresponding to the crystallographic directions.

The growth of a hollow cylindrical single crystal was then accomplished as follows: The seed was placed in the bottom of the crystal growing mold and oriented by visually sighting down the axis of the mold so that a ⟨111⟩ direction was parallel with the axis. The previously-cast billet was slipped over the graphite plug-rod for this mold which had been fabricated smaller than the rod in the casting mold to allow this to be done at room temperature. The mold was assembled with the plug-rod raised about 3 mm above its shoulder, and placed in the induction furnace. The furnace was evacuated and the induction coil positioned so that its bottom was at the level of the center of the seed. The mold was heated to red heat in a vacuum and 1 atm of helium was added. The silver was then melted down to approximately the center of the seed. This was accomplished by judicious adjustment of the height of the coil and the power setting while observing the temperature of the mold with an optical pyrometer which had been calibrated to account for the absorption of the fused quartz vacuum envelope. The induction coil was then raised at the rate of 5 mm/hr and the single crystal grown up from the seed. The furnace was then slowly cooled over a period of about two hours. The rod was pulled from the crystal as before, and the seed cut off with the Servomet spark machine. The hollow crystal was then sliced to length and the ends planed perpendicular to the axis, again with the spark machine. Several crystals were fabricated in this manner.

The fabrication of these samples was no mean task. Success was found to depend on slow cooling of the molds, elimination of the vibration in the apparatus, and prevention of stresses on the silver due to the differing thermal expansivities of the silver and graphite. The growing speed was also found to be important, since striations developed in the crystals at higher speeds.

The dislocation structure and density produced by this method of fabrication is not known, but the stresses developed when the crystal was cooled on

the graphite rod and when the rod was pulled from it no doubt increased the density over that expected for crystals of simpler shape. Etch pit counting was not performed.

Some of the silver used in growing the final sample had already been melted more than six times because of the difficulty in producing a single crystal in such an unusual shape.

D. TEMPERATURE MEASUREMENT AND CONTROL— THE CRYOSTAT FURNACE

As mentioned above, careful measurement and control of temperature is essential to the success of experiments of this type. This is particularly important in the region near liquid helium temperature and immediately above.

To accomplish this, the cryostat furnace pictured in Fig. 2 was designed and built. The basis of this apparatus is a Cryenco stainless steel liquid helium Dewar. The inner chamber of this Dewar measures 101.6 mm i.d. × 914.4 mm deep. The bottom 610 mm is double-walled and vacuum-insulated. The inner wall is made of stainless steel, while the outer wall, in contact with liquid nitrogen, is made of copper. The upper 305 mm is single-walled, 0.381-mm-thick, stainless steel. Fittings were attached to the side of the Dewar at the top, to provide for filling of the nitrogen chamber. There is a stainless steel collar at the top of the Dewar, which is tapped for 6.35 mm bolts and contains an O-ring groove. This collar mates with the main flange of the heater-buffer assembly.

The heater-buffer assembly consists of two concentric cylindrical chambers (called the specimen and buffer chambers), the main supporting tube, the thermocouple tubes, the main flange, and a polyurethane plug. The specimen chamber is made of stainless steel, to allow for high-temperature oxygen experiments. The thermocouple tubes enter the inner can but are hermetically sealed from it. The tips of these tubes are fitted with small thermal anchors that were welded to the inside of the inner can at its center height. The tubes extend up through the main flange and terminate in fittings that ensure a vacuum seal and allow for pump-out.

The heater is a 400-W tubular stainless-steel-sheathed Nichrome element with magnesia insulation. It was wound helically onto the specimen chamber, held in place with small stainless steel strips spot-welded to the chamber, and vacuum-brazed in place with gold-nickel alloy. The entire specimen chamber with its heater was electroplated with a 1.6-mm-thick layer of copper and a thin coating of gold. This specimen chamber design is advantageous in that it allows oxygen experiments to be done because of the stainless steel liner, but retains the beneficial high thermal conductivity of copper to

reduce thermal gradients. The integral design provides tight thermal linking of the heater and thermocouples for precise control.

The buffer is a copper can, 88.9 mm in diameter and 0.762 mm thick, surrounding the specimen chamber and heater assembly. It has a pump-out tube extending up to the main flange so that it can be evacuated or filled with exchange gas independently of the inner can. The heater leads, inside their sheath, extend to the top flange through the buffer pump-out tube. This provides insulation to minimize liquid helium boil-off. It was necessary to mount the top of the heater sheath in a bellows, to allow for differential thermal expansion. The top of the bellows was thermally linked to the top flange with copper braid to prevent overheating.

The main flange contains several fittings. First is the center hole for the main tube. The hole is surrounded by an O-ring groove and a tapped bolt circle that mates with the flange on the electrode-sample holder assembly. The main flange also contains the thermocouple wand seals, the thermocouple pump-out fittings, the buffer pump-out line, the heater leads, the vacuum-jacketed fill line for the 101.6-mm-i.d. Dewar chamber, the Dewar-chamber vent and pump-out line, and a Dewar-chamber probe hole. Molded onto the upper 300 mm of the main tube is a polyurethane plug that prevents collapse of the Dewar wall when the Dewar chamber is evacuated, and reduces gas-column conduction when the Dewar contains liquid helium.

The heater-buffer assembly is lowered into the Dewar chamber and bolted to the collar. This provides the third concentric vacuum tight chamber. With this combination it is possible to control the temperature of the sample in the inner can over a wide range. For the lowest temperatures, liquid helium is fed into the Dewar chamber and helium gas into the buffer and inner can. With this arrangement, it is possible to reach approximately 2 K by pumping on the liquid helium with a mechanical pump (normally it is open to the atmosphere through a check valve). Using the heater, the temperature can be controlled up to about 80 K. For higher temperatures, the helium is allowed to boil off, and the Dewar jacket is kept filled with liquid nitrogen. This can be used up to room temperature by evacuating the buffer. Above room temperature, a recirculating water system is connected to the Dewar chamber. It consists of a pump, hoses, and a combination reservoir, heat exchanger, and surge chamber. The system is filled with deionized water and exchanges heat with the Laboratory cooling water loop. The capacity of this system is such that the deionized water temperature rises only a few degrees at full heater power.

The actual measurement and control of the temperature is accomplished by a thermocouple control system. Thermocouples are fitted into wands made of thin-wall stainless steel tubing. These contain Kovar seals at the top and are inserted into the thermocouple tubes. The bottom tips of the wands are

chamfered to mate with the thermal anchors. The tops of the thermocouple tubes contain O-ring seals so that they can be evacuated and backfilled with helium gas.

The low-temperature thermocouples were made of 0.076-mm wire to reduce heat transfer. Au-2.1% Co/Cu thermocouples were chosen for their high output. The wires are glass-insulated, and junctions were made by spot welding. The beads are insulated from the wands with Teflon tape. For medium temperatures, copper/constantan thermocouples are used. The high-temperature thermocouples are Pt/Pt-10% Rh surrounded by ceramic insulators. The low-temperature thermocouples were calibrated against a Honeywell germanium resistance thermometer that was attached to a wand and lowered into one of the thermocouple tubes in the same manner. The Au-2.1% Co/Cu thermocouples are never allowed to rise above room temperature.

The thermocouples are referenced to an automatic ice-point reference standard made by Kaye Instruments, Inc. The output of one thermocouple can be measured accurately with a Leeds and Northrup K-3 potentiometer, while that of the other is used for control. The control system is shown on the block diagram, Fig. 3. It contains an operational amplifier which is connected to give a gain of 100. The output of this amplifier is then bucked by a regulated 1-V power supply, and the difference is fed to a Leeds and Northrup Series 60 C.A.T. controller. The controller output drives a magnetic amplifier, which in turn feeds a voltage-dividing resistor bank connected to the cryostat heater. A separate difference signal is also fed to the strip chart recorder. A motor drive on the bucking circuit enables one to drive the control temperature in either direction at various speeds.

The accuracy of the temperature control system is $\pm 1/2$ K in absolute value and $\pm 1/4$ K in relative value during a given isothermal run. The final temperature calibration for the runs reported here was made by replacing the sample with a dummy silver sample of the same size into which a 40-gauge copper/constantan thermocouple was crimped. The thermocouple wires were passed out the center of the electrode through a Kovar feedthrough. The conditions of specimen chamber pressure and temperature during each run were duplicated and the sample temperature was calibrated against the chamber temperature. Corrections were then applied for the temperature changes due to insertion of the source, as discussed in Section G.

E. SAMPLE MOUNTING AND ELECTRODE ALIGNMENT

A bar that is to be driven in longitudinal vibration ideally should be mounted exactly at its nodal plane with zero-thickness mounts that will support the sample over the entire temperature range of interest without

stressing the material or allowing it to loosen. The mount should be either infinitely compliant or infinitely rigid, to avoid absorbing energy from the vibration.

In practice, it is not possible to achieve these goals completely, but satisfactory results have been obtained by various workers using wires, knife edges, and needles. The wire system, though very compliant, is not satisfactory for vertical sample orientation; and the knife edges and needles, although very rigid, deform the sample and require accurate correction for thermal-expansion differences between the sample and the mount. To eliminate these difficulties, we decided to mount the sample on four sliding pins, spaced 90° apart on the nodal plane. The pins were made by turning down the tips of stainless steel set screws to a diameter of 0.38 mm. After some development, they were electroplated with a thin layer of cobalt to prevent sintering to the silver and coated with a layer of colloidal graphite to promote sliding. The importance of this is discussed in Part VI.

Four holes were spark-machined into the sample using the Servomet on range 6. The cutting electrode used consisted of a size 80 drill bit chucked upside down. Accurate alignment of these holes was achieved by using a specially-built jig. The jig incorporated a V-block with a stainless steel sample sleeve. The sleeve had four holes spaced at 90°, which registered with a pin on the V-block. In use, the sample was first located with a micrometer screw. Then it was glued inside the sleeve, which had a Teflon liner, with a home-made conducting glue that was soluble in acetone but not in kerosene, which was the cooling fluid used in the Servomet machine. This glue was made by adding powdered graphite to Duco cement. The spark machine was then aligned by matching the cutting electrode to a small hole drilled at the proper place in the V-block. The cutting electrode was backed off, and the sample sleeve was glued to the V-block, matching one of its holes to the pin. The first hole was then spark-machined into the sample. After it was completed, the glue holding the sleeve to the V-block was dissolved with acetone on a Q-tip, taking care not to dissolve the glue holding the sample to the sleeve. The sleeve and sample were then rotated 90°, glued, spark-machined, and so on, until all four holes were completed. The glue holding the sample inside the sleeve was then dissolved and the sample was removed and washed with acetone.

The sample was then carefully mounted in the sample holder by lining up the holes with the pins and screwing the pins in against the shoulders provided in the sample holder. The sample holder was then installed in the mounting assembly, which is shown in Fig. 1. Differences in horizontal thermal expansion are compensated by sliding of the sample on the pins, and the small size of the pins makes thermal-expansion differences between the pin and hole diameters unimportant. By saturating a silver sample with oxygen to pin its dislocations the background decrement due to this mounting was found to be

less than 1.4×10^{-5}, about an order of magnitude below the other measurements made in this work. Actually, it may have been lower than this, since it is not known whether the oxygen eliminated all internal friction in the sample, itself.

To align the sample and the electrode accurately, four adjustments were provided. The adjustment sequence was as follows:

1. The sample-holder mounting assembly was first aligned approximately horizontally with the electrode tube axis, using its three mounting screws and lock nuts (Fig. 1).
2. The sample holder was then tilted, using its supporting screws until the sample center hole was parallel with the axis of the electrode.
3. The electrode was then moved horizontally by adjusting the position of the electrode centering spider using three screws.
4. The electrode cap was then tilted by means of four set screws arranged on two axes that are perpendicular to each other and separated vertically by 25.4 mm. Only two of the screws are shown in Fig. 1. This cap design was suggested by a fellow graduate student, Ronald M. Finnila.[109]

The last adjustment was made by first shining a bright light through the gap and tilting the electrode cap until it was as nearly parallel to the sample end face as could be judged with the naked eye. Then the 5-MHz carrier signal was applied, and the electrode was carefully lowered until a small arc occurred. Its location was noted and the electrode was backed off and tilted slightly to increase the gap at that point. This procedure was continued until no further improvement could be made.

This design and procedure is effective in coping with variations in dimensions between different samples, and allows rapid and precise adjustment of the alignment. It is stable during annealing, protects the sample from mechanical disturbance, and guarantees gap alignment to better than 13 micrometers over the width of the sample. This is very essential, because it allows a small gap and hence a low strain amplitude to be used in order to avoid the amplitude-dependent damping region during experiments.

F. ELECTRONIC SYSTEM

The electronic equipment is shown in the block diagram, Fig. 3. Most of the system was assembled by M. W. Guinan, who has described it elsewhere.[105] Its functions are to control the sample—electrode gap, to drive the sample at its resonant frequency and a preselected strain amplitude, and to measure and record the resonant frequency and drive voltage continuously. In

addition, it must be able to plot resonance curves and to monitor the decay of free vibrations. The temperature control and monitoring system is also shown. Switches are shown in the normal, closed-loop control position.

The essential concept is that the electrode—sample combination forms a capacitor that is effectively located in the tuning circuit of an FM oscillator. The resonant frequency of the oscillator is 5 MHz; and it is modulated by the sample vibration, which causes the effective capacitance of the gap to vary. The frequency of the modulation corresponds to the vibration frequency of the sample, and the absolute amount by which the modulation shifts the oscillator frequency corresponds to the amplitude of the sample vibration.

The oscillator output is fed to a discriminator circuit, which puts out two signals. The first is a d.c. signal that corresponds to the average oscillator frequency. It therefore reflects the average value of the electrode-sample capacitance, which is inversely proportional to the average gap spacing. This signal is fed to a servo amplifier driving a pulse motor that raises and lowers the electrode to maintain a constant gap spacing.

The other signal coming from the discriminator is an a.c. signal whose frequency is that of the sample vibration and whose amplitude is proportional to the sample vibration amplitude. This signal is amplified and filtered to remove noise, its frequency is counted to ±0.3 Hz reproducibly and is recorded by the strip chart, and it is passed through a phasing control and a variable gain amplifier. The amplifier gain is varied in order to keep the sample vibration at constant amplitude, as indicated by the discriminator signal. The phasing control varies the phase relation between its input and output signals by a few degrees at a rate of 1 Hz and controls the average phase at the value that produces equal increases in the required drive signal as the phase is varied in each direction. The voltage of the output or drive signal is then measured to about 1% accuracy and recorded as it is applied to the electrode. The high- and low-pass filters are used to prevent interference between the lower-frequency drive signal and the higher-frequency oscillator carrier signal. The decay gate is used to calibrate the drive-signal voltage measurement, so that the relationship between the internal friction and the required drive voltage for a given vibration amplitude can be known. It is essentially a differential discriminator that allows the counter to count the number of cycles between two specified vibration amplitudes in a free decay. To use it, the counter is switched to the decay gate output, the drive is temporarily turned off, and the number of cycles whose amplitude lie inside the "window" is counted as the vibration decays.

The d.c. voltage supply provides an adjustable bias to the electrode so that a wide range of damping and strain amplitude can be accommodated. It also ensures that the drive signal frequency and oscillation frequency are

equal instead of being related by a factor of two, as would be the case with pure a.c. drive. The d.c. voltage can be known to an accuracy of better than 0.1%.

The VTVM allows precise setting of the strain amplitude. The control level of the variable gain amplifier is set by reference to it.

The oscilloscope provides a convenient monitor for the system. During stable operation, it displays an elliptical 1:1 Lissajous figure which is steady in size and rocks gently back and forth at 1 Hz with the phase modulation. Any instabilities such as electrode arcing, loss of control, or amplifier distortion are immediately apparent.

To plot resonance curves, the other three switches shown in Fig. 3 are placed in the "down" position. This connects the variable audio oscillator and amplifier to the electrode so that the forcing frequency can be swept across resonance. The oscillator frequency dial is attached to a potentiometer that varies the d.c. voltage from a small power supply and drives the X-axis of the X-Y plotter. The Y-axis then responds to the specimen vibration amplitude, through the a.c.-to-d.c. converter. This makes it possible to plot amplitude versus frequency in a quick and convenient manner. The resonance curves give the damping value to a reproducibility of 1%.

The output data continuously printed by the strip chart recorder are temperature, resonant frequency, and drive voltage as functions of time.

G. IRRADIATION SYSTEM

The irradiation system consists of the sources, the remote control source transfer mechanism, and the storage and shielding pit.

The three sources are composed of cobalt partially activated to ^{60}Co, and were obtained from General Electric Corporation, Vallecitos Nuclear Center, Pleasanton, California. The nominal activities of the sources are 1.0, 10, and 100 Ci. The exact activities are calculated for each experiment by using calibration data supplied by the manufacturer and a half-life of 5.263 years.[110] The calibrations are certified to be accurate to ±5%.

The cobalt is in the form of 1-mm-diameter by 1-mm-long cylindrical pellets uniformly spaced in sealed stainless steel tubes of total length 8.5 cm. These tubes in turn are inserted into outer stainless steel tubes that are soft-soldered to threaded plugs above the heated zone. The plugs are screwed into the ends of Teflon rods. The top of each rod is fitted with an eye screw, an O-ring, and a cap that screws onto the top of the electrode shaft at the top of the cryostat furnace. This provides a vacuum seal when the source is in the cryostat furnace.

Because the sources are metallic, it is necessary to provide an electrostatic shield between the sample and the source, which is inserted into it.

Otherwise, insertion of a source would cause a large change in the apparent electrode sample capacitance which would increase the automatically controlled gap, which would in turn raise the strain amplitude and possibly the observed damping. A thin-walled stainless steel tube was therefore welded to the end of the electrode tube, independent of the electrode cap. It passes through the cap and the sample, extending a few mm below it. This tube also prevents the source from rubbing the sample during insertion and withdrawal. The gamma-ray attenuation of this tube is negligible.

This source-sample geometry provides maximum efficiency and fairly uniform irradiation, making it possible to obtain a flux of about 3.6×10^{11} gammas/(cm^2-sec) from a 100-Ci source in a sample of 2.5 cm^3 volume, with 90% of the sample volume receiving within ±25% of the average damage rate as mentioned previously.

The disadvantages of this design are that it is not possible to obtain isothermal data until about 1 hr after the source is inserted, and it appears that insertion of the source causes a small initial change in the damping, amounting to at most 4.3% in this work.

The reason for the 1-hr delay is that the source insertion changes the sample temperature, and this length of time is required before a new thermal balance is restored. The temperature change is due to gamma heating and the additional heat-leak path to the cooling bath that is contributed by the source. These effects were separated by inserting sources with the apparatus held at room temperature by a water cooling bath. In this case the heat-leak effect should not be present. The change in vibrational frequency, which is inversely proportional to the temperature change, was observed. It was found that gamma heating is negligible (less than 0.1°C) with the 1.0-Ci source, which was used in the quantitative experiments of the present work. The combined effects amounted to about 0.4°C for the highest temperature run used in this work (53°C). This was taken into account in calculating the actual sample temperatures.

The cause of the small damping change when the source is inserted is not completely clear. Since it occurs instantaneously, compared to the pinning observed during the anneals, it seems not to be due to a radiation pinning effect. Neither can it be attributed to mechanical shaking of the sample during insertion of the source, since it does not occur with a dummy source. Rather, it appears to be due to the rapid initial change in temperature of the sample relative to its mounting, necessitating sliding of the mounting pins in the sample mounting holes. Although precautions were taken to reduce pin-sample friction, as discussed earlier, it seems probable that the small friction which remains gives rise to small deformations near the mounting pins, which change the damping slightly. As a consequence of this, the initial damping

value has been treated as a variable parameter with narrow limits in the data analysis as will be discussed later.

The transfer mechanism (Fig. 4) is used for raising the sources and transferring them between the cryostat and the storage area. It consists of a movable, 110-mm-thick lead shield mounted on a trolley, which in turn rolls on an overhead I-beam. The shield can be raised and lowered by means of pulleys, cables, and a counterweight, in order to keep the source covered at all times. The trolley can be locked in position by means of a spring-loaded pin that engages holes in the I-beam. The sources themselves are carried by a hook which attaches to the eye screws mentioned above. The hook in turn is affixed to a cable which passes up inside the shield to the trolley and thence over a pulley and out to the control point. All the control cables for this source, shield, trolley, and lock pin extend overhead to the control point 5 m away, where they pass over pulleys and terminate in fobs. Remote control is accomplished by the use of these fobs and strategically placed mirrors.

The storage and shielding pit is constructed from 12 tons of lead brick. The bricks are placed in such a way that the sources are surrounded by 200 mm of lead when in the cryostat, and by 250 mm when in the adjacent storage area. This effectively protects personnel but retains convenience of operation. The highest dose rate to operators occurs during transfer of the largest source and does not exceed 80 mR/hr for a period of 1 min.

H. STRAIN AMPLITUDE AND DAMPING CALIBRATION

To interpret the data from the apparatus described above, one must be able to convert the measurements of drive voltage at the electrode—sample gap and discriminator output voltage into the logarithmic decrement and the strain amplitude. To do this it is necessary to solve the equation of motion of the sample and apply the equations governing the behavior of the electronic measuring and control system. This has been done by Guinan,[105] and is repeated here with some changes.

Consider first a uniform rod of arbitrary cross section with ends perpendicular to its axis, center plane mounting, and length L. This represents the silver sample. The equation of motion of such a rod, driven electrostatically at $x = L/2$ by a sinusoidal signal, is[111]

$$\rho \frac{\partial^2 u}{\partial t^2} = E \frac{\partial^2 u}{\partial x^2} + \delta\left(x - \frac{L}{2}\right)\sigma_o e^{i\omega t} \qquad \text{(V-H-1)}$$

where

ρ is the mass density (kg/m^3)

u is the displacement from equilibrium in the x-direction (m)

E is Young's modulus, complex to allow for damping (Pa)

t is time (sec)

σ_o is the peak value of the applied stress (Pa)

ω is the circular frequency of the driving signal (sec^{-1})

and $\delta\left(x - \frac{L}{2}\right)$ has dimensions of 1/length, so that

$$\int_{-\infty}^{+\infty} \delta\left(x - \frac{L}{2}\right) dx = 1.$$

Using the boundary conditions

$$u(0,t) = 0 \text{ and } \frac{\partial u(x,t)}{\partial x}\bigg|_{x=\frac{L}{2}} = 0,$$

this equation of motion can be solved by separation of variables and eigenfunction expansion. The solution is shown to be

$$u(x,t) = \sum_{n=0}^{\infty} \text{Re}\left[A_n \sin(a_n x)\, e^{i\omega_n t}\right], \qquad \text{(V-H-2)}$$

where

$$A_n = \frac{\sigma_o}{\rho L\left(\frac{E}{\rho} a_n^2 - \omega_n^2\right)}. \qquad \text{(V-H-3)}$$

Here, Re denotes the real part,

$$a_n = \frac{(2n \pm 1)\pi}{L}, \qquad \text{(V-H-4)}$$

and

$$\omega_n = a_n \sqrt{\frac{E}{\rho}}. \qquad \text{(V-H-5)}$$

In determining the coefficients A_n, it is assumed that the driving frequency is equal to one of the normal mode frequencies, i.e.,

$$\omega = \omega_n = \sqrt{a_n^2 \frac{E}{\rho}}. \tag{V-H-6}$$

To allow for damping, we set

$$E = E_o\left(1 + \frac{i\Delta}{\pi}\right), \tag{V-H-7}$$

where Δ is the logarithmic decrement. Then

$$u(x,t) = \frac{\pi\sigma_o}{\rho L\Delta} \sum_{n=0}^{\infty} \frac{1}{\omega_n^2} \sin\left[\frac{(2n+1)\pi x}{L}\right] \sin \omega_n t. \tag{V-H-8}$$

Finally, if the bar is driven at its fundamental mode (n = 0), the solution becomes

$$u(x,t) = \frac{\sigma_o}{4\pi\rho L f_o^2 \Delta} \sin\frac{\pi x}{L} \sin 2\pi f_o t, \tag{V-H-9}$$

where f_o is the frequency of the fundamental (Hz). It is now necessary to relate this solution to the parameters of the control system. Since the strain is defined as $\epsilon = \partial u/\partial x$, its maximum value occurring at the center plane of the rod is

$$\epsilon_o = \frac{\sigma_o}{4\rho L^2 f_o^2 \Delta}. \tag{V-H-10}$$

Also, since the increment of length (u_{max}) is given by

$$\delta L = \frac{\sigma_o}{4\pi\rho L f_o^2 \Delta} \tag{V-H-11}$$

it follows that

$$\epsilon_o = \pi \frac{\delta L}{L}. \tag{V-H-12}$$

This relates the maximum strain in the rod to the deflection of its end, for simple harmonic motion. It is the motion of the end that is important to the control system, as will be seen.

The basis of the electrostatic drive system is that a capacitor is formed by the electrode and the top end of the silver rod. Its area is equal to the cross-sectional area of the rod. Then, neglecting edge effects[112]

$$C_g = \frac{8.842 \times 10^{-12} A}{d_g} \qquad \text{(V-H-13)}$$

where

C_g is the capacitance of the gap in F,

A is the area in m^2, and

d_g is the gap spacing in m.

Also,

$$\delta d_g = \frac{-8.842 \times 10^{-12} A \, \delta C_g}{C_g^2} \qquad \text{(V-H-14)}$$

where δd_g and δC_g represent small changes in the gap and capacitance, respectively. The frequency change of the FM oscillator is related to δC_g by

$$\frac{\delta C_g}{C_o} = \frac{-2\delta f_H}{f_H}, \qquad \text{(V-H-15)}$$

where f_H is the FM oscillator frequency. This equation defines C_o (in F) which is actually a composite of the fixed and variable capacitors in the oscillator circuit and filters, and the stray capacitance of the apparatus. Since $\delta L = \delta d_g$, the maximum strain amplitude is given by

$$\epsilon_o = \frac{7.86 \times 10^{-11} A C_o \gamma V_o}{L f_H G C_g^2} \qquad \text{(V-H-16)}$$

where γ is a constant relating the discriminator output to the frequency change δf_H: ($\delta f_H = \gamma V_d$), and V_d is the peak voltage of the discriminator output. V_d in turn is related to the VTVM reading by

$$V_d = \frac{\sqrt{2}}{G} V_o,$$

where V_o is the VTVM reading in V rms and G is the voltage gain of the amplifier located between the discriminator and the VTVM. This result provides a method of determining the maximum strain amplitude with no knowledge of the damping or drive voltage. A and L can be obtained by measuring the sample. C_o is obtained by calibrating the change in oscillator frequency for known values of inserted capacitance. f_H is read from the counter. G can be measured by using the VTVM and audio oscillator. γ is obtained from a calibration of the discriminator output voltage versus oscillator frequency. C_g is found

by raising the electrode, manually adjusting the FM oscillator frequency to the desired value, lowering the electrode, resetting the frequency, and noting the difference on the calibrated dial. V_o is read from the VTVM.

It is also possible to obtain an independent measure of the strain amplitude if the damping and drive voltages are known. This provides a check on the system. To accomplish this, it is necessary to express the strain amplitude in terms of the drive voltage.

As was shown above,

$$\epsilon_o = \frac{\sigma_o}{4L^2 f_o^2 \Delta \rho}. \qquad \text{(V-H-10)}$$

The stress on a capacitor plate is given by[113]

$$\sigma = \frac{V^2}{7.2 \times 10^{10}\, \pi\, d_g^2} \qquad \text{(V-H-17)}$$

where σ is expressed in pascals, d_g in meters, and V in volts. Since the electrode receives both an a.c. signal and a d.c. bias,

$$V = V_D + \sqrt{2}\, v_o \sin \omega_D t, \qquad \text{(V-H-18)}$$

where V_D is expressed in volts d.c., v_o is the rms a.c. drive voltage, and ω_D is the drive frequency. Then

$$V^2 = V_D^2 + 2\sqrt{2}\, v_o V_D \sin \omega_D t + 2v_o^2 \sin^2 \omega_D t$$

$$= V_D^2 + 2\sqrt{2}\, v_o V_D \sin \omega_D t + v_0^2 - v_o^2 \cos 2\omega_D t. \qquad \text{(V-H-19)}$$

In the present case, $V_D \gg v_o$ (by a factor of at least 15) so that the sample is driven at the frequency of the a.c. signal, and

$$\sigma_o = \frac{1.60 \times 10^{-19} v_o V_D C_g^2}{A^2}. \qquad \text{(V-H-20)}$$

Finally,

$$\epsilon_o = \frac{4.00 \times 10^{-20} v_o V_D C_g^2}{L^2 f_o^2 \Delta \rho A^2}. \qquad \text{(V-H-21)}$$

In using this equation, Δ must be determined by taking a resonance curve or by the free decay method.

A final approach is to combine Eqs. (V-H-16) and (V-H-21) and solve for Δ. Then, if Δ is obtained independently by resonance curves or free decay, a comparison can be made quickly, as a continuous check of the system. This calculation results in the equation

$$\Delta = \frac{5.09 \times 10^{-10} v_o V_D c_g^4 f_H G}{L f_o^2 \rho A^3 C_o V_o}. \qquad \text{(V-H-22)}$$

During operation, the actual practice was to periodically obtain the ratio $\Delta/(v_o V_D)$, where Δ was obtained from free decays. This ratio varied as much as 10% over the course of a 600-hr irradiation, but the use of frequent free-decay calibrations made it possible to determine the damping to a precision of about 1%.

The calibration standard for all values of Δ was taken to be the resonance-curve method, since this is independent of all other parameters so long as they remained constant during the period of about 1 min that was required to plot a curve. That they did was demonstrated by the smoothness and reproducibility of the curves that were obtained.

VI. Survey Experiments

Several survey experiments were conducted in preparation for the isothermal irradiations discussed in Part VII. The purposes of these experiments were to test and improve the operation of the newly fabricated apparatus and to obtain a qualitative understanding of the processes to be studied. Because these purposes were accomplished simultaneously, high precision was not possible in this phase of the work, but considerable information was obtained, and a firm foundation was laid for the more quantitative work which followed. To present a more coherent account, we have chosen to present the experimental procedure and the results together. Discussion and conclusions drawn from the survey experiments will follow and will set the stage for discussion of the isothermal irradiations.

A. EXPERIMENTAL PROCEDURE AND RESULTS

After mounting in the cryostat furnace, the first single crystal sample (labeled No. SC4a) was annealed overnight in high vacuum at a temperature of 600°C. This anneal lowered the room-temperature decrement by about a factor of 2.5 from the freshly mounted value to 2.8×10^{-3}. The resonant frequency at room temperature after annealing was about 24.7 kHz.

The first experiment was a room-temperature irradiation with the 20-Ci source for 120 hr. The purpose was to find out whether this source would cause large enough changes in the damping and frequency in a few hours to be readily observed. The irradiation resulted in a 93% reduction in the decrement and a frequency increase of about 100 Hz. Following this, the sample was annealed overnight several times at 600°C in high vacuum, cooling to room temperature between anneals. This was done to find out whether the room-temperature damping value would change with successive anneals. It was found that the first anneal raised the decrement to near the value before irradiation. Each succeeding anneal lowered the decrement by a decreasing amount. After six anneals, the room-temperature damping became constant within a few percent.

Sample No. SC4a was replaced by a second single crystal (labeled No. SC9t) for the next series of experiments, because apparatus difficulties caused No. SC4a to recrystallize, rendering it unusable. This second crystal was annealed overnight four times at 600°C in high vacuum. After each of the first three anneals, a dummy source was inserted to check and adjust its alignment with the hole in the sample. Each time, the sample was disturbed, and the damping rose slightly. After the fourth anneal the alignment of the source was properly adjusted, and its insertion did not result in a damping increase. The room-temperature damping at this point was 1.1×10^{-3}, and the resonant frequency was about 26.7 kHz.

The annealed sample then was cooled to 4.2 K, and the damping and frequency were monitored during a continuous warm-up to room temperature. The purpose was to establish the preirradiation values of the monitored parameters. The warm-up revealed a single broad peak in the internal friction as a function of temperature. The decrement rose from a value of about 9×10^{-4} at 4.2 K to about 5×10^{-3} at 81 K, with a slope that was concave downward. Then it decreased at a slower rate to room temperature, where it was equal to about 1.1×10^{-3} as mentioned above. The slope was concave upward on the high side of the peak. The half-maximum values of the decrement occurred at about 25 K and 190 K. The warm-up was repeated to check reproducibility, with the result that the temperature of maximum damping was reproducible to within about 3 K, the decrement values to within about 2%, and the frequency values to within about 0.02%.

Once the starting values were established, the next objective was to find out at what temperatures observable changes due to irradiation would occur. The sample was cooled to 4.2 K and the 20-Ci source* was inserted. The sample was irradiated for about 8 hr, during which time its temperature never rose above 20 K, and then it was slowly warmed to room temperature. Because of apparatus difficulties (formation of air ice in the electrode), it was not possible to remove the source before the warm-up, so the irradiation was continued during this period. The damping and frequency were continuously monitored during the warm-up, but apparatus difficulties precluded smooth temperature control. Upon reaching room temperature, the source was removed after a total irradiation time of about 26 hr. At this time the damping was observed to have decreased to 9.0×10^{-4} from its former value of 1.1×10^{-3}. The frequency had increased by about 44 Hz. The sample then was allowed to anneal at room temperature for about 35 hr. During this time the temperature rose briefly to about 35°C as a result of controller malfunction, but spent the majority of the time at room temperature. This anneal caused the damping to decrease to 4.7×10^{-4}, and the frequency rose an additional 27 Hz.

The sample was cooled again to 4.2 K, and another monitored warm-up to room temperature was performed. The objective of this warm-up was to determine whether the effects of irradiation that were seen after room-temperature annealing could be observed over the entire temperature range. A decrease in the damping was observed, which ranged from about 15% at 4.2 K to about 48% at room temperature. The observed peak was decreased about 32% in height and shifted down in temperature to 70 K.

*This source later decayed to become the 10-Ci source.

Using the results from this warm-up as a new set of starting values, the sample was again irradiated with the 20-Ci source near liquid helium temperature, this time for about 21 hr. Because of difficulties in transferring liquid helium, the temperature rose to 20 K for about 4 min during this period and momentarily rose to 36 K. When the temperature was lowered again, however, no changes were observed in damping or frequency arising from this problem. The source was raised from the sample, and another monitored warm-up to room temperature was performed. This experiment was conducted to see if a larger irradiation dose and better temperature control during warm-up would reveal temperature regions where changes in dislocation pinning occur. The results showed an increase in frequency of about 0.06% between 65 K and 90 K when this run was compared to the previous warm-up, which appeared to be significant in comparison to the scatter in the data. There was no significant change in the damping over the temperature range during the time of the warm-up. After annealing was done at room temperature for 3 days, however, the damping had decreased to 3.2×10^{-4}.

In order to estimate the damping due to the sample mounting, the sample was held at 540°C for 5 hr in the presence of 200 kPa of oxygen. This procedure resulted in a decrease of the room temperature damping to 1.5×10^{-5}. Annealing at 725°C overnight raised the damping back to only 6×10^{-5}. Since this was too low for quantitative experiments, the sample was unmounted and plastically deformed in axial compression about 0.25%. After the remounting and annealing, the damping was about 3×10^{-4}. An irradiation with the 96-Ci source for 9 hr at 100°C showed little damping change. Sample No. SC9t was therefore unmounted and set aside.

A third single crystal, No. SC10t, was mounted and annealed several times for periods of one hour each time in high vacuum, at a temperature of 600°C. It was found that the room-temperature damping was relatively constant with successive anneals after the first anneal.

The next experiments were long irradiations designed to observe the time scale of parameter changes due to the irradiation-produced defects. In these experiments, changes in damping appeared to saturate while the frequency continued to increase, even at rather long times. For example, in a 35°C irradiation with the 96-Ci source, the damping was essentially constant after 120 hr while the frequency was still increasing after 600 hr. In a 75°C run with the same source, the damping had essentially stopped changing in less than 10 hr while the frequency was still increasing at 550 hr.

In the course of repeated annealing of this and the earlier samples, the internal friction was usually monitored during warm-up until the temperature reached about 315°C, when the electrode was raised to prevent roughening of its polished surface due to condensation of silver. When an annealed sample was warmed from room temperature, the internal friction was observed to

rise abruptly as the warm-up was begun to an apparent maximum at about 50°C. It then decreased at a more-or-less constant rate until about 300°C, when it reached a minimum. Above 300°C, it increased until measurements were ceased at about 375°C. The height of the initial damping rise appeared to be greater when the heating rate was increased. During cooling from an anneal that took place at a much slower rate, the damping did not retrace this path, but rather decreased to a broad minimum at about 190°C and then rose monotonically as the temperature decreased to room temperature, arriving finally at about the same value as was observed before the warm-up. The cooling curve appeared to match with the data obtained from 4.2 K to room temperature in a more satisfactory manner than the warm-up curves did, since the slopes were of opposite sign.

In addition to this, it was observed that, when a source was inserted, the damping underwent a prompt increase. These observations led to a series of experiments designed to investigate the effects of sintering at the mounting. The mounting pins were first electroplated with a thin layer of silver. After mounting, the sample was annealed at 600°C several times to sinter it to the pins. (The sintering was confirmed later upon unmounting, when it was found that the pins were firmly attached to the sample.) The 96-Ci source was inserted with the sample heated to 30°C. In a time of about 1/2 hr, the frequency was observed to drop by 60 Hz, and the damping rose by 60% on the same time scale. Then both parameters reversed themselves and changed at a much slower rate in the opposite directions. These prompt changes were greater than had been observed earlier with bare stainless steel pins.

Following this, the sample was unmounted and new pins were electroplated with a layer of cobalt and coated with colloidal graphite. Since neither cobalt nor carbon are soluble in silver, it is expected that sintering would not occur and the sample would be able to slide more freely on the pins. After being remounted, the sample was annealed several times at 500°C for 1 hr. The room-temperature damping was stable after the first anneal. In addition, the damping rose only slightly when the succeeding warm-ups were begun, and reached a minimum at about 250°C rather than at 300°C as observed previously. After the sample was annealed, the 96-Ci source again was inserted. The observed frequency change was now 21 Hz, and the damping increased only 4%. When the 10-Ci source was used, the prompt frequency decrease was 2.7 Hz, and the prompt damping rise again was about 4%. With the 1-Ci source there was no measurable change in frequency, but the prompt damping change was still about 4%. Modification of the electronic system to permit a lower strain amplitude reduced the prompt damping change to less than 2% at 36°C. Insertion and removal of the dummy source did not result in a change in damping.

The next survey experiment consisted of an observation of the depinning process. The purpose was to find out at what temperature it was necessary to anneal to remove the effects of irradiation. Before this time, we had chosen

somewhat arbitrarily 600℃; but, now that it was desired to avoid sintering, the lowest satisfactory annealing temperature was sought. The sample was irradiated at 35℃ with the 10-Ci source for 355 hr, which lowered the decrement from 1.7×10^{-3} to 1.7×10^{-4} and raised the resonant frequency from 26,610 Hz to 26,854 Hz. The source was removed, and an isochronal anneal was performed. In each cycle of this anneal the specimen chamber was heated to a new temperature, held there for 2-1/2 hr, and cooled back to 35℃, where it was left overnight. The new temperature was 20 K higher each time; and the parameters were measured both at 35℃ and at the annealing temperature, as a function of time. Figure 6 shows the frequency and decrement measured at 35℃ plotted against the preceding annealing temperature. Two values are shown for most temperatures; one was observed as soon as the sample cooled to 35℃ (after the thermal lag), and the other was observed after the sample had remained there overnight. It can be seen that annealing began at about 120℃, was half completed at about 220℃, and was essentially finished at about 360℃, if account is taken only of the data observed immediately after cooling. However, it can also be seen that, from 220℃ to at least 340℃, considerable retrenchment in the measured values occurred at 35℃. (An immediate value was not recorded at 360℃.) After annealing at 500℃ and cooling over the weekend, the room-temperature value of the damping was within 2.4%, and the frequency within 2 Hz, of the preirradiation values. In addition to the 35℃ data shown, the measurements at the annealing temperatures also revealed a trend. At temperatures up to 220℃, the damping and frequency exhibited apparent pinning while held at the annealing temperature. At higher

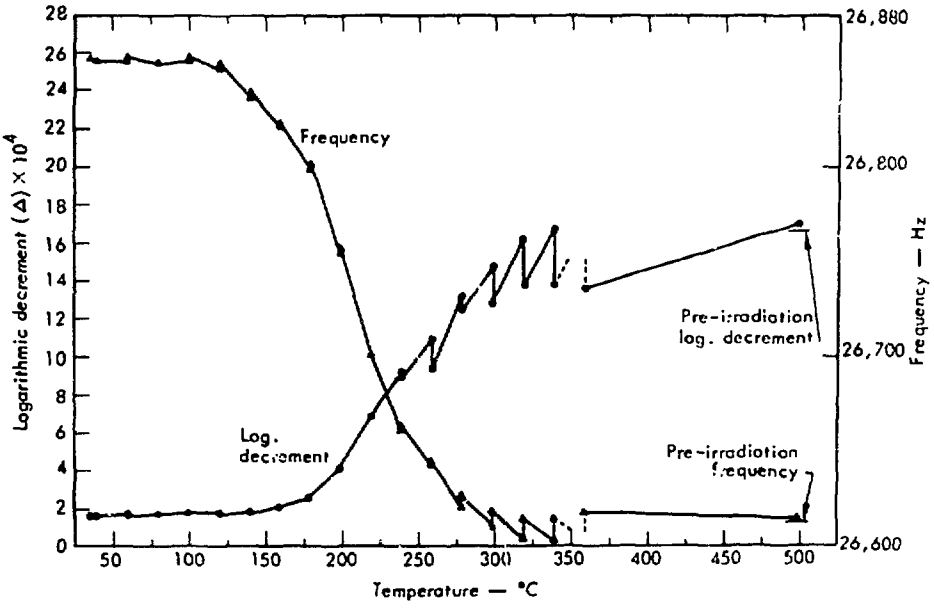

Fig. 6. Depinning data.

temperatures, both parameters showed evidence of depinning at the annealing temperature.

B. DISCUSSION

The survey experiments provide useful information about apparatus operation, sample annealing, preirradiation values of the frequency and decrement, temperatures at which pinning occurs, temperature range over which the effects of pinning can be observed, approximate rates of pinning for different temperatures and sources, and behavior of frequency and decrement at long times.

With regard to the apparatus, the experiments show that the use of a hollow single-crystal sample with a cylindrical irradiation geometry is feasible and makes it possible to observe changes in internal friction and modulus in a reasonable time with a rather small source. They also show that gamma heating is not observed if the source size is about 1 Ci, but it becomes significant if this is increased by an order of magnitude. However, with the larger sources the temperature change due to heating can be calculated from the observed frequency change.

The oxygen-saturation experiment shows that the damping due to the mounting could not be greater than 1.5×10^{-5}. Of course, it may be considerably less than this value. Since the final damping values after irradiations were always about an order of magnitude larger than this, the damping due to the mounting is not expected to interfere with the pinning experiments. It is also clear that the oxygen is able to remove sources of internal friction that are not removed by gamma irradiation.

The experiments with different coatings on the mounting pins indicate that free sliding of the pins in the mounting holes is necessary if the sample is to remain undisturbed when a source is inserted or the temperature is changed. It is probable that differential thermal expansion between the sample and sample holder gives rise to such motion. If the pins are sintered to the sample, the resulting stresses unpin some dislocations or generate new ones near the mounting holes, causing an increase in the decrement. Since this would occur when a source was inserted, it might be inferred that the irradiation-produced defects initially caused the damping to rise. However, these experiments show that, in the present case, at least most of the damping rise that was observed in the initial experiments was an artifact due to the mounting and could be eliminated. We suspect that the small remaining increase is also due to this effect or to the change in strain amplitude that occurs when a source is inserted, because of its effect on the capacitance. A particularly telling point is that the prompt damping change occurs in a time that is comparable to that required to reach temperature equilibrium and less than that

which is characteristic of the later decreases observed. The question of damping increase at the beginning of irradiation is important because it bears on the model proposed by Simpson and Sosin,[114] which attributes such an increase to the process of defect dragging by dislocations. In the present work we are convinced that the small observed increases are instrumental and not physical in origin.

The source-sample alignment problems led to the use of a concentric tube to prevent the source from touching the sample. This tube also serves to reduce the capacitance change that occurs when the source is inserted.

The results of repeated anneals after mounting sample No. SC4a show that about six anneals were necessary to obtain a relatively constant room-temperature damping value. This could also have been due to sintering at the mount. It might be expected that, after repeated warming and cooling, the volume of the crystal near the mounting pins would reach a more-or-less stable dislocation configuration so that the damping would no longer change.

The broad peak in the preirradiation decrement, when plotted as a function of temperature, can be identified as the Bordoni peak. First observed by Bordoni,[115] it has been studied extensively, and several theories have been advanced to explain it.[116] The peak temperature observed in the present work (81 K) agrees fairly well with that found by Bordoni et al.[117] at comparable frequencies (75.8 K at 18.58 kHz and 81.0 K at 50.55 kHz) in silver, and the curve shape is also similar. Perhaps the most surprising aspect of the peak observed in this work is that it appears in an annealed crystal. Since fully-annealed crystals do not exhibit a Bordoni peak,[116] its presence here indicates that there were still some internal strains present, although the large peak width corresponds to a small amount of cold work. Since these observations were performed before the mounting pins were coated to eliminate sintering, it is possible that differential thermal expansion caused some deformation near the pins on cooling from 600°C. Apparently this effect was not significant on cooling below room temperature, since the peak was reproducible after recooling to 4.2 K from room temperature. The decrease in peak height as a result of gamma-irradiation at low temperature and annealing at room temperature is consistent with the work of Routbort and Sack[118] with aluminum. Such a decrease has also been observed following neutron irradiation of copper[119,120] and silver.[121] Niblett and Wilkes[119] observed a decrease of the peak temperature after neutron irradiation of copper by about 4 K, as compared to the 11 K lowering observed in this work.

The frequency of the annealed sample decreases with rising temperature in the manner predicted by the temperature variation of the elastic modulus. The frequency variation in the vicinity of the peak was not examined in detail.

An important question in point defect theory asks at what temperature long range migration of a defect first occurs. Since dislocation pinning during

a warm-up after irradiation requires the long range motion of defects, internal friction and modulus measurements are able to aid in finding the answer. In the present work the source strength and irradiation time used were able to give only an indication, but it appears that the modulus changed a significant amount between 65 K and 90 K. Although these temperatures are somewhat above the range where Stage I is normally observed, it must be pointed out that this work involved a steady warm-up rather than the usual isochronal anneals, and the defect concentration was considerably lower than in resistivity experiments. Therefore, it appears that long-range migration of a defect was observed in Stage I. The damping change that should have accompanied the frequency change was probably below the precision of measurement. Stage I dislocation pinning in silver after low-temperature electron bombardment has been reported by Keefer and Robinson.[122] These workers also reported three continuous stages between 60 and 200 K, which they tentatively attributed to release of trapped Stage I interstitials. Additional evidence for long range migration at low temperatures in silver has been obtained in resistivity experiments. This work has been reviewed by Schilling et al.[68]

When the irradiated sample was allowed to anneal at room temperature, subsequent cooling demonstrated that the effects of pinning could be seen in decreased damping over the entire temperature range. Taken together, the survey experiments show that, while a small change occurs at low temperatures, a much larger pinning effect is observed in the region near room temperature and above. It was decided that quantitative experiments could best be done in the latter region with the apparatus and sources available. It was seen that changes there occurred in times long compared to the time required for temperature stabilization (about 1 hr), but still short enough to allow experiments of practicable duration.

The results of the long irradiations have important consequences. First, the inability to saturate the modulus change means that it is not possible to obtain a value for the modulus in the completely pinned state with the sources available. The quantitative interpretation of modulus changes requires a knowledge of this value and is therefore not possible in this work. Second, the apparent saturation of decrement changes at much shorter times in comparison indicates that the vibrating string model with a single dislocation type is not followed, since this model requires simultaneous changes in the two parameters. More will be said about this later.

The depinning experiments show that a temperature of 500°C for 2-1/2 hr is sufficient to remove the effects of irradiation. As a result of these observations, later sample annealing was done at 500°C for 1 hr at a time and proved to give reproducible room temperature decrement values. The depinning results will be discussed in more detail later, when a model is invoked to explain the isothermal irradiation results.

VII. Quantitative Experiments

A. EXPERIMENTAL PROCEDURE AND RESULTS

In view of the results of the survey experiments, it was decided that the most definitive work which could be done with the present apparatus would be a series of isothermal irradiations just above room temperature using the 1-Ci source.

The sample used for these experiments was No. SC 10t. Because the thermal history of a sample has been shown to be a significant factor in internal friction experiments, it will be reviewed in detail. After growing, single crystal No. SC 10 was pulled from the graphite rod at a temperature of about 750°C in high vacuum and then was furnace cooled. Sample No. SC 10t was spark-machined from the top section of the crystal and stored at room temperature in air for 41 mo. The ends of the crystal were spark-planed flat and parallel, and the crystal was given a light etch with 50% reagent grade nitric acid in deionized water to remove sharp edges and surface tarnish. Mounting holes were spark-machined into the sample, and it was cleaned with reagent grade acetone and mounted on silver-plated mounting pins to test the effects of sintering, as discussed in Part VI. During the course of experiments, the sample was annealed 16 times at a temperature of 600°C for 1 hr each time. The first five anneals were conducted in high vacuum and the rest with 100 kPa of purified helium, to promote temperature uniformity and reduce silver evaporation.

Following this, the sample was unmounted and the nonsintering mounting pins were installed, after which the sample was annealed eleven times at 500°C for 1 hr each time in 100 kPa of purified helium before the quantitative isothermal irradiations were begun. A similar 1-hr anneal was performed once after each irradiation. The cooling after anneals was always done at the rate of 135°C per hour down to a temperature of 32°C, where the heater was turned off and the furnace was allowed to cool at its own (slower) rate to room temperature.

Five isothermal irradiations then were performed in the following sequence: 34.8, 71.2, 44.0, 53.0, and 24.8°C. In each case, after cooling at least overnight from the anneal, the helium gas was pumped out to a pressure of about 67 Pa. Previously, it had been determined that the presence of helium at this pressure did not cause an observable damping increase. The damping was measured by resonance curve to ascertain whether it had returned to its unirradiated value. The temperature monitor was checked against the potentiometer and adjusted if necessary. The furnace was heated to the chosen temperature as measured by a copper/constantan thermocouple in the specimen chamber, while the sample was maintained in vibration. In the 34.8°C

experiment, the sample was held at temperature for 1 day before proceeding, because of noise in the electronic system, which was corrected. In the other runs no such difficulty arose, and it was possible to proceed immediately with transfer of the source.

Then the driving signal was turned off and the electrode was raised a small distance. The furnace was backfilled with 100 kPa of purified helium and the top was screwed off the electrode shaft. The 1-Ci ^{60}Co source was then moved from the storage area to the cryostat furnace and secured with its center 0.12 m above the center of the sample. The electrode cap on the source wand was tightened and the cryostat furnace was evacuated to about 0.7 mPa. Fresh purified helium was then admitted to a pressure of 67 Pa. The electrode was lowered and the vibration drive signal was applied. The damping and frequency were monitored until the frequency became constant with time, indicating that the sample temperature had stabilized. This occurred about 1 hr after the specimen chamber had reached temperature.

An initial resonance curve then was made, and damping readings were taken with the decay gate for cross-calibration. The electrode was raised slightly, and the source was lowered by hand into the sample. In the 71.2°C experiment, insertion of the source caused a prompt damping increase of about 10%. For reasons to be discussed, this increase was judged to be instrumental in origin. Because of its large magnitude it was decided to terminate this run before complete pinning occurred, but to use it as a test of whether depinning would occur at long times. Accordingly, the source was raised 0.12 m after an irradiation of 21.35 hr and the sample vibration parameters were monitored for a total of 117 hr.

Because of the large damping increase observed in the 71.2°C run, it was decided to lower the source over a period of 5 min for the later runs in order to minimize the thermal shock. The temperatures of these runs were also lower. The beginning of these later irradiations was taken as the midtime of the lowering operation. The electrode then was lowered and the vibration drive was turned on. The drive voltage, frequency, and temperature were recorded continuously from this point on. After about 1 hr, the sample temperature again was stable, as indicated by a constant vibration frequency. At this point, a second resonance curve was made, and the decay readings were taken again. The isothermal irradiation was then allowed to proceed and resonance curves and decay readings were taken periodically to correct for changes in the gain of the control loop. The irradiation was continued until no further change in damping was observed over a 1-day period. In the 24.6°C and 34.8°C runs, the 1-Ci source was replaced by the 100-Ci source in an attempt to saturate the pinning. The large source was left in for 162 and 142 hr, respectively, when the damping was no longer observed to

change over a 1-day period. The small source was reintroduced to duplicate the measurement conditions during the experiments and was left in until the damping no longer changed over a 1-day period.

The results of the isothermal irradiations are shown in Figs. 6 through 16. The data are given in detail in Tables 1 through 5. The frequency data were taken from the strip chart and corrected for changes in calibration and control loop tracking error by comparison with the resonance curves taken periodically throughout the runs. The damping data were likewise corrected

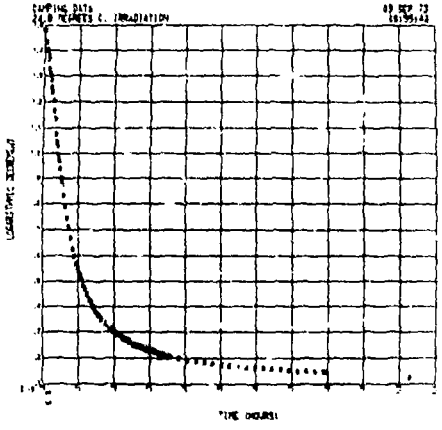

Fig. 7. Damping data for irradiation at 24.8°C.

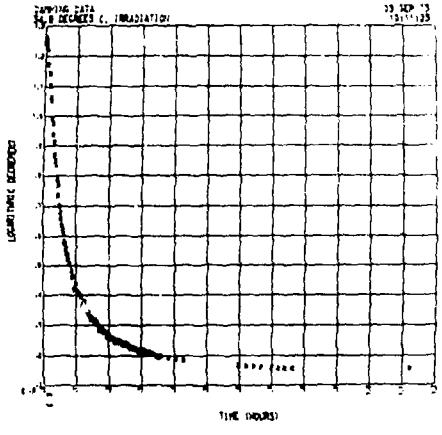

Fig. 8. Damping data for irradiation at 34.8°C.

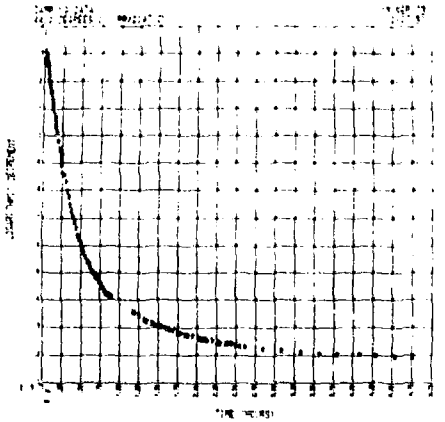

Fig. 9. Damping data for irradiation at 44.0°C.

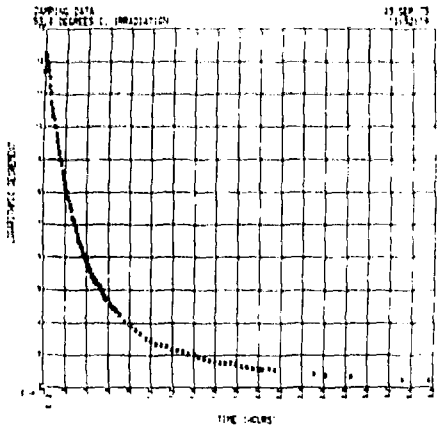

Fig. 10. Damping data for irradiation at 53.0°C.

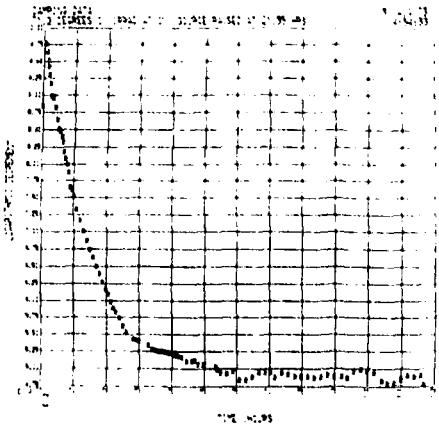

Fig. 11. Damping data for irradiation at 71.2°C (source raised at 21.35 hr).

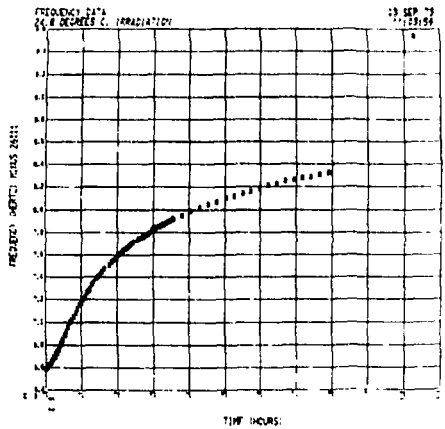

Fig. 12. Frequency data for irradiation at 24.8°C.

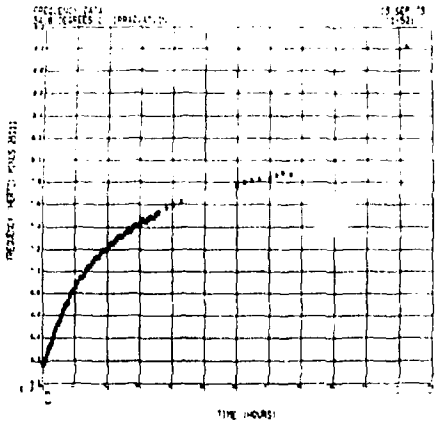

Fig. 13. Frequency data for irradiation at 34.8°C.

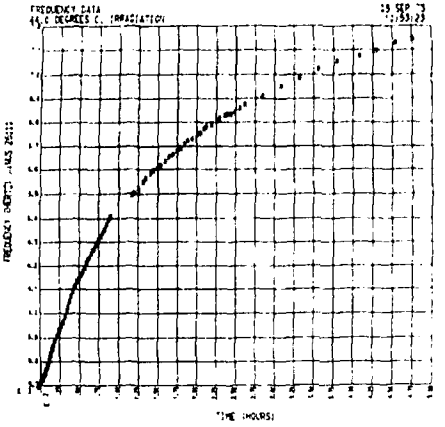

Fig. 14. Frequency data for irradiation at 44.0°C.

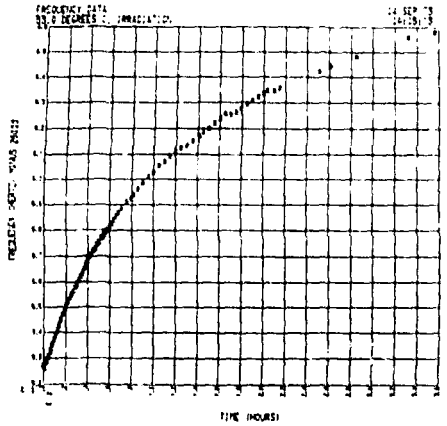

Fig. 15. Frequency data for irradiation at 53.0°C.

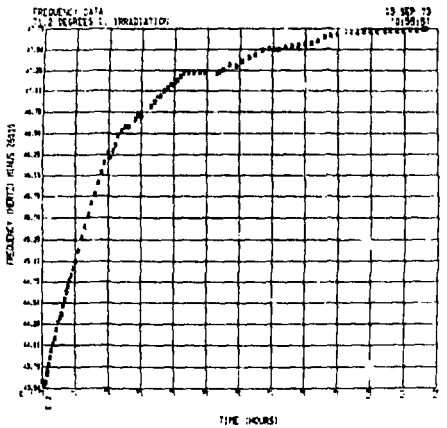

Fig. 16. Frequency data for irradiation at 71.2°C (source raised at 21.35 hr).

Table 1. Experimental data from 24.8℃ irradiation.

	Time (hr)	Log Decr	Freq (Hz) (grams 26,000)		Time (hr)	Log Decr	Freq. (Hz) (grams 26,000)
1	.0E+00	1.480E-03	6.577E+02	51	2.100E+02	2.450E-04	7.688E+02
2	5.000E+00	1.480E-03	6.585E+02	52	2.146E+02	3.620E-04	7.624E+02
3	7.500E+00	1.430E-03	6.602E+02	53	2.200E+02	2.800E-04	7.631E+02
4	1.000E+01	1.400E-03	6.610E+02	54	2.262E+02	2.720E-04	7.648E+02
5	1.250E+01	1.380E-03	6.618E+02	55	2.300E+02	2.670E-04	7.662E+02
6	1.500E+01	1.360E-03	6.628E+02	56	2.350E+02	2.650E-04	7.678E+02
7	1.750E+01	1.320E-03	6.644E+02	57	2.400E+02	2.630E-04	7.691E+02
8	2.000E+01	1.300E-03	6.659E+02	58	2.450E+02	2.580E-04	7.708E+02
9	2.257E+01	1.280E-03	6.676E+02	59	2.550E+02	2.460E-04	7.724E+02
10	2.500E+01	1.250E-03	6.684E+02	60	2.618E+02	2.450E-04	7.739E+02
11	2.750E+01	1.230E-03	6.696E+02	61	2.650E+02	2.400E-04	7.743E+02
12	3.100E+01	1.200E-03	6.711E+02	62	2.700E+02	2.480E-04	7.746E+02
13	3.227E+01	1.160E-03	6.721E+02	63	2.747E+02	2.360E-04	7.757E+02
14	3.500E+01	1.130E-03	6.738E+02	64	2.800E+02	2.350E-04	7.771E+02
15	3.750E+01	1.070E-03	6.752E+02	65	2.859E+02	2.310E-04	7.782E+02
16	4.000E+01	1.040E-03	6.774E+02	66	2.900E+02	2.320E-04	7.765E+02
17	4.250E+01	1.020E-03	6.794E+02	67	2.950E+02	2.260E-04	7.800E+02
18	4.500E+01	9.900E-04	6.812E+02	68	3.000E+02	2.240E-04	7.814E+02
19	4.700E+01	9.660E-04	6.829E+02	69	3.050E+02	2.230E-04	7.822E+02
20	5.000E+01	9.340E-04	6.843E+02	70	3.100E+02	2.210E-04	7.834E+02
21	5.500E+01	8.960E-04	6.875E+02	71	3.150E+02	2.220E-04	7.836E+02
22	5.700E+01	8.750E-04	6.888E+02	72	3.200E+02	2.180E-04	7.843E+02
23	6.000E+01	8.280E-04	6.914E+02	73	3.250E+02	2.130E-04	7.854E+02
24	6.500E+01	7.950E-04	6.954E+02	74	3.300E+02	2.120E-04	7.858E+02
25	7.005E+01	7.410E-04	6.994E+02	75	3.341E+02	2.110E-04	7.864E+02
26	7.400E+01	7.070E-04	7.011E+02	76	3.400E+02	2.080E-04	7.879E+02
27	8.000E+01	6.640E-04	7.035E+02	77	3.450E+02	2.040E-04	7.888E+02
28	8.600E+01	6.240E-04	7.073E+02	78	3.500E+02	2.020E-04	7.897E+02
29	9.000E+01	5.940E-04	7.109E+02	79	3.550E+02	2.020E-04	7.909E+02
30	9.572E+01	5.640E-04	7.144E+02	80	3.578E+02	2.020E-04	7.909E+02
31	1.000E+02	5.400E-04	7.162E+02	81	3.816E+02	1.940E-04	7.942E+02
32	1.050E+02	5.220E-04	7.187E+02	82	4.053E+02	1.880E-04	7.978E+02
33	1.100E+02	5.030E-04	7.216E+02	83	4.297E+02	1.830E-04	8.014E+02
34	1.150E+02	4.780E-04	7.238E+02	84	4.541E+02	1.790E-04	8.040E+02
35	1.200E+02	4.620E-04	7.260E+02	85	4.777E+02	1.750E-04	8.059E+02
36	1.250E+02	4.420E-04	7.284E+02	86	5.040E+02	1.680E-04	8.090E+02
37	1.305E+02	4.230E-04	7.318E+02	87	5.258E+02	1.660E-04	8.111E+02
38	1.350E+02	4.150E-04	7.341E+02	88	5.497E+02	1.640E-04	8.130E+02
39	1.418E+02	3.960E-04	7.373E+02	89	5.729E+02	1.600E-04	8.149E+02
40	1.450E+02	3.880E-04	7.385E+02	90	5.978E+02	1.570E-04	8.178E+02
41	1.500E+02	3.740E-04	7.401E+02	91	6.215E+02	1.550E-04	8.204E+02
42	1.560E+02	3.630E-04	7.424E+02	92	6.459E+02	1.530E-04	8.220E+02
43	1.600E+02	3.590E-04	7.443E+02	93	6.700E+02	1.500E-04	8.245E+02
44	1.659E+02	3.440E-04	7.465E+02	94	6.937E+02	1.490E-04	8.251E+02
45	1.787E+02	3.280E-04	7.498E+02	95	7.175E+02	1.450E-04	8.268E+02
46	1.850E+02	3.160E-04	7.522E+02	96	7.412E+02	1.460E-04	8.275E+02
47	1.898E+02	3.100E-04	7.540E+02	97	7.657E+02	1.420E-04	8.300E+02
48	1.950E+02	3.080E-04	7.551E+02	98	7.900E+02	1.400E-04	8.314E+02
49	2.000E+02	2.990E-04	7.565E+02	99	7.955E+02	1.410E-04	8.312E+02
50	2.050E+02	2.900E-04	7.589E+02	100	1.030E+03	1.200E-04	9.531E+02

Table 2. Experimental data from 34.0℃ irradiation.

	Time (hr)	Log Decr.	Freq. (Hz) (minus 26,000)		Time (hr)	Log Decr.	Freq. (Hz) (minus 26,000)
1	.0E+00	1.240E-03	6.160E+02	51	1.700E+02	2.780E-04	7.115E+02
2	1.650E+00	1.260E-03	6.155E+02	52	1.750E+02	2.790E-04	7.119E+02
3	2.500E+00	1.250E-03	6.159E+02	53	1.800E+02	2.830E-04	7.150E+02
4	5.900E+00	1.240E-03	6.163E+02	54	1.850E+02	2.740E-04	7.172E+02
5	7.500E+00	1.220E-03	6.179E+02	55	1.900E+02	2.750E-04	7.163E+02
6	1.000E+01	1.170E-03	6.196E+02	56	1.950E+02	2.600E-04	7.183E+02
7	1.500E+01	1.140E-03	6.239E+02	57	2.000E+02	2.570E-04	7.190E+02
8	1.750E+01	1.100E-03	6.264E+02	58	2.050E+02	2.570E-04	7.219E+02
9	2.000E+01	1.060E-03	6.288E+02	59	2.100E+02	2.530E-04	7.236E+02
10	2.250E+01	1.050E-03	6.302E+02	60	2.150E+02	2.520E-04	7.248E+02
11	2.500E+01	9.560E-04	6.311E+02	61	2.200E+02	2.430E-04	7.245E+02
12	2.750E+01	9.710E-04	6.323E+02	62	2.261E+02	2.450E-04	7.264E+02
13	3.000E+01	9.350E-04	6.338E+02	63	2.300E+02	2.430E-04	7.281E+02
14	3.250E+01	9.090E-04	6.359E+02	64	2.350E+02	2.400E-04	7.300E+02
15	3.500E+01	8.650E-04	6.384E+02	65	2.400E+02	2.380E-04	7.307E+02
16	3.750E+01	8.430E-04	6.413E+02	66	2.450E+02	2.310E-04	7.309E+02
17	4.000E+01	8.230E-04	6.439E+02	67	2.499E+02	2.320E-04	7.312E+02
18	4.262E+01	7.830E-04	6.464E+02	68	2.550E+02	2.330E-04	7.334E+02
19	4.500E+01	7.640E-04	6.484E+02	69	2.604E+02	2.260E-04	7.352E+02
20	4.700E+01	7.320E-04	6.502E+02	70	2.650E+02	2.200E-04	7.351E+02
21	5.035E+01	6.960E-04	6.516E+02	71	2.700E+02	2.230E-04	7.341E+02
22	5.300E+01	6.750E-04	6.530E+02	72	2.750E+02	2.210E-04	7.361E+02
23	5.500E+01	6.550E-04	6.543E+02	73	2.800E+02	2.210E-04	7.386E+02
24	5.700E+01	6.330E-04	6.567E+02	74	2.846E+02	2.180E-04	7.400E+02
25	6.000E+01	6.190E-04	6.592E+02	75	2.900E+02	2.080E-04	7.395E+02
26	6.300E+01	6.020E-04	6.621E+02	76	2.950E+02	2.130E-04	7.393E+02
27	6.500E+01	5.770E-04	6.636E+02	77	3.000E+02	2.130E-04	7.415E+02
28	6.700E+01	5.710E-04	6.653E+02	78	3.050E+02	2.110E-04	7.433E+02
29	7.000E+01	5.540E-04	6.672E+02	79	3.100E+02	2.130E-04	7.447E+02
30	7.200E+01	5.380E-04	6.680E+02	80	3.150E+02	2.060E-04	7.433E+02
31	7.600E+01	5.320E-04	6.693E+02	81	3.200E+02	2.030E-04	7.435E+02
32	7.750E+01	5.180E-04	6.700E+02	82	3.250E+02	2.060E-04	7.458E+02
33	8.000E+01	5.050E-04	6.713E+02	83	3.300E+02	2.020E-04	7.471E+02
34	8.600E+01	4.790E-04	6.763E+02	84	3.350E+02	2.000E-04	7.473E+02
35	9.000E+01	4.570E-04	6.794E+02	85	3.450E+02	1.930E-04	7.471E+02
36	9.600E+01	4.130E-04	6.819E+02	86	3.500E+02	1.920E-04	7.497E+02
37	1.000E+02	4.330E-04	6.819E+02	87	3.550E+02	1.910E-04	7.509E+02
38	1.049E+02	4.090E-04	6.846E+02	88	3.586E+02	1.950E-04	7.517E+02
39	1.100E+02	3.980E-04	6.864E+02	89	3.812E+02	1.900E-04	7.556E+02
40	1.160E+02	3.900E-04	6.926E+02	90	4.045E+02	1.850E-04	7.583E+02
41	1.200E+02	3.630E-04	6.932E+02	91	4.286E+02	1.810E-04	7.613E+02
42	1.250E+02	3.700E-04	6.938E+02	92	5.972E+02	1.620E-04	7.760E+02
43	1.296E+02	3.490E-04	6.961E+02	93	6.211E+02	1.600E-04	7.788E+02
44	1.350E+02	3.410E-04	7.000E+02	94	6.450E+02	1.590E-04	7.804E+02
45	1.404E+02	3.340E-04	7.027E+02	95	6.682E+02	1.570E-04	7.811E+02
46	1.450E+02	3.140E-04	7.029E+02	96	7.019E+02	1.570E-04	7.823E+02
47	1.500E+02	3.260E-04	7.036E+02	97	7.219E+02	1.530E-04	7.851E+02
48	1.544E+02	3.110E-04	7.069E+02	98	7.410E+02	1.530E-04	7.876E+02
49	1.600E+02	3.110E-04	7.091E+02	99	7.654E+02	1.530E-04	7.860E+02
50	1.648E+02	3.000E-04	7.112E+02	100	1.125E+03	1.500E-04	9.018E+02

Table 3. Experimental data from 44.0℃ irradiation.

	Time (hr)	Log. Decr.	Freq. (Hz) (minus 26,000)		Time (hr)	Log. Decr.	Freq (Hz) (minus 26,000)
1	.0E+00	1.270E-03	5.700E+02	51	7.200E+01	4.730E-04	6.283E+02
2	9.800E-01	1.310E-03	5.704E+02	52	7.400E+01	4.650E-04	6.297E+02
3	2.000E+00	1.290E-03	5.711E+02	53	7.600E+01	4.570E-04	6.307E+02
4	3.000E+00	1.290E-03	5.717E+02	54	7.800E+01	4.430E-04	6.319E+02
5	3.500E+00	1.270E-03	5.720E+02	55	8.000E+01	4.330E-04	6.330E+02
6	4.000E+00	1.260E-03	5.724E+02	56	8.200E+01	4.210E-04	6.344E+02
7	5.000E+00	1.260E-03	5.733E+02	57	8.400E+01	4.160E-04	6.355E+02
8	5.500E+00	1.250E-03	5.737E+02	58	8.600E+01	4.140E-04	6.370E+02
9	6.000E+00	1.230E-03	5.740E+02	59	8.800E+01	4.110E-04	6.387E+02
10	7.000E+00	1.210E-03	5.750E+02	60	9.000E+01	4.070E-04	6.399E+02
11	8.000E+00	1.190E-03	5.761E+02	61	9.100E+01	4.040E-04	6.404E+02
12	9.000E+00	1.150E-03	5.771E+02	62	1.169E+02	3.490E-04	6.469E+02
13	1.000E+01	1.160E-03	5.781E+02	63	1.200E+02	3.480E-04	6.500E+02
14	1.100E+01	1.150E-03	5.787E+02	64	1.250E+02	3.390E-04	6.517E+02
15	1.200E+01	1.130E-03	5.799E+02	65	1.317E+02	3.240E-04	6.545E+02
16	1.300E+01	1.110E-03	5.809E+02	66	1.350E+02	3.170E-04	6.559E+02
17	1.400E+01	1.090E-03	5.819E+02	67	1.411E+02	3.090E-04	6.578E+02
18	1.500E+01	1.070E-03	5.829E+02	68	1.450E+02	3.040E-04	6.590E+02
19	1.600E+01	1.060E-03	5.841E+02	69	1.500E+02	3.000E-04	6.600E+02
20	1.650E+01	1.040E-03	5.845E+02	70	1.541E+02	2.950E-04	6.612E+02
21	1.700E+01	1.030E-03	5.853E+02	71	1.600E+02	2.900E-04	6.630E+02
22	1.800E+01	1.010E-03	5.863E+02	72	1.651E+02	2.840E-04	6.650E+02
23	2.000E+01	9.740E-04	5.883E+02	73	1.700E+02	2.850E-04	6.658E+02
24	2.200E+01	9.450E-04	5.899E+02	74	1.750E+02	2.750E-04	6.671E+02
25	2.400E+01	9.330E-04	5.915E+02	75	1.792E+02	2.730E-04	6.682E+02
26	2.500E+01	9.190E-04	5.923E+02	76	1.850E+02	2.660E-04	6.703E+02
27	2.550E+01	9.000E-04	5.924E+02	77	1.889E+02	2.650E-04	6.716E+02
28	2.600E+01	8.880E-04	5.929E+02	78	1.950E+02	2.640E-04	6.725E+02
29	2.800E+01	8.500E-04	5.945E+02	79	2.024E+02	2.560E-04	6.744E+02
30	3.005E+01	8.260E-04	5.959E+02	80	2.050E+02	2.520E-04	6.749E+02
31	3.200E+01	7.980E-04	5.979E+02	81	2.100E+02	2.520E-04	6.769E+02
32	3.413E+01	7.710E-04	6.000E+02	82	2.130E+02	2.490E-04	6.778E+02
33	3.600E+01	7.420E-04	6.020E+02	83	2.200E+02	2.470E-04	6.785E+02
34	3.800E+01	7.220E-04	6.043E+02	84	2.264E+02	2.420E-04	6.802E+02
35	4.000E+01	7.020E-04	6.064E+02	85	2.300E+02	2.390E-04	6.811E+02
36	4.200E+01	6.820E-04	6.083E+02	86	2.367E+02	2.370E-04	6.824E+02
37	4.400E+01	6.620E-04	6.102E+02	87	2.400E+02	2.380E-04	6.829E+02
38	4.600E+01	6.340E-04	6.113E+02	88	2.450E+02	2.380E-04	6.831E+02
39	4.800E+01	6.220E-04	6.127E+02	89	2.500E+02	2.310E-04	6.841E+02
40	5.000E+01	6.040E-04	6.138E+02	90	2.550E+02	2.270E-04	6.855E+02
41	5.200E+01	5.840E-04	6.149E+02	91	2.615E+02	2.270E-04	6.870E+02
42	5.400E+01	5.680E-04	6.160E+02	92	2.848E+02	2.200E-04	6.907E+02
43	5.600E+01	5.530E-04	6.173E+02	93	3.091E+02	2.130E-04	6.947E+02
44	5.800E+01	5.360E-04	6.185E+02	94	3.334E+02	2.080E-04	6.981E+02
45	6.000E+01	5.320E-04	6.203E+02	95	3.570E+02	2.020E-04	7.016E+02
46	6.200E+01	5.170E-04	6.219E+02	96	3.801E+02	1.990E-04	7.049E+02
47	6.400E+01	5.030E-04	6.230E+02	97	4.088E+02	1.980E-04	7.069E+02
48	6.600E+01	4.940E-04	6.249E+02	98	4.299E+02	1.930E-04	7.093E+02
49	6.800E+01	4.840E-04	6.260E+02	99	4.543E+02	1.900E-04	7.128E+02
50	7.000E+01	4.790E-04	6.271E+02	100	4.766E+02	1.870E-04	7.143E+02

Table 4. Experimental data from 53.0°C irradiation.

	Time (hr)	Log. Decr.	Freq. (Hz) (minus 26,000)		Time (hr)	Log. Decr.	Freq. (Hz) (minus 26,000)
1	.0E+00	1.170E-03	5.268E+02	51	4.900E+01	5.810E-04	5.741E+02
2	1.000E+00	1.220E-03	5.252E+02	52	5.000E+01	5.150E-04	5.748E+02
3	2.000E+00	1.210E-03	5.268E+02	53	5.238E+01	5.070E-04	5.742E+02
4	3.000E+00	1.190E-03	5.261E+02	54	5.300E+01	5.050E-04	5.763E+02
5	4.000E+00	1.170E-03	5.294E+02	55	5.400E+01	4.940E-04	5.769E+02
6	4.500E+00	1.150E-03	5.298E+02	56	5.500E+01	4.890E-04	5.777E+02
7	5.000E+00	1.150E-03	5.303E+02	57	5.600E+01	4.790E-04	5.783E+02
8	6.000E+00	1.100E-03	5.316E+02	58	5.700E+01	4.740E-04	5.790E+02
9	7.000E+00	1.070E-03	5.330E+02	59	5.800E+01	4.680E-04	5.798E+02
10	8.000E+00	1.050E-03	5.344E+02	60	6.000E+01	4.630E-04	5.813E+02
11	9.000E+00	1.030E-03	5.356E+02	61	6.200E+01	4.540E-04	5.822E+02
12	1.000E+01	1.020E-03	5.369E+02	62	6.400E+01	4.430E-04	5.837E+02
13	1.100E+01	9.960E-04	5.382E+02	63	6.600E+01	4.410E-04	5.851E+02
14	1.216E+01	9.730E-04	5.396E+02	64	6.800E+01	4.330E-04	5.862E+02
15	1.300E+01	9.530E-04	5.407E+02	65	7.078E+01	4.280E-04	5.880E+02
16	1.400E+01	9.340E-04	5.419E+02	66	7.600E+01	3.980E-04	5.907E+02
17	1.500E+01	9.160E-04	5.431E+02	67	8.000E+01	3.930E-04	5.922E+02
18	1.600E+01	8.960E-04	5.445E+02	68	8.200E+01	3.890E-04	5.935E+02
19	1.700E+01	8.830E-04	5.459E+02	69	8.600E+01	3.740E-04	5.955E+02
20	1.800E+01	8.590E-04	5.468E+02	70	9.000E+01	3.630E-04	5.980E+02
21	1.900E+01	8.480E-04	5.481E+02	71	9.600E+01	3.470E-04	6.006E+02
22	2.000E+01	8.260E-04	5.489E+02	72	1.000E+02	3.430E-04	6.025E+02
23	2.100E+01	8.170E-04	5.502E+02	73	1.050E+02	3.310E-04	6.049E+02
24	2.200E+01	8.030E-04	5.514E+02	74	1.100E+02	3.280E-04	6.065E+02
25	2.300E+01	7.820E-04	5.523E+02	75	1.150E+02	3.230E-04	6.088E+02
26	2.395E+01	7.700E-04	5.532E+02	76	1.200E+02	3.120E-04	6.109E+02
27	2.500E+01	7.550E-04	5.543E+02	77	1.250E+02	3.100E-04	6.120E+02
28	2.600E+01	7.420E-04	5.551E+02	78	1.300E+02	3.070E-04	6.130E+02
29	2.700E+01	7.170E-04	5.568E+02	79	1.350E+02	2.990E-04	6.148E+02
30	2.850E+01	7.090E-04	5.571E+02	80	1.412E+02	2.980E-04	6.166E+02
31	2.900E+01	7.030E-04	5.576E+02	81	1.450E+02	2.910E-04	6.182E+02
32	3.000E+01	6.910E-04	5.584E+02	82	1.500E+02	2.860E-04	6.196E+02
33	3.100E+01	6.790E-04	5.593E+02	83	1.550E+02	2.790E-04	6.217E+02
34	3.200E+01	6.620E-04	5.602E+02	84	1.600E+02	2.770E-04	6.232E+02
35	3.300E+01	6.480E-04	5.611E+02	85	1.653E+02	2.740E-04	6.252E+02
36	3.400E+01	6.380E-04	5.618E+02	86	1.700E+02	2.710E-04	6.251E+02
37	3.500E+01	6.300E-04	5.626E+02	87	1.750E+02	2.720E-04	6.259E+02
38	3.600E+01	6.200E-04	5.637E+02	88	1.796E+02	2.680E-04	6.272E+02
39	3.700E+01	6.040E-04	5.647E+02	89	1.850E+02	2.600E-04	6.290E+02
40	3.800E+01	5.960E-04	5.657E+02	90	1.895E+02	2.560E-04	6.305E+02
41	3.900E+01	5.890E-04	5.669E+02	91	1.950E+02	2.530E-04	6.321E+02
42	4.000E+01	5.850E-04	5.679E+02	92	2.000E+02	2.520E-04	6.331E+02
43	4.100E+01	5.750E-04	5.686E+02	93	2.034E+02	2.520E-04	6.342E+02
44	4.200E+01	5.670E-04	5.697E+02	94	2.100E+02	2.550E-04	6.342E+02
45	4.300E+01	5.580E-04	5.703E+02	95	2.151E+02	2.510E-04	6.354E+02
46	4.400E+01	5.530E-04	5.713E+02	96	2.515E+02	2.360E-04	6.419E+02
47	4.500E+01	5.400E-04	5.716E+02	97	2.625E+02	2.340E-04	6.439E+02
48	4.600E+01	5.360E-04	5.722E+02	98	2.857E+02	2.280E-04	6.479E+02
49	4.700E+01	5.290E-04	5.726E+02	99	3.330E+02	2.170E-04	6.556E+02
50	4.800E+01	5.220E-04	5.734E+02	100	3.569E+02	2.150E-04	6.579E+02

Table 5. Experimental data from 71.2℃ irradiation.

	Time (hr)	Log Decr	Freq. (Hz) (minus 26,000)		Time (hr)	Log Decr	Freq. (Hz) (minus 26,000)
1	.0E+00	8.640E-04	4.357E+02	46	3.600E+01	5.230E-04	4.694E+02
2	4.800E-01	9.760E-04	4.353E+02	47	3.700E+01	5.230E-04	4.700E+02
3	1.000E+00	9.640E-04	4.356E+02	48	3.800E+01	5.220E-04	4.703E+02
4	1.500E+00	9.500E-04	4.366E+02	49	3.900E+01	5.210E-04	4.707E+02
5	1.660E+00	9.410E-04	4.369E+02	50	4.000E+01	5.200E-04	4.707E+02
6	2.000E+00	9.290E-04	4.377E+02	51	4.100E+01	5.170E-04	4.712E+02
7	2.500E+00	9.180E-04	4.385E+02	52	4.200E+01	5.160E-04	4.716E+02
8	3.000E+00	8.970E-04	4.394E+02	53	4.320E+01	5.140E-04	4.720E+02
9	3.500E+00	8.940E-04	4.401E+02	54	4.453E+01	5.090E-04	4.721E+02
10	4.000E+00	8.810E-04	4.408E+02	55	4.600E+01	5.090E-04	4.721E+02
11	4.500E+00	8.630E-04	4.416E+02	56	4.800E+01	5.050E-04	4.721E+02
12	5.000E+00	8.560E-04	4.406E+02	57	4.952E+01	5.040E-04	4.721E+02
13	5.500E+00	8.470E-04	4.432E+02	58	5.338E+01	5.010E-04	4.720E+02
14	6.000E+00	8.390E-04	4.436E+02	59	5.400E+01	4.970E-04	4.721E+02
15	6.500E+00	8.310E-04	4.446E+02	60	5.500E+01	4.980E-04	4.724E+02
16	7.000E+00	8.160E-04	4.454E+02	61	5.700E+01	4.910E-04	4.730E+02
17	7.500E+00	8.060E-04	4.462E+02	62	5.900E+01	4.940E-04	4.729E+02
18	8.000E+00	7.980E-04	4.469E+02	63	6.100E+01	4.920E-04	4.734E+02
19	8.430E+00	7.860E-04	4.476E+02	64	6.300E+01	4.920E-04	4.739E+02
20	9.000E+00	7.640E-04	4.483E+02	65	6.500E+01	4.860E-04	4.743E+02
21	9.500E+00	7.600E-04	4.491E+02	66	6.700E+01	4.930E-04	4.747E+02
22	1.000E+01	7.510E-04	4.499E+02	67	6.900E+01	4.930E-04	4.750E+02
23	1.100E+01	7.310E-04	4.512E+02	68	7.055E+01	4.930E-04	4.749E+02
24	1.200E+01	7.150E-04	4.527E+02	69	7.200E+01	4.850E-04	4.749E+02
25	1.300E+01	6.990E-04	4.540E+02	70	7.400E+01	4.920E-04	4.751E+02
26	1.400E+01	6.850E-04	4.554E+02	71	7.600E+01	4.900E-04	4.753E+02
27	1.500E+01	6.720E-04	4.567E+02	72	7.800E+01	4.870E-04	4.754E+02
28	1.600E+01	6.610E-04	4.578E+02	73	8.000E+01	4.870E-04	4.755E+02
29	1.700E+01	6.480E-04	4.591E+02	74	8.200E+01	4.870E-04	4.756E+02
30	1.800E+01	6.370E-04	4.603E+02	75	8.400E+01	4.850E-04	4.759E+02
31	1.900E+01	6.250E-04	4.615E+02	76	8.600E+01	4.860E-04	4.763E+02
32	2.000E+01	6.150E-04	4.627E+02	77	8.800E+01	4.890E-04	4.765E+02
33	2.068E+01	6.080E-04	4.622E+02	78	9.000E+01	4.860E-04	4.767E+02
34	2.135E+01	5.960E-04	4.630E+02	79	9.230E+01	4.870E-04	4.769E+02
35	2.217E+01	5.870E-04	4.637E+02	80	9.400E+01	4.850E-04	4.769E+02
36	2.300E+01	5.810E-04	4.647E+02	81	9.600E+01	4.940E-04	4.769E+02
37	2.400E+01	5.720E-04	4.653E+02	82	9.800E+01	4.970E-04	4.770E+02
38	2.500E+01	5.600E-04	4.658E+02	83	1.000E+02	4.940E-04	4.770E+02
39	2.600E+01	5.520E-04	4.658E+02	84	1.020E+02	4.920E-04	4.770E+02
40	2.920E+01	5.420E-04	4.667E+02	85	1.045E+02	4.810E-04	4.770E+02
41	2.900E+01	5.400E-04	4.671E+02	86	1.060E+02	4.770E-04	4.771E+02
42	3.000E+01	5.380E-04	4.670E+02	87	1.080E+02	4.780E-04	4.771E+02
43	3.283E+01	5.320E-04	4.682E+02	88	1.100E+02	4.830E-04	4.771E+02
44	3.400E+01	5.260E-04	4.687E+02	89	1.120E+02	4.880E-04	4.772E+02
45	3.500E+01	5.250E-04	4.691E+02	90	1.140E+02	4.870E-04	4.772E+02
				91	1.160E+02	4.880E-04	4.773E+02
				92	1.170E+02	4.760E-04	4.773E+02

to the results from free decays, which were capable of higher precision in the damping measurement than were the resonance curves in this damping range. Consider first the damping data in the four long runs. The initial values of Δ ranged between 1.17×10^{-3} and 1.48×10^{-3} for the four experiments. Immediately after the source was inserted, a change in damping was observed, which ranged from a decrease of 0.7% in the 24.8°C run to an increase of 1.3% in the 53.0°C run. This change occurred in a time that was short compared to the time scale of later damping changes, but comparable to the time required for the sample to reach a new steady temperature, as determined by previous experiments. Since this change was also largest when the sample temperature was most different from that of the inserted source, it is believed to be due to the temperature change caused by source insertion and its interaction with the sample mounting as discussed earlier, and not due to the influence of radiation-produced defects. Hence, it will not be discussed further.

After a steady temperature was established, the damping monotonically decreased at an increasing rate, reached an inflection point, and then leveled out and appeared to asymptotically approach a final value. The rate of decrease of damping increased as the temperature was raised. The final value of Δ appeared to be a monotonically increasing function of temperature for the four runs. The total change in damping ranged from a factor of about 10 for the lowest temperature to a factor of about 5 for the highest temperature.

In the case of the frequency data for the four long runs, the initial values were inversely proportional to the temperature. There was a small change immediately after the source was inserted, presumably due to the temperature change. It was largest in the 53.0°C run, where it amounted to about +8 Hz, corresponding to a temperature decrease of about 1.8°C. After about 1/2 hr, the frequency leveled out, presumably because a new temperature was reached. At the three lowest temperatures, the frequency was then essentially unchanged from its value before source insertion. In the 53.0°C run it was lower by about 1.8 Hz. Since this would imply a temperature increase upon source insertion if it were attributed directly to a temperature change, and since gamma heating is not significant with this source strength as discussed earlier, the decrease in frequency must be explained by other changes in the sample or mounting. It seems probable that the thermal shock effect accounts for it, for the reasons discussed above, and therefore it is not attributed to the influence of radiation-produced defects.

The frequency then rose monotonically, with the lower-temperature runs appearing to exhibit an inflection point. The rate of change then decreased for the duration of the experiment but did not reach a constant final value within the time scale of the observations. The initial rate of change increased with temperature, but the total frequency change at 400 hr amounted to slightly more than 0.5% for all the runs.

As was mentioned above, in two of the runs the 1-Ci source was replaced by the 100-Ci source to attempt saturation of the pinning. The results were as follows: In the 24.6°C run, the decrement (measured under identical conditions) decreased from 1.41×10^{-4} to 1.20×10^{-4}, while the frequency increased an additional 0.45%. In the 34.8°C run, the decrement decreased from 1.53×10^{-4} to 1.50×10^{-4}, while the frequency increased 0.43%. In both cases the damping reached a constant value while the frequency continued to rise, albeit at an ever-decreasing rate. The frequency change never reached saturation in the time scale of the experiments. In the 71.2°C experiment, the damping decreased rapidly and the frequency correspondingly rose at a high rate. After 21 hr the source was raised, and, 40 hr later, the rates of change reached lower, more-or-less constant values, which persisted for the duration of the measurements. It should be noted that the sample continues to be irradiated when the source is in the raised position, but the flux is over two orders of magnitude less than when it is inserted. After these runs were completed, the variation in damping as a function of strain amplitude was measured at 53°C for both the irradiated and annealed states. The variation of damping with maximum strain amplitude for the annealed state is shown in Fig. 17. The range of strain amplitudes used in the isothermal irradiations is

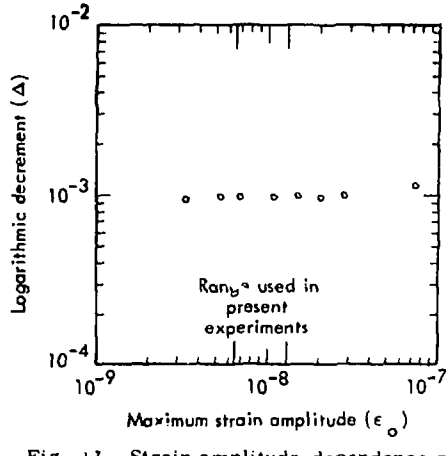

Fig. 17. Strain amplitude-dependence of damping.

indicated. In the pinned state the damping was constant within experimental uncertainty from a maximum strain amplitude of 4.5×10^{-9} to 7.5×10^{-8}.

To see if the frequency and decrement would change in the absence of irradiation, the sample was held at 34.8°C for 5.5 days in the annealed state. The results were as follows:

Time (days)	Frequency (Hz)	Δ (× 10^3)
0	26,613.6	1.61
0.5	26,617.9	1.49
1.5	26,619.7	1.47
2.5	26,621.4	1.41
3.5	26,621.9	1.38
5.5	26,623.4	1.39

As can be seen, the frequency continued to change after 5.5 days at an average rate of +1.8 Hz per day. The damping stopped changing within measurement uncertainty after 3.5 days, where its total decrease had amounted to about 14%. After these measurements, the sample was heated to 500°C overnight in the presence of 200 kPa of oxygen in order to pin the dislocations as completely as possible and to observe the remaining damping, as another check on the sample mounting. The room-temperature damping was reduced to 1.35×10^{-5} by this treatment.

Finally, the sample was unmounted and replaced by a dummy silver sample for the temperature calibration, as discussed in Section V.D. above. A section was cut out of the sample at a location midway between the center plane and one end. It was etched with 50% reagent grade nitric acid in deionized water, washed in reagent grade methyl alcohol, and submitted to the Analytical Chemistry Section of the Lawrence Livermore Laboratory for spectrochemical analysis. The results of this analysis are shown in Table 6.

Table 6. Spectrochemical analysis report for Plate No. 3099, Sample SS-0856, of silver sample No. SC10t3.

Values are approximate ppm by weight for the impurity elements listed.

Analysis ppm		Elements not detected
Si	30	< 150 As
Ca	8	< 40 Ba, Ge, Pb, Sb, W
Cu	8	< 15 B, Bi, Cd, In, Nb, Sn, V, Zn, Zr
Al	≲ 3	< 4 Cr, Mn, Ni, Sr
Mg	< 3	< 2 Be, Co, M , Ti
Fe	1	

B. ANALYSIS

A first step in analyzing data of this type is to normalize the changes in damping and modulus defect to the total changes over the course of the experiment. In doing this, one defines the parameters Y and Z:

$$Y = \frac{E(\infty) - E(t)}{E(\infty) - E(0)} \simeq \frac{f(\infty) - f(t)}{f(\infty) - f(0)} \qquad \text{(VII-B-1)}$$

$$Z = \frac{\Delta(t) - \Delta(\infty)}{\Delta(0) - \Delta(\infty)} \qquad \text{(VII-B-2)}$$

In these equations, Y and Z are the fractional amounts of the total modulus defect and damping change that are present at time t, E is Young's modulus, f is the frequency, and Δ is the logarithmic decrement. Y and Z are equal to 1 at the beginning of an experiment. If the KGL model holds, Y and Z should both monotonically decrease toward zero as the irradiation proceeds. If the SS model applies, it is possible for Z first to increase to a value greater than 1 and then to decrease toward zero, as discussed previously. If the KGL model with a single dislocation type applies, it should be found in addition that $Y^2 = Z$, since the modulus defect in this model is proportional to the square of the dislocation loop length, while the decrement is proportional to the fourth power. Such behavior was observed by Thompson and Holmes,[27] and Thompson *et al.*[32] in copper, and by Fornerod[123] in silver. In many other copper experiments, however, this behavior was not observed.[100,124-127] In the SSJ work, the relation between Y and Z was found to be simply $Y = Z$.

In the present work, Z can be evaluated from the irradiation data, since the decrement reached a constant value at long times. Y, on the other hand, cannot be evaluated in a straightforward manner, because the frequency continued to change throughout the irradiations. Nevertheless, the fact that the frequency underwent a large fraction of its total observed change while the damping was essentially constant within experimental error, as in the high dose rate part of the 34.8°C run, clearly demonstrates that neither $Y = Z$ nor $Y^2 = Z$ is satisfied by the present data. Without further analysis, therefore, it is possible to conclude that the present work cannot be explained either by the KGL model with a single dislocation type or by the SSJ approach. As noted above, it has not been unusual for this to occur in past experiments. In response to such a situation, Thompson and Paré[100] proposed the existence of two or more types of dislocations, of which some are pinned more rapidly than others. A similar approach was used by several other workers.[124,128-130] Some workers have suggested that the two types can be identified with edge and screw dislocations, respectively. Paré and Guberman[96] found that their results could be explained by the assumption of two dislocation components, one

of which is present in much smaller concentration than the other but has a much greater average loop length. However, they rejected this explanation on the grounds that the large difference between the average loop lengths of the two groups, which was necessary to explain the data, did not seem plausible and that the two-component model does not resolve the disagreement between the observed frequency dependence of the damping at low frequencies and that predicted by the KGL model.

It appears that there are two possibilities for obtaining a fit of the present data to theory by invoking more than one dislocation component: It might be possible to obtain a fit to either the SS or the KGL theory. We have chosen not to attempt a fit to the SS model for the following reasons:

1. In the present experiment, we do not believe that the damping ever exhibits an initial increase that is due to radiation-produced defects. Although such an increase is not required in the SS theory, it was the main reason for invoking this theory in the SSJ work.
2. The damping due to the dragging effect is proportional to ω^{-1}, while that due to rigid pinning is proportional to ω^{+1}. If a direct comparison can be made between the SSJ copper work and the present silver work, the relative importance of the rigid pinning compared to the dragging effect should be more than a factor of 2500 greater in the present work because ω is a factor of 50 greater. This assumes that the dislocation parameters in the two experiments are similar, which is not unreasonable, given the similarity of copper and silver. Support for this argument comes from the TBBH experiments conducted in copper at a frequency midway between the SSJ work and the present work. These experiments were explained very well with the rigid-pinning KGL model, indicating that rigid pinning is already dominant at 11 kHz in copper.

In view of these arguments, we chose to attempt to fit the data to the KGL model, using more than one dislocation component. In doing this we have assumed that there are two groups, that both groups may contribute to the modulus defect, and that only one group is responsible for the pinnable damping. The reason for using only two groups is that this is quite obviously the simplest case beyond a single group. In general, one might expect that both groups would contribute to both the modulus defect and damping. However, it is clear from the experiments using the large source at the end of the 24.8°C and 34.8°C runs that the modulus defect change nearly doubled itself with little or no concomitant change in the decrement. This suggests that the second dislocation group did not contribute significantly to the damping changes observed earlier in the experiments.

Using this approach, we calculated the number of pinning points as a function of time, using the equation

$$n_D = \frac{1}{\Delta} - 1, \qquad \text{(VII-B-3)}$$

in accordance with the KGL model. Δ was evaluated by using the observed values for $\Delta(0)$ and $\Delta(\infty)$. $\Delta(0)$ was taken as the maximum value measured. In the lowest-temperature run this was the value prior to source insertion, and in the others it was the value observed 1 hr after source insertion. The plots of n_D versus time obtained from this calculation displayed the following behavior: At ($t = 0$, $n_D = 0$) the curves had zero slope. As the time increased, the slope increased until an inflection point was reached, where the slope began decreasing. At longer times, the slope became approximately constant until the damping became so low that experimental uncertainty caused too much scatter in the data for the analysis to be significant. The slope of the straight-line portions of the curves increased as the temperature increased. The intercept of the straight line portions at $t = 0$ was always positive and decreased as the temperature increased.

When these observations were coupled with the results of the short 71.2°K irradiation, which indicate that the pinning points do not disappear at long times, at least not at a rate greater than 1% of the pinning rate, it became clear that this behavior is very similar to that found in copper by TBBH. In fact, as mentioned earlier, those authors showed that all the features of the TBHB model were required by these same observations. Accordingly, we decided to attempt to fit the present data to the TBHB model.

In analyzing the TBBH experiments, the authors found that an excellent fit could be obtained by using only one transient term from the TBHB theory, as described earlier. Once the linear part of n_D was subtracted off, it was possible to obtain a straight line on a semilogarithmic plot with the remainder, indicating a single transient whose relaxation time could be determined from the slope. In the present case, however, a straight line was not obtained, indicating that more than one transient was present. Accordingly, the $n = 1$ term in the sum shown by TBHB was retained, giving the following equation for n_D:

$$n_D = \left[\frac{8(\phi - A)\ell_o^2}{\pi^4 D}(1 - g_o) - (\phi - A)g_o\tau_{LE}\right] + [(\phi - A)g_o]t$$

$$+ \left[\frac{8(\phi - A)\ell_o^2}{\pi^4 D}(1 - g_o)\frac{\tau_1}{\tau_{LE} - \tau_1}\right]\exp(-t/\tau_1)$$

$$+ \left[(\phi - A)g_o\tau_{LE} - \frac{8(\phi - A)\ell_o^2}{\pi^4 D}(1 - g_o)\frac{\tau_{LE}}{\tau_{LE} - \tau_1}\right]\exp(-t/\tau_{LE}), \qquad \text{(VII-B-4)}$$

or, in a more convenient form,

$$n_D = I + St + \left[(I + S\tau_{LE}) \frac{\tau_1}{\tau_{LE} - \tau_1}\right] \exp(-t/\tau_1)$$

$$+ \left[S\tau_{LE} - (I + S\tau_{LE}) \frac{\tau_{LE}}{\tau_{LE} - \tau_1}\right] \exp(-t/\tau_{LE}), \qquad \text{(VII-B-5)}$$

where I is the intercept of the straight-line portion at $t = 0$, and S is the slope of the straight-line portion. As can be seen, this equation contains two transients in addition to the intercept and straight-line terms.

Because of the complexity of this equation, it was decided to make the fits with the help of a computer. This was accomplished on a Control Data Corporation 7600 computer, using a program called GAP (General Analysis and Plotting[131]) developed by David Y. F. Lai of the Lawrence Livermore Laboratory. This program in turn makes use of a program called MLR (Minimize Linear Residuals[132]) developed by R. E. von Holdt, also of LLL.

Rather than fit to the Δ data directly, it was decided to fit to log Δ, in order to give equal weight to all the data points, since the program minimizes the sum of the squares of the differences between the observed and calculated values. The fitting equation was then

$$\log \Delta = \log \left(\Delta(\infty) + [\Delta(0) - \Delta(\infty)] \left\{1 + I + St\right.\right.$$

$$+ \left[(I + S\tau_{LE}) \frac{\tau_1}{\tau_{LE} - \tau_1}\right] \exp(-t/\tau_1)$$

$$\left.\left. + \left[S\tau_{LE} - (I + S\tau_{LE}) \frac{\tau_{LE}}{\tau_{LE} - \tau_1}\right] \exp(-t/\tau_{LE})\right\}^{-4}\right). \qquad \text{(VII-B-6)}$$

In performing the four fits, $\Delta(\infty)$, I, S, τ_{LE}, and τ_1 were considered as variable parameters for each run, while the $\Delta(0)$ values were taken directly from the data, as described above.

This analysis resulted in much closer fits to the data. However, two problems appeared: First, it was now impossible to mathematically distinguish between τ_{LE} and τ_1, since interchanging them does not change the equation. Even though they arise from different physical processes (lattice diffusion and pipe diffusion, respectively), they were now algebraically identical. Second, it was not clear that the higher-order terms from the sum were insignificant, in view of the fact that the first term had made an important contribution. Accordingly, the magnitudes of the higher-order terms were examined,

and it was found that only the n = 3 term, in addition to the n = 1 term, was significant. Inclusion of the n = 3 term produced the following equation for n_D:

$$n_D = I + St + \left(S\tau_{LE} - \frac{81}{80}\tau_{LE}(I + S\tau_{LE}) \times \left\{\frac{1}{\tau_{LE} - \tau_1} - \frac{1}{81[\tau_{LE} - (\tau_1/q)]}\right\}\right)\exp(-t/\tau_{LE}) + \left[\frac{81}{80}(I + S\tau_{LE})\frac{\tau_1}{\tau_{LE} - \tau_1}\right]\exp(-t/\tau_1) - \left\{\frac{1}{80}(I + S\tau_{LE})\frac{\tau_1/q}{[\tau_{LE} - (\tau_1/q)]}\right\}\exp(-9t/\tau_1). \quad \text{(VII-B-7)}$$

As can be seen, there were now three transient terms in addition to the intercept and linear terms. τ_1 and τ_{LE} were now algebraically distinguishable. Another set of fits for the four runs was obtained, again fitting to log Δ, using the new expression for n_D in the fitting equation:

$$\log \Delta = \log\left\{\Delta(\infty) + [\Delta(0) - \Delta(\infty)](1 + n_D)\right]^{-4}\}. \quad \text{(VII-B-8)}$$

The same parameters were varied as before.

The result of this procedure was a set of values for $\Delta(\infty)$, I, S, τ_{LE}, and τ_1 for each of the four irradiations. The values for $\Delta(\infty)$ were not very different from those measured in the cases in which the large source was used to complete the pinning. The standard deviations for all four data sets were about 1%. When plotted on Arrhenius graphs, the values for S, τ_{LE}, and τ_1 exhibited approximate straight lines.

In view of this success, we decided to fit all four data sets to the TBHB model simultaneously, requiring exact Arrhenius behavior of S, τ_{LE}, and τ_1. An additional equation linking the parameters was obtained as follows: As shown above, the intercept is given by

$$I = \frac{8(\phi - A)\ell_o^2}{\pi^4 D}(1 - g_o) - (\phi - A)g_o\tau_{LE}, \quad \text{(VII-B-9)}$$

and the slope is given by

$$S = (\phi - A)g_o. \quad \text{(VII-B-10)}$$

From Eq. (IV-J-12),

$$\tau_1 = \frac{\ell_o^2}{\pi^2 D}. \tag{VII-B-11}$$

Because the slope in the TBHB work was temperature-dependent in the Arrhenius fashion, increasing as the temperature increased, the authors were able to make the assumptions $g_o << 1$ and $A << \phi$. Since this is also observed in the present work, these assumptions are adopted here as well.

Combining equations and using these assumptions, one finds that

$$I \cong \frac{8}{\pi^2} \phi \tau_1 - S\tau_{LE}. \tag{VII-B-12}$$

As noted above,

$$\phi = \frac{\ell_o}{\Lambda} N_A \Phi \sigma_D. \tag{IV-J-6}$$

Since ℓ_o and Φ are not the same for the four irradiations, the following parameters were used for normalization:

$$\Phi^* \equiv \frac{\Phi}{\Phi_{34.8}} \tag{VII-B-13}$$

and

$$\ell^* \equiv \frac{\ell_o}{\ell_{o_{24.8}}}, \tag{VII-B-14}$$

where $\Phi_{34.8}$ is the average gamma ray flux in the 34.8°C irradiation, and $\ell_{o_{24.8}}$ is the average dislocation loop length in the 24.8°C irradiation.

Inserting these equations into Eq. (VII-B-12), one obtains the final equation linking the parameters for each run:

$$I \cong K \ell^* \Phi^* \tau_1 - S\tau_{LE}, \tag{VII-B-15}$$

where

$$K = \frac{8}{\pi^2} \frac{\ell_{o_{24.8}}}{\Lambda} N_A \sigma_D \Phi_{34.8}. \tag{VII-B-16}$$

K was assumed constant for all the runs, since Λ should not change for a well-annealed crystal. The values of Φ^* were calculated by using the half-life of ^{60}Co, which is 5.263 yr.[110] The values of ℓ^* were obtained by the following method: The initial damping values for the four long runs were plotted as a

function of temperature. The values for the 24.8, 44.0, and 53.0°C runs formed a smooth curve sloping downward as temperature increased, as had been observed in previous warm-ups and cool-downs above room temperature. The 34.8°C value lay below this curve. We reasoned that the curve represented the normal high-temperature tail of the Bordoni peak in which damping should be proportional to the fourth power of the loop length. Since the 34.8°C run was the only one that had been held at temperature overnight prior to the beginning of the irradiation, we surmised that pinning must have occurred during this time, lowering the average loop length and damping from the smooth curve exhibited by the others. Indeed, the inferred decrease of 9.4% in the damping is about the same amount as observed in the self-pinning experiment described above. The value of ℓ^* required to place the damping values on the same smooth curve was then computed by assuming the fourth power loop-length dependence. The final values of Φ^* and ℓ^* for the four runs were thus calculated to be the following:

Temperature (°C)	Date of Midpoint	Φ^*	ℓ^*
24.8	Jan. 20, 1973	0.95694	1.0000
34.8	Sept. 10, 1972	1.00000	0.9729
44.0	Nov. 17, 1972	0.97568	1.0000
53.0	Dec. 9, 1972	0.96803	1.0000

It should be noted that TBBH chose to correct for variation in the initial average loop lengths of their runs by a different procedure. They assumed that the damping coefficient is proportional to temperature as predicted by Leibfried's theory,[133] and they adjusted the loop lengths to account for the observed deviations in predicted damping. We have assumed, on the other hand, that the damping coefficient varies with temperature in the manner predicted by the Seeger and Schiller theory[134] of the Bordoni peak in this range.

Because τ_1 and τ_{LE} are proportional to ℓ_o^2, the loop-length correction has also been applied to them. Since the slope is equal to Φg_o in this approximation, and since both Φ and g_o are proportional to ℓ_o in the same approximation, the loop-length correction has likewise been applied to S. Finally, the source decay factor Φ^* is also applied to S, since it is proportional to Φ.

The final equations for the simultaneous fit of the four sets of data were then Eq. (VII-B-8) and the following four equations:

$$\tau_1 = \ell^{*2}\, \tau_{1_o} \exp(-E_1/kT) \qquad \text{(VII-B-17)}$$

$$\tau_{LE} = \ell^{*2}\, \tau_{LE_o} \exp(-E_{LE}/kT) \qquad \text{(VII-B-18)}$$

$$S = \ell^{*2}\, \Phi^*\, S_o \exp(-E_S/kT) \qquad \text{(VII-B-19)}$$

$$I = K \Phi^{*} L^{*} \tau_1 - S\tau_{LE}. \qquad \text{(VII-B-20)}$$

Because of the complexity of the equations, the fit was obtained using an n-dimensional least-squares fit routine developed by Richard N. Stuart[135] of Lawrence Livermore Laboratory on a CDC 7600 computer. The initial values for this fit were taken from the results of the individual fits described above. The following parameters were varied to obtain the minimum standard deviation: $\Delta(0)$, $\Delta(\infty)$, E_1, E_{LE}, E_S, τ_{1_0}, τ_{LE_0}, S_0, and K. The resulting fit was tested by interchanging the parameters for τ_1 and τ_{LE}, whereupon the computer changed them back in the course of refitting. This result indicated that they had been assigned correctly.

The fit was also tested by starting from different initial values, and the fitting procedure again reached the same values. The standard deviation for the best fit obtained was 1.2%, which is comparable to the uncertainty in the data. The final values for the varied parameters are shown in Table 7. The results of the fitting are shown in Figs. 18 through 22. Figures 18 through 21 show comparisons of the calculated to the measured logarithmic decrement values. Figure 22 shows comparisons of the average number of pinning points per dislocation loop, as calculated from the data by assuming a fourth power loop-length dependence and as predicted from the theory by using the fitted values for the parameters in Eq. (VII-B-7). As can be seen, the fits are very good, with the possible exception of small deviations at the beginning of the decrement curves. These result from the fact that $\Delta(0)$ was treated as a variable parameter rather than held fixed. This was done because of the known uncertainty introduced in $\Delta(0)$ by insertion of the source.

Table 7. Fitted values of parameters obtained when $\Delta(0)$ was allowed to vary.

Irradiation temperature (°C)	$\Delta(0)$	$\Delta(\infty)$
24.8	14.5	1.15
34.8	12.9	1.38
44.0	12.8	1.72
53.0	11.7	2.04

$E_{LE} = 0.51$ eV
$E_1 = 0.24$ eV
$E_S = 0.32$ eV
$\tau_{LE_0} = 8.58 \times 10^{-8}$ hr
$\tau_{1_0} = 9.29 \times 10^{-3}$ hr
$S_0 = 4.10 \times 10^{2}$ hr^{-1}
$K = 4.64 \times 10^{-3}$ hr^{-1}

Another fit was made under the same conditions as the first fit except that the $\Delta(0)$ values were held to within 1% of the values measured after source insertion. This was done to test whether the values of the parameters would be sensitive to the initial damping value. This second fit reached a standard deviation of 1.4%, slightly greater than the first fit, as expected. The values of the parameters are shown in Table 8. As can be seen, E_{LE} and K remained nearly the same, while the other parameters changed by varying

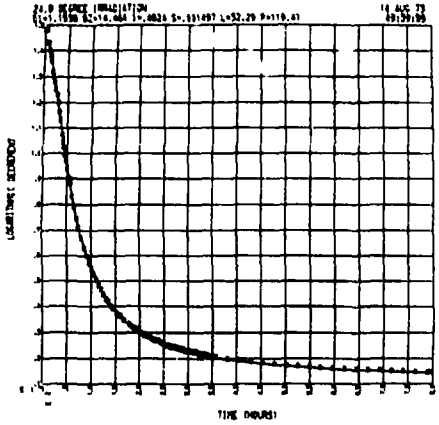

Fig. 18. Irradiation at 24.8°C; Δ(0) varied.

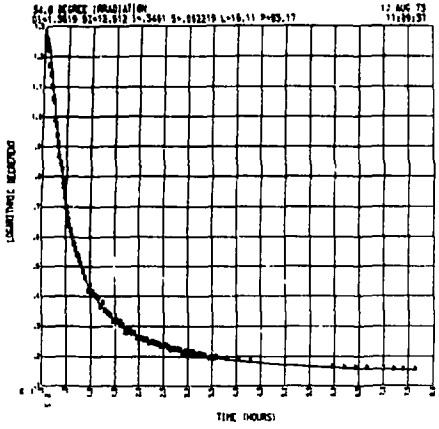

Fig. 19. Irradiation at 34.8°C; Δ(0) varied.

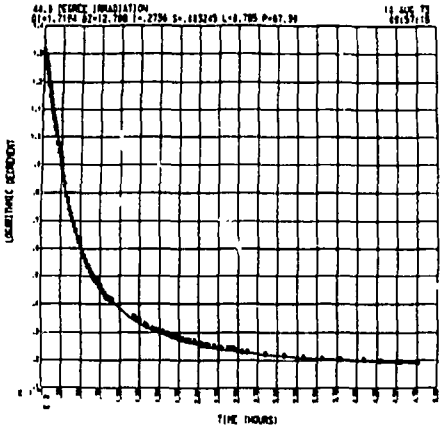

Fig. 20. Irradiation at 44.0°C; $\Delta(0)$ varied.

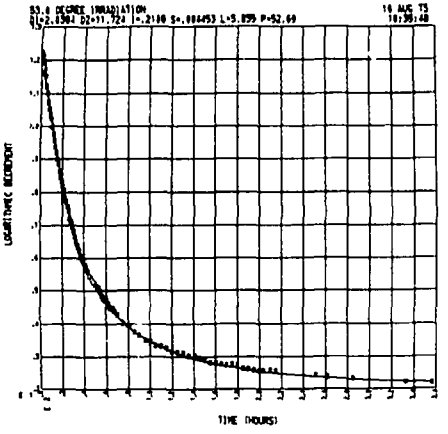

Fig. 21. Irradiation at 53.0°C; $\Delta(0)$ varied.

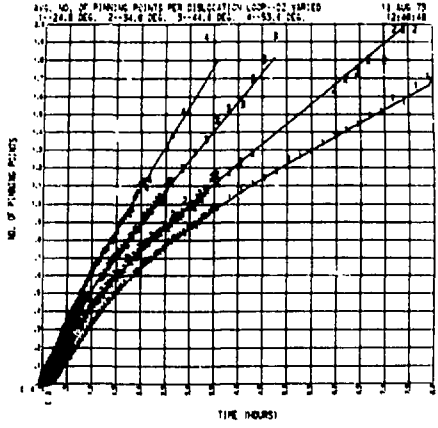

Fig. 22. Average number of pinning points per dislocation loop; $\Delta(0)$ varied.

Table 8. Fitted values of parameters obtained when $\Delta(0)$ was held fixed.

Irradiation temperature (°C)	$\Delta(0)$	$\Delta(\infty)$
24.8	14.6	1.08
34.8	12.7	1.33
44.0	12.8	1.71
53.0	12.1	2.09

E_{LE} = 0.48 eV
E_1 = 0.30 eV
E_s = 0.43 eV
τ_{LE_o} = 1.86×10^{-7} hr
τ_{1_o} = 1.45×10^{-3} hr
S_o = 2.22×10^{4} hr^{-1}
K = 4.49×10^{-3} hr^{-1}

degrees. The results of the second fit are plotted in Figs. 23 through 27. As can be seen, this fit also appears to be very satisfactory. It is difficult to choose between the two fits on the basis of their standard deviations, which are both comparable to the uncertainty in the data. Therefore, we will discuss the two fits together.

C. DISCUSSION

Before discussing the implications of these results, it is important to point out the sources of uncertainty in the data and the analysis and to examine whether the results are quantitatively reasonable. The chief source of uncertainty is the assumption that the entire decrease in the damping arises from pinning caused by radiation-produced defects, whereas, in fact, part of the decrease appears to be due to rearrangement of defects already present in the crystal. As was noted above, the spontaneous decrease in damping amounted to about 14% over the first 3.5 days at 34.8°C. However, since the crystal was held for about 1 day at this temperature prior to irradiation, the relevant change for the 34.8°C run is that occurring after the first day, which amounted to about 7%.

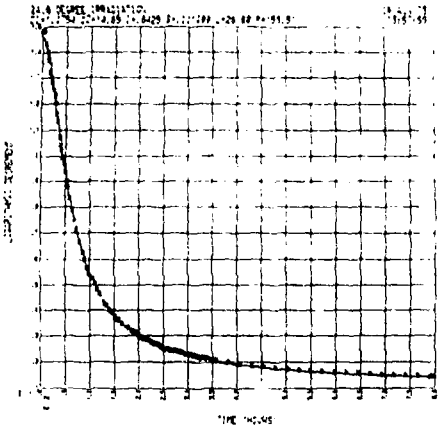

Fig. 23. Irradiation at 24.8°C; Δ(0) fixed.

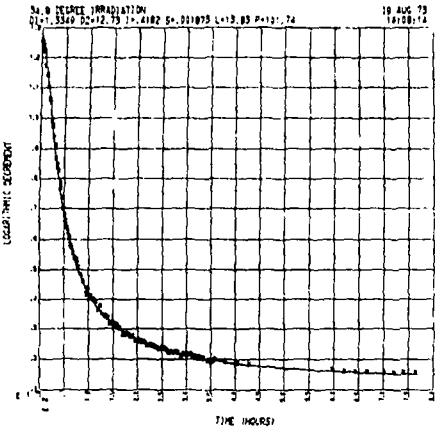

Fig. 24. Irradiation at 34.8°C; Δ(0) fixed.

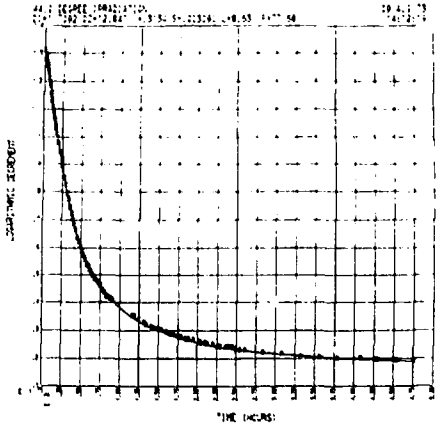

Fig. 25. Irradiation at 44.0℃; Δ(0) fixed.

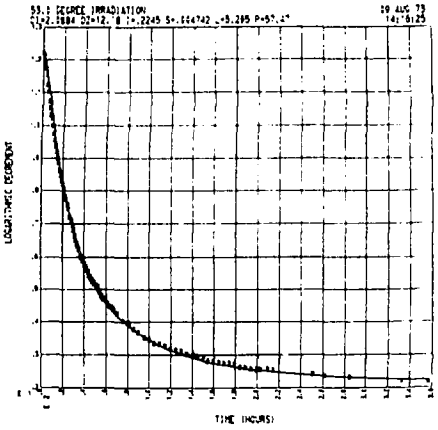

Fig. 26. Irradiation at 53.0℃; Δ(0) fixed.

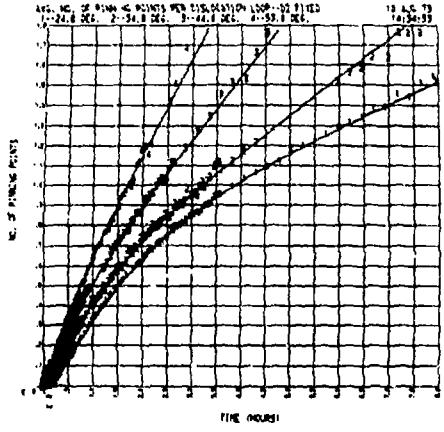

Fig. 27. Average number of pinning points per dislocation loop; $\Delta(0)$ fixed.

This is to be compared to the 51% total change observed after 2.5 days in the 34.8°C irradiation. Unfortunately, no attempt was made in this work to separate the spontaneous damping decrease from that due to the irradiation. This could have been done, for example, by holding the sample at temperature a few days prior to irradiating, until the spontaneous change had saturated. It is not known whether previous workers have carried out such a procedure, but these results show it to be desirable.

A second source of uncertainty is the prompt damping change upon insertion of the source. As noted, this amounts to less than 5% for all the runs used in the analysis.

Finally, as pointed out above, we have assumed that the pinning of a single dislocation component is responsible for the entire damping decrease whereas, in fact, the second dislocation component may also contribute a measurable change. However, this contribution is expected to be small for the reason mentioned.

Because we do not have accurate knowledge of the magnitudes of these uncertainties or of their behavior as a function of temperature, it is not possible to assign error limits to the final results.

Let us next examine whether the results obtained from this analysis are quantitatively reasonable, considering the physical basis of the TBHB model, the measured data itself, and the results of other, previous experiments. First to be considered are the values of $\Delta(0)$ and $\Delta(\infty)$. It can be seen by a comparison of the values given in Tables 7 and 8 with the data shown in Tables 1 through 4 that $\Delta(0)$ deviates from the measured initial value of the

decrement by about 3% in the worst case. This seems reasonable in view of the fact that the uncertainty in the initial value due to source insertion effects was as much as 4.3% in the worst case. The $\Delta(\infty)$ value in every case is below the last measured value of the decrement, as it should be.

The energy, E_{LE}, according to the TBHB model, represents the migration energy of the defects responsible for the dislocation pinning. If the process is free (untrapped) lattice migration, the value of E_{LE} can be compared with those determined for Stage III annealing of silver in other experiments. Table 9 is a list of these values. It can be seen that the present values (0.48 and 0.51 eV) are less than the majority of those shown, but agree with the lowest of them. They therefore do not seem unreasonable.

The term τ_{LE_o} is the preexponential term in the relaxation time for the lattice diffusion process. It can be related to that in the unit jump time of the diffusing defect by Eq. (IV-J-7):

$$\tau_{LE_o} \cong \frac{\ell_o^2}{a^2} \tau_{LU_o}.$$

If one uses the generally accepted range of values for τ_{LU_b}, 10^{-12} to 10^{-13} sec (comparable to the reciprocal of the Debye frequency[88]), one obtains the

Table 9. Stage III migration energies observed in other experiments.

Type of experiment	Migration energy (eV)	Reference
cw - resist.	0.2 - 0.5 (first part) 0.55 ± 0.03 (second part)	136
q - resist.	0.57	137
e (1.6 and 3.0 MeV)-resist.	0.57 ± 0.04 to 0.71 ± 0.02	138
cw	0.60 ± 0.05	139
n (fast spectrum) - int. frict.	0.64 ± 0.06	123
cw	0.65	140
d (10 MeV)	0.67 ± 0.04	141
cw	0.7	142

Key

cw - cold work
q - quenching
e - electron irradiation
n - neutron irradiation
d - deuteron irradiation
resist. - electrical resistivity measurement
int. frict. - internal friction measurement

result $\ell_o/a \cong 2$ to 8×10^4 for the two fits considered together. Since a is equal to 4.0862×10^{-8} cm in silver,[143] ℓ_o must be of the order of 10^{-3} cm. This is a reasonable spacing between dislocation lines for crystals grown in the same manner as the present ones, since, if a simple cubic network of dislocations is assumed, the relation $\Lambda \ell_o^2 \cong 1$ would yield a dislocation density of 10^6 cm/cm^3. This is a value commonly observed in crystals seeded for growth with close-packed external surfaces.[74]

The question of whether the lattice diffusion is trapped or untrapped can also be answered by consideration of τ_{LE_o}. As shown by Thompson and Buck,[34] if the motion is untrapped, the attempt frequency, which should be comparable to the Debye frequency, is given by

$$\nu_o = \frac{N_A^{2/3}}{\Lambda \tau_{LE_o}}, \qquad \text{(VII-C-1)}$$

where N_A is the number of atoms per cm^3 (5.85×10^{22} for silver), and Λ is the dislocation density in (cm/cm^3). Using a value of $\Lambda = 10^6$ cm/cm^3, which was calculated above, one finds that ν_o is in the range 2 to 5×10^{12} sec^{-1}, which is reasonable.[86] On the other hand, if the motion involves trapping by impurities in the crystal, ν_o would be given by[34]

$$\nu_o = \frac{12\, N_A^{2/3}\, P}{\Lambda \tau_{LE_o}}, \qquad \text{(VII-C-2)}$$

where P is the concentration of impurity atoms. From the spectrochemical analysis, P is estimated to be in the range of 10 ppm, or 10^{-5} fractional concentration. Again, assuming $\Lambda = 10^6$ cm/cm^3, one finds that ν_o would be in the range of 10^8 sec^{-1}, which is unreasonably low.[86]

As pointed out by Thompson and Buck,[34] another test to differentiate the trapped and untrapped cases can be made by estimating the diffusion length of the defect by use of the Einstein relation [Eq. (IV-D-4)], Eqs. (VII-C-1) and (VII-C-2), and the approximate equation

$$\overline{x^2} \cong D\tau_{LE}, \qquad \text{(VII-C-3)}$$

where $\sqrt{\overline{x^2}}$ is the diffusion length. The value of the diffusion length should be comparable to the spacing between dislocations. Applying these equations for the untrapped case, one finds that $\sqrt{\overline{x^2}}$ is about 5×10^{-4} cm, which is about half the value obtained for the dislocation spacing and is therefore reasonable. For the trapped case, the result for $\sqrt{\overline{x^2}}$ is about two orders of magnitude smaller, which is unreasonably short.

It must be pointed out that these arguments do not rule out the existence of deep impurity traps. If sufficiently deep traps are present, migrating defects will not escape from them in the timescale of the experiment, and their only effect will be to reduce the effective rate of production of possible dislocation pinners.

In summary, the results of the fits for E_{LE} and τ_{LE_o} are consistent with the interpretation that they represent the free lattice migration of a Stage III defect. As noted by Thompson and Buck,[34] the reason the migration of such a defect is observed at a temperature usually characteristic of Stage IV in resistivity experiments is that the defect concentration is so much smaller and the diffusion lengths are longer in the present experiments.

Turning to the examination of the values for $E_1 (= E_{DU})$ we note that the TBHB theory interprets it as the activation energy for migration of the defects along the dislocation lines, i.e., as the migration part of what is usually known as the pipe diffusion energy. As mentioned in Section IVG, other work[82] predicts that its value must be considerably less than 0.78 to 0.85 eV. The present values, 0.24 and 0.30 eV, satisfy this requirement. In addition, they are considerably less than the value obtained for the lattice migration energy, E_{LE}. This is reasonable, in that migration along the core of a dislocation is known to be easier than migration through the lattice.[84] It is interesting that the ratio of E_1 to E_{LE} for the fit in which $\Delta(0)$ was held fixed is about 0.63, compared to about 0.66 in the TBHB copper work. This is to be expected, in view of the similarity in structure of the two metals, and may shed some light on the relative validity of the two fits made here, since the other fit gives a ratio of 0.47.

The energy E_S, which is equal to $E_{ND} - E_1$, is interpreted as the binding energy of the defects to the nodes on the dislocation lines. Thomson and Balluffi[144] have argued that E_S should asymptotically approach the formation energy of the defects in the dislocations as the nodal points become large. One might therefore expect that the ratio of E_S to E_1 might be nearly equal for metals that are similar in structure, just as is true for the corresponding parameters in the bulk. This ratio has values of 1.4 and 1.3 for the two fits, compared to 1.6 in the TBHB copper work. Again, the fit with $\Delta(0)$ held fixed gives closer agreement. The smaller relative value for E_S in silver (0.43 or 0.32 eV versus 0.68 eV in copper) may be explained by the fact that the stacking fault energy of this metal is believed to be much less than that of copper,[72] leading to more extended nodes. These in turn would produce smaller stresses in the crystal and lower interaction energies with defects.

Interpretation of the remaining parameters is somewhat less straightforward. The term τ_{1_o} is the preexponential factor in the lowest-order relaxation time for pipe diffusion. Making use of Eq. (IV-J-12), we find that

$$\tau_{l_o} = \frac{2}{\pi^2} \frac{\ell_o^2}{a^2} \tau_{DU_o}, \qquad \text{(VII-C-4)}$$

where ℓ_o is the average length of the dislocation loops, a is the lattice parameter, and τ_{DU_o} is the preexponential factor in the relaxation time for a single jump along the dislocation line. Using the values of ℓ_o/a derived above, one obtains values of τ_{DU_o} on the order of 10^{-8} sec, which is quite long in comparison to the reciprocal of the Debye frequency.[86] There appear to be two possible explanations. The first is that, because of the low stacking-fault energy, the dislocations are widely split. In this case, as Love pointed out,[84] the defects on the line would also partially "extend," in that their exact atomic position would be undetermined within the stacking-fault width. Migration of such a defect would require the cooperative motion of a number of atoms, introducing a considerable negative activation entropy for the process.[145] Since τ_{DU_o} is the product of approximately the reciprocal of the Debye frequency and the entropy factor $e^{-S_m/k}$, where S_m is the entropy of migration and k is Boltzmann's factor, a large negative entropy could explain this result and make a value of 10^{-8} sec reasonable.

A second possible explanation is that the average length of the dislocations whose pinning gives rise to the observed damping change is much greater than the average distance which the pinning defects have traveled before reaching them. If this explanation alone is to explain the discrepancy, the required dislocation length would be of the order of 1 mm. There are two objections raised to such an explanation. First, it does not seem plausible that dislocation loops would be this long, in view of the thickness of the specimen and the manner of preparation. Secondly, a fundamental assumption in the derivation of the TBHB model was that the dislocation length and the spacing between them are equal, i.e., the dislocations are arranged in a cubic lattice. When this assumption is removed and the derivation is repeated, the result is that additional terms of the form t^2 and $te^{-\alpha t}$ must be added to the equation for n_D. Inclusion of these terms would increase the complexity of the fitting equations and add another unknown parameter. However, it could not measurably improve the fit, since the standard deviations of the present fits are already within the uncertainty in the data. Therefore, it would not be possible to judge whether or not the more complex formulation were more nearly correct. More importantly, the fact that the present fits match the data to the degree they do indicate that the simpler formulation is adequate. For these reasons, we believe that the entropy explanation accounts for at least part of the discrepancy in τ_{DU_o}.

The terms S_o and K can be interpreted by a consideration of the equation

$$S = \frac{\phi}{2} \frac{\ell_o}{a} \frac{\tau_{DU_o}}{\tau_{ND_o}} \exp\left[-(E_{ND} - E_{DU})\right]/kT, \qquad \text{(VII-C-5)}$$

which results from Eqs. (VII-B-10) and (IV-J-11), with the assumptions, justified by TBHB, that $A \ll \phi, (2\,a/\ell_o)(\tau_{ND}/\tau_{DU}) \gg 1$, and $\tau_{LE}/\tau_{DL} \ll (2a/\ell_o)(\tau_{ND}/\tau_{DU})$. From Eq. (VII-C-5),

$$S_o = \frac{\phi}{2}\,\frac{\ell_o}{2}\,\frac{\tau_{DU_o}}{\tau_{ND_o}}. \qquad \text{(VII-C-6)}$$

The parameter ϕ can be evaluated from the fitted value of K by using Eqs. (IV-J-6), (VII-B-13), (VII-B-14), and (VII-B-16). Combining these relations and solving for τ_{DU_o}/τ_{ND_o} by using $\ell_o/a = 5 \times 10^4$, one obtains a ratio of about 200 for the fixed-$\Delta(0)$ fit, and a ratio of about 3 for the varied-$\Delta(o)$ fit. If one uses the value of 10^{-8} sec obtained above for τ_{DU_o}, one obtains a value for τ_{ND_o} in the r nge of 10^{-11} sec for the first case and 10^{-9} sec for the second case. The first value seems more plausible in comparison to the reciprocal of the Debye frequency, supporting the fixed-$\Delta(o)$ fit. If, on the other hand, one uses a value for τ_{DU_o} that is nearer the reciprocal of the Debye frequency, then the varied-$\Delta(o)$ fit gives a more reasonable result for τ_{ND_o}.

Another check on the fitted value of K can be made by using Eq. (VII-B-16) and the calculated values for the displacement cross section and gamma ray flux from Section IV.B. This produces the result that $\ell_o/\Lambda = 1.5 \times 10^{-13}$ cm^3. If ℓ_o is assumed to be 10^{-3} cm, as computed above, the value of Λ comes out to be 7×10^9 (cm/cm^3), which is higher than one would expect for annealed crystals and higher than one would calculate, assuming a square dislocation network, from the relationship $\Lambda \ell_o^2 \cong 1$.

An alternative approach is to assume that only part of the defects that were created acted as pinners for the dislocations that gave rise to the damping. Using values of $\ell_o = 10^{-3}$ cm and $\Lambda = 10^6$(cm/cm^3), the result is that only about one defect in 10^4 acted as a damping pinner. There are three possible reasons why this might be true. First, it is known that not all displacements give rise to freely migrating defects, but that many annihilate. For example, Corbett et al.[146] found that, in copper, about 80% of the damage created by 1.4 MeV electrons annealed in substages Ia-Id, which are believed to result from annihilation of close or correlated Frenkel pairs. A second possible reason why only a small part of the defects may have acted as pinners is that there was a high relative concentration of impurities, which may have acted as deep traps. In fact, the average distance from a radiation-produced defect to an impurity atom was of the order of 10^{-6} cm, whereas the average distance to a dislocation was calculated at 10^{-3} cm. Whether or not the defects would be bound to the impurities probably depends on the species and is not known. However, TBHB concluded that 100% of the defects in their copper experiments migrated to dislocations.

A third possible reason for such a low pinning efficiency is that a large fraction of the defects migrate to dislocations that do not give rise to significant damping. Indeed, we already suspected from the frequency data that such dislocations were present and were being pinned. This explanation is reminiscent of one of the possibilities considered by Paré and Guberman[96]—namely, that there are two categories of dislocations, one of which has a much longer average loop length than the other but is present in much smaller concentration. The group of longer dislocations could then give rise to virtually all of the observed damping, because the damping is proportional to the fourth power of the loop length. However, because of its much lower density, it would gather only a small portion of the point defects as pinners. At the same time, since the modulus defect is proportional to only the second power of the loop length, the shorter dislocation group could make a significant contribution to modulus changes if they compensate in density for what they lack in loop length relative to the first group.

As discussed in Section VII-B, Paré and Guberman[96] rejected the two-dislocation-component model on the grounds that it did not explain the discrepancies in the frequency dependence of the damping in copper, and that it did not seem plausible. Since the frequency dependence was not studied in this work, we will confine our discussion to the plausibility of the model for the present crystals.

The best evidence for deciding whether this model is plausible would be produced by observation of the dislocation structure of the samples, either by electron microscopy or etch-pit studies. Neither of these techniques was applied to the present samples, but considerable insight can be gained from observations on crystals having similar purity, method of growth, and thermal and mechanical history. Electron microscopy has been performed on dislocations in silver by Bailey and Hirsch[147] and by Moon and Robinson.[148] Etch pit studies were carried out by Levinstein and Robinson,[149] Worzala and Robinson,[150] Sabol and Robinson,[151] and Chen and Hendrickson.[152] All these workers found that the dislocation structure of silver crystals is far different from the cubic lattice assumed in the TBHB theory. Although much of the work involved silver that had been heavily cold-worked, the papers by Levinstein and Robinson,[149] Chen and Hendrickson,[152] and Worzala and Robinson[150] discuss observations on as-grown, annealed, and lightly deformed crystals. It should be noted that the present crystals can best be classified as lightly deformed and annealed. The deformation came about because of the thermal contraction difference of about 1.2% between the silver and the graphite rod on which it was grown, the subsequent pulling to remove the rod, and the handling involved in spark-machining and mounting. The annealing was done at tempertures of 800°C and 500°C, as discussed earlier, which are lower than those used in the etch-pit studies. Levinstein and Robinson[149] found that as-grown

crystals had dislocation densities in the neighborhood of $1\text{-}5 \times 10^7$ cm^{-2}. The dislocations appeared to fall into two categories. Most were distributed more-or-less randomly and exhibited small etch pits. These dislocations were believed to be in the form of small loops, each of which produced two etch pits where they intersected the surface. As material was removed, these loops were etched away and were replaced by other loops, as they in turn intersected the surface. In this way, the size of the randomly located pits remained small. The other category of pits was located on low-angle boundaries and slip lines. These pits grew as etching proceeded, indicating that the dislocations giving rise to them had longer line lengths.

Levinstein and Robinson[149] found that a 3% deformation resulted in slip bands with a cellular appearance; that is, they were "made up of regions of high dislocation density surrounding regions in which there are no dislocation lines intersecting the surface."

Chen and Hendrickson[152] *found that their as-grown crystals had dislocation densities of* $1\text{-}5 \times 10^6$ cm^{-2}. A 2-week anneal at 940°C reduced the density to about 5×10^4 cm^{-2}. The annealed crystals contained "randomly dispersed dislocation etch pits with a few subboundaries." When these authors lightly deformed an annealed crystal through handling, and reannealed it at 940°C for 2 weeks, they observed well-defined polygonization boundaries, which they found "somewhat surprising" in view of the low stacking-fault energy of silver.

Worzala and Robinson[150] described the dislocation structure of silver in the easy glide region. A typical specimen had an average dislocation density after annealing of 1.8×10^6 cm^{-2}. The dislocations were arranged both randomly and in low-angle boundaries. Deformation of 0.1%, which was just past the yield point, gave rise to clusters of dislocations, which became more dense as deformation was increased.

In view of these observations, it seems clear that the present crystals could very likely have had a dislocation structure incorporating a low density of long dislocations and a higher density of short ones, either as a result of ingrown subboundaries or of polygonization arising from deformation and annealing.

The parameter E_{ND} is interpreted as the sum of the binding energy of the defect to the node and its migration energy on the dislocation. Its value thus can be obtained as the sum of E_S and E_{DU}, which is 0.73 eV in the case of the fixed-$\Delta(0)$ fit, and 0.56 eV for the varied-$\Delta(0)$ fit. Using the argument of Thomson and Balluffi cited above,[144] TBHB compared E_{ND} to the measured pipe diffusion energy. For silver, this energy has been measured at 0.78 eV and 0.85 eV by different authors.[82] Again, a comparison in the present case reveals that a more favorable agreement is obtained with the fixed-$\Delta(0)$ fit.

The parameter E_{DL}, which corresponds to the energy required to return a defect from a dislocation to the lattice, has not been evaluated in these experiments. TBHB obtained an estimate by assuming that the defects were all accounted for by the sum of those present on the dislocations, on the nodes, and freely migrating in the lattice. Because of the presence of the second dislocation component and the possible presence of deep impurity traps, we cannot make this assumption here. For the same reason, we are not able to calculate the efficiency of dislocations in trapping defects.

In view of the considerations discussed here, it appears that the fixed $-\Delta(0)$ fit is more nearly correct than the varied-$\Delta(0)$ fit, in spite of its having a slightly higher standard deviation. It should be noted that, because the fitting scheme gives equal weight to all the data points, and because only a few points are located at early enough times to have a large effect in determining the parameters in the transient terms, it is not surprising that the early points were not well fitted when $\Delta(0)$ was allowed to vary, or that the standard deviation increased slightly when $\Delta(0)$ was fixed.

To summarize the discussion presented in this section thus far, it appears that the following statements are true: 1) More reasonable values for the parameters in the theory are obtained when $\Delta(0)$ is constrained to match the value measured after source insertion and temperature stabilization than when it is allowed to vary; 2) the parameters determined in this way are plausible if one allows for wide splitting of dislocations and the presence of two dislocation components; 3) these two assumptions are supported by the observed stacking-fault energy and dislocation structures in silver; 4) the time and temperature dependence of the observed pinning is consistent with the free migration to dislocations of a single type of defect, pipe diffusion along the dislocations, and binding of the defects to nodes; and 5) the best value for the lattice migration energy of the defect is about 0.48 eV. It remains to discuss the identity of the migrating defect.

Gordon[138] recently reviewed the proposed models for Stage III annealing in silver. These include the two-interstitial model, the di-interstitial model, the trapped interstitial model, the interstitial cluster break-up model, and the vacancy model. In analyzing his data for Stage III resistivity recovery of electron-irradiated silver, Gordon interpreted the results in terms of the migration of vacancies to interstitial clusters and the formation of divacancies in the anneal, followed by migration of divacancies in the latter part of Stage III. In doing so, he assumed that the migration energy of the vacancy far from any clusters is 0.71 eV, and that the migration energy of divacancies 0.57 eV. This value for the vacancy migration energy is considerably less than the values determined by Quéré,[153] Doyama and Koehler,[154] Gertsriken and Novikov,[155] and Ramsteiner, et al.[156] in quenching and annealing experiments, which range from 0.83 to 0.88 eV. It is also less than that obtained by subtracting the vacancy formation energy determined in quenching experiments

from the best value of the self-diffusion energy in 1970 as summarized by Mehrer and Seeger.[157] However, the latest self-diffusion energy measurements by Lam et al.[83] indicate that the monovacancy self-diffusion energy is 1.76 eV. Subtracting vacancy formation energies in the range of 1.0 to 1.1 eV (Ref. 157) then gives good agreement with Gordon's result. It is conceivable, then, that the vacancy migration energy could be as low as 0.71 eV. The author knows of no serious suggestion that the activation energy for free migration of monovacancies in silver is less than this value, particularly not as low as 0.48 eV. The divacancy migration energy assumed by Gordon is in good agreement with other measured results, as summarized by Mehrer and Seeger.[157]

In identifying the defect responsible for pinning in the present experiments, several possibilities can be ruled out. Single vacancies, although known to be created by gamma irradiation, simply have too high a migration energy to account for the results. Although the uncertainty in E_{LE} as determined in the present work may be sizeable, it is not likely to be as high as 40%. Support for this contention is found in the fact that the fit with $\Delta(0)$ held fixed produced a value for E_{LE} that was within 6% of that obtained when $\Delta(0)$ was varied. It therefore does not seem to be very sensitive to the fitting constraints.

Divacancies, although their migration energy is not very different from that determined here, can also be ruled out on the basis that they are not likely to be formed in any significant number in the present experiments. Direct formation by the irradiation is unlikely because of the energy argument given in Section IV.B. Formation by the migration together of two vacancies is not likely because of the small defect concentration present. The same arguments rule out di-interstitials and interstitial clusters. The only possibility left is the free migration of single interstitial atoms. Since there is general agreement that some type of interstitial migrates in Stage I, and since we have seen evidence of this migration in the survey experiments, we are thus led to embrace the two-interstitial model to explain the present results. It must be emphasized that this conclusion applies only to the present experimental conditions. It does not rule out the possibility that different defects may cause significant effects in Stage III under different conditions of radiation type or energy or higher defect concentrations.

Now that we have settled upon the single interstitial as the responsible defect, it is interesting to attempt an explanation of the depinning results discussed in Part VI. As was stated in Section VI.A, when the pinned sample was heated to annealing temperatures up to 220°C, the damping and frequency exhibited apparent pinning while held at the annealing temperature. In the framework of the present model, this can be explained by interstitial atoms being "boiled off" the nodes onto the dislocation lines, raising the average

number of pinning points. For annealing temperatures less than about 120°C, this was the only effect which occurred appreciably, so that, when the sample was cooled back to 35.5°C, the extra pinning points returned to the nodes, reestablishing the original equilibrium distribution and returned the damping and frequency to their original values, as observed. At annealing temperatures between about 120°C and 220°C, an appreciable number of interstitials are also "boiled off" the dislocation lines into the lattice. The parameters still exhibit apparent pinning when the sample is held at the annealing temperature, since more interstitials are added to the lines from the nodes than are lost to the lattice. When the sample is then cooled to 35.5°C, some of the interstitials return from the lattice, but a greater number return to the nodes, causing the average number of pinning points to decrease, as observed. For annealing temperatures between about 220°C and 340°C, more interstitials are boiled off into the lattice than are supplied by the nodes, so that a net unpinning is observed at the annealing temperature. When cooled back to 35.5°C, however, the interstitials returning from the lattice now dominate those that return to the nodes, and a net pinning is observed when the sample is held at 35.5°C. This last step is somewhat analogous to what took place in the original irradiation, when a net pinning occurred because not all the interstitials that reached the lines migrated on to the nodes. Finally, annealing at 500°C enables the interstitials to escape completely from the dislocations and undergo longer-range migration in the lattice, so that they annihilate the vacancies, which were always present as comparatively inanimate partners throughout the lower-temperature pinning-depinning process. In addition, at 500°C the vacancies are sufficiently mobile that their migration will also contribute to permanent depinning. It is thus seen that the TBHB model with the interstitial as the migrating defect is able to explain, at least qualitatively, all the depinning observations.

VIII. Conclusions

A. The Koehler-Granato-Lücke vibrating string model applied to a single dislocation component cannot explain the present dislocation pinning results.

B. These pinning results are consistent with the vibrating string model if two dislocation components are assumed, one of which has a much higher average loop length than the other. Such a structure may result from polygonization or the presence of low-angle boundaries.

C. The results of survey experiments are consistent with long-range migration in Stage I in silver.

D. The activation energy for migration of the defect which pins dislocations in Stage III in silver using ^{60}Co gamma irradiation and low defect concentrations is about 0.48 eV. This defect is most likely the single interstitial atom.

E. Pipe diffusion is necessary to explain the pinning behavior as a function of time and temperature in these experiments. The migration of point defects and their interaction with dislocations can be explained by the model of Thompson, Buck, Huntington, and Barnes.

F. The efficiency of the dislocations in trapping the point defects could not be estimated because of the presence of two dislocation components, only one of which contributed significantly to the measured damping.

Acknowledgments

I want here to acknowledge the help given to me by several individuals and organizations during the course of this work. Without their assistance I would certainly have been unable to complete a project of this scope and duration.

I would like to thank Dr. Edward Teller, who first interested me in applied science and invited me to study in the Department of Applied Science of the College of Engineering, University of California, Davis-Livermore.

Although I can no longer thank him personally, I wish to acknowledge the encouragement given me by the late Dr. Albert Kirschbaum in the earliest days.

Dr. Richard J. Borg provided encouragement and support as well as helpful discussions.

Mr. David Lai gave invaluable assistance in apparatus design, in programming, and in my introduction to the versatility and power of the high-speed computer.

Dr. Richard Stuart provided help with the simultaneous fitting of all the data.

Dr. Jack B. Mitchell provided helpful advice in understanding the microstructure of metals.

Messrs. Bert Tuckey, Sid Egan, Robert France, and Gene Stiles aided me in design and fabrication of the cryostat furnace and other mechanical apparatus.

Mr. Akinobu Kuramoto designed and fabricated the vibration amplitude and phase control system.

Mrs. Doree Coronado painstakingly typed the manuscript.

Mr. Larry Fagan and the staff of the Technical Information Department of Lawrence Livermore Laboratory edited and produced the final copy.

Financial support was provided by the Fannie and John Hertz Engineering Scholarship Foundation, the taxpayers of the United States of America through the Atomic Energy Commission and the Lawrence Livermore Laboratory, and the taxpayers of the state of California through the University of California. My gratitude goes out to all of them.

The experimental work was performed under the auspices of the Inorganic Materials Division of the Chemistry and Materials Science Department of the Lawrence Livermore Laboratory. My thanks go to several members of the staff who provided support and helpful suggestions.

Finally, I want to thank my advisor, Dr. Michael W. Guinan, who suggested the topic of the work, gave me constant assistance and guidance, and supplied unfaltering encouragement through many trying times. It has been a privilege to be associated with him.

References

1. F. Seitz, "Radiation Effects in Solids," Phys. Today 5 (6) 6 (June 1952).
2. R. H. J. Silsbee, J. Appl. Phys. 28, 1246 (1957).
3. G. H. Kinchin and R. S. Pease, Repts. on Prog. in Phys. 18, 1 (1955).
4. F. Seitz and J. S. Koehler, Solid State Physics 2, F. Seitz and D. Turnbull, Eds. (Academic Press, New York, 1956), p. 305.
5. D. S. Billington and J. H. Crawford, Jr., Radiation Damage in Solids (Princeton University Press, Princeton, New Jersey, 1961).
6. M. W. Thompson, Defects and Radiation Damage in Metals (Cambridge University Press, London, 1969).
7. R. Hooke, Micrographia, (1665), p. 85.
8. R. Haüy, Traite elementaire de Physique, Vol. 1 (De L'Imprimerie de Delance et Leseur, Pris, 1803).
9. A. Bravais, Etudes crystallographiques (Gautier-Villars, Paris, 1866).
10. H. G. Van Bueren, Imperfections in Crystals (North-Holland, Amsterdam, 1961), 2nd ed.
11. J. Frenkel, Zeits. Physik 35, 652 (1926).
12. A. Joffe, Ann. d. Phys. 72, 481 (1923).
13. C. Wagner and W. Schottky, Zeits. physik. Chem. B11, 163 (1930); C. Wagner, Zeits. physik. Chem., Bodenstein Fest., 177 (1931) and B22, 181 (1933).
14. H. B. Huntington and F. Seitz, Phys. Rev. 61, 315 (1942); H. B. Huntington, Phys. Rev. 61, 325 (1942).
15. G. H. Vineyard, J. Phys. Chem. Solids 3, 121 (1957).
16. Reference 10, p. 302.
17. A. C. Damask and G. J. Dienes, Point Defects in Metals (Gordon and Breach, New York, 1963).
18. J. Frenkel, Zeits. Physik 37, 572 (1926).
19. L. Prandtl, Z. Angew. Math. Mech. 8, 85 (1928); G. Masing and M. Polanyi, Ergeb. exact. Naturw. 2, 177 (1923); U. Dehlinger, Ann. Physik 5, 2, 749 (1929); G. I. Taylor, Proc. Royal Soc. A145, 362 (1934); G. I. Taylor, J. Inst. Met. 62, 307 (1938); E. Orowan, Z. Physik 89, 614, 635 (1934); M. Polanyi, Z. Physik 98, 660 (1934); J. M. Burgers, Proc. Kon. Ned. Acad. Wet. 47, 293, 378 (1939).
20. Sir L. Bragg, Proc. Phys. Soc. 52, 54 (1940).
21. N. F. Mott and F. R. N. Nabarro, Proc. Phys. Soc. 52, 86 (1940).
22. A. H. Cottrell, Report on the Strength of Solids (Physical Society, London, 1948).
23. C. Zener, Elasticity and Anelasticity of Metals (Chicago, Chicago University Press, 1948).
24. T. A. Read, Phys. Rev. 58, 371 (1940).

25. J. S. Koehler, Imperfections in Nearly Perfect Crystals (Wiley, New York, 1952), p. 197.
26. A. Granato and K. Lücke, J. Appl. Phys. 27, 583, 789 (1956); 28, 635 (1957).
27. D. O. Thompson and D. K. Holmes, J. Appl. Phys. 27, 713 (1956).
28. D. O. Thompson and D. K. Holmes, J. Phys. Chem. Solids 1, 275 (1956).
29. H. Dieckamp and A. Sosin, J. Appl. Phys. 27, 1416 (1956).
30. R. M. Stern and A. V. Granato, Acta Met. 10, 358 (1962).
31. V. K. Paré, "Analysis of Internal Friction in Copper at Megacycle Frequencies," in Solid State Division Annual Progress Report, Oak Ridge National Laboratory, Rept. ORNL-3364 (1962), pp. 74-77; D. O. Thompson, V. K. Paré, and F. W. Young, Jr., "Effect of Fast-Neutron Irradiation on Internal Friction in Copper Single Crystals at Megacycle Frequencies," in Solid State Division Annual Progress Report, Oak Ridge National Laboratory, Rept. ORNL-3017 (1960), pp. 40-41.
32. D. O. Thompson, O. Buck, R. S. Barnes, and H. B. Huntington, J. Appl. Phys. 38, 3051 (1967).
33. D. O. Thompson, O. Buck, H. B. Huntington, and P. S. Barnes, J. Appl. Phys. 38, 3057 (1967).
34. D. O. Thompson and O. Buck, J. Appl. Phys. 38, 3068 (1967).
35. V. K. Paré and H. D. Guberman, J. Appl. Phys. 44, 32 (1973).
36. D. O. Thompson and V. K. Paré, "Use of Anelasticity in Investigating Radiation Damage and the Diffusion of Point Defects," in Physical Acoustics, Vol. III, Part A, W. P. Mason, Ed. (Academic Press, New York, 1966), pp. 293-359.
37. R. D. Evans, "Gamma Rays," in American Institute of Physics Handbook, D. E. Gray, Ed. (McGraw-Hill, New York, 1963), p. 8-81.
38. R. A. Dugdale, Report of Bristol Conference on Defects in Crystalline Solids (Physical Society, London, 1955).
39. D. O. Thompson and D. K. Holmes, J. Phys. Chem. Solids 1, 275 (1957).
40. R. S. Barnes, N. H. Hancock, and E. C. H. Silk, Phil. Mag. 3, 518 (1958); R. M. Stern and A. V. Granato, Acta Met. 10, 358 (1962); and P. L. Gruzin, Yu. D. Zharov, and Yu. A. Polikarpov, Sov. Phys. Dokl. 9, 1118 (1965).
41. J. H. E. Mattauch, W. Thiele, and A. H. Wapstra, Nucl. Phys. 67, 1 (1965).
42. E. F. Plechaty and J. R. Terrall, "Photon Cross Sections 1 keV to 100 MeV," Lawrence Livermore Laboratory, Rept. UCRL-50400, Vol. VI (1968), p. 99.
43. D. S. Billington and J. H. Crawford, Jr., Radiation Damage in Solids (Princeton University Press, Princeton, New Jersey, 1961), p. 28

[Results taken from O. S. Oen and D. K. Holmes, J. Appl. Phys. 30, 1289 (1959)].

44. P. Marmier and E. Sheldon, Physics of Nuclei and Particles, Vol. I (Academic Press, New York, 1969), p. 113.
45. Ibid., p. 106.
46. R. D. Evans, "Compton Effect," in Handbuch der Physik, Bd. XXXIV, S. Flugge, Ed. (Springer-Verlag, Berlin, 1958), p. 218.
47. P. Marmier and E. Sheldon, Physics of Nuclei and Particles, Vol. I (Academic Press, New York, 1969), p. 188.
48. J. W. Corbett, Electron Radiation Damage in Semiconductors and Metals (Academic Press, New York, 1966).
49. F. Seitz and J. S. Koehler, Solid State Physics 2, p. 305.
50. A. Sosin and W. Bauer, in Studies in Radiation Effects in Solids, Vol. 3, G. J. Dienes, Ed. (Gordon and Breach, New York, 1969), p. 153.
51. P. G. Lucasson and R. M. Walker, Disc. Faraday Soc. 31, 57 (1961); and Phys. Rev. 127, 485 (1962).
52. C. G. Roberts, W. P. Rickey, and P. E. Shearin, J. Appl. Phys. 37, 4517 (1966).
53. O. S. Oen and D. K. Holmes, J. Appl. Phys. 30, 1289 (1959); and unpublished data received from O. S. Oen for Z = 40 and Z = 50.
54. A. Hedgran and S. Hultberg, Phys. Rev. 94, 498 (1954).
55. A. Sosin and W. Bauer, p. 280 in Studies in Radiation Effects in Solids, Vol. 3, G. J. Dienes, Ed. (Gordon and Breach, New York, 1969), p. 280.
56. C. G. Roberts W. P. Rickey, and P. E. Shearin, J. Appl. Phys. 37, 4517 (1966).
57. Reference 48, p. 200.
58. J. B. Gibson, A. N. Goland, M. Milgram, and G. H. Vineyard, Phys. Rev. 120, 1229 (1960); K. H. Benneman, Phys. Rev. 124, 669 (1961); A. Seeger, E. Mann, and R. v. Jan, J. Phys. Chem. Solids 23, 639 (1962); R. A. Johnson and E. Brown, Phys. Rev. 127, 446 (1962); P. Hoekstra and D. R. Behrendt, Phys. Rev. 128, 560 (1962).
59. H. Paneth, Phys. Rev. 80, 708 (1950).
60. H. J. Wollenberger, "Production Rates of Frenkel Defects During Low-Temperature Irradiations," in Vacancies and Interstitials in Metals, A. Seeger et al., Eds., Proceedings of the International Conference held at Julich, Germany, on 23-28 September 1968 (North-Holland, Amsterdam, 1970), p. 215.
61. H. M. Simpson and A. Sosin, Radiation Effects 3, 1 (1970).
62. P. Shewmon, Diffusion in Solids (McGraw-Hill, New York, 1963).
63. A. Einstein, Investigations on the Theory of Brownian Movement (Dover Pub., New York, 1956).
64. A. Fick, Pogg. Ann. 94, 59 (1855).

65. B. S. Chandrasekhar, Revs. Mod. Phys. 15, 1 (1943).
66. Reference 17, p. 79.
67. G. H. Vineyard, J. Phys. Chem. Solids 3, 121 (1957).
68. W. Schilling, G. Burger, K. Isebeck, and H. Wenzl, "Annealing Stages in the Electrical Resistivity of Irradiated FCC Metals," in Vacancies and Interstitials in Metals, A. Seeger et al., Eds., Proceedings of the International Conference held at Julich, Germany, on 23-28 September 1968 (North-Holland, Amsterdam, 1970), p. 255.
69. J. W. Corbett, "On the Interpretation of the Recovery Stages of FCC Metals," in Vacancies and Interstitials in Metals, A. Seeger et al., Eds., Proceedings of the International Conference held at Julich, Germany, on 23-28 September 1968 (North-Holland, Amsterdam, 1970), p. 997.
70. A. Seeger, "Introduction to the Panel Discussion," in Vacancies and Interstitials in Metals, A. Seeger et al., Eds., Proceedings of the International Conference held at Julich, Germany, on 23-28 September 1968 (North-Holland, Amsterdam, 1970), p. 999.
71. A. Seeger, D. Schumacher, W. Schilling, and J. Diehl, Eds., Vacancies and Interstitials in Metals, Proceedings of the International Conference held at Julich, Germany, on 23-28 September 1968 (North-Holland, Amsterdam, 1970).
72. J. P. Hirth and J. Lothe, Theory of Dislocations (McGraw-Hill, New York, 1968).
73. Ibid., p. 764
74. F. W. Young, Jr., and J. R. Savage, J. Appl. Phys. 35, 1917 (1964).
75. R. Bullough and R. C. Newman, Repts. Prog. Phys. 33, 101 (1970)
76. F. R. N. Nabarro, Theory of Crystal Dislocations (Clarendon Press, Oxford, 1967).
77. A. H. Cottrell and B. A. Bilby, Proc. Phys. Soc. 62, 49 (1949).
78. H. Pfeiderer, A. Seeger, and E. Kröner, Z. Naturforsch. 15a, 758 (1960).
79. J. D. Eshelby, Proc. Roy. Soc. A241, 376 (1957).
80. L. A. Girifalco and D. Kuhlmann-Wilsdorf, J. Phys. Soc. Japan 18, Suppl. II, 230 (1963).
81. A. A. Hendrickson and E. S. Machlin, Trans. AIME, J. Metals 6, (9), Sect. 2 1035 (1954); D. Turnbull and R. E. Hoffman, Acta Met. 2, 419 (1954); G. Love and P. G. Shewmon, Acta Met. 11, 899 (1963).
82. D. Turnbull and R. E. Hoffman, Acta Met. 2, 419 (1954); G. Love and P. G. Shewmon, Acta Met. 11, 899 (1963).
83. Nghi Q. Lam, S. J. Rothman, H. Mehrer, and L. J. Nowicki, Phys. Stat. Solidi (b) 57, 225 (1973).
84. G. R. Love, Acta Met. 12, 731 (1964).
85. R. Hooke, De potentia restitutiva (London, 1678).

86. C. Kittel, Introduction to Solid State Physics (Wiley, New York, 1966), 3rd ed.
87. A. S. Nowick, "Internal Friction in Metals," in Prog. in Met. Phys. 4, B. Chalmers, Ed. (Pergamon, New York, 1961), p. 1.
88. A. Granato and K. Lücke, J. Appl. Phys. 27, 583 (1956); 27, 789 (1956); and 28, 635 (1957).
89. T. A. Read, Phys. Rev. 58, 371 (1940).
90. J. Weertman, J. Appl. Phys. 26, 202 (1955).
91. O. S. Oen, D. K. Holmes, and M. T. Robinson, "Inertia-Free Model of Dislocation Line Motion," in Solid State Division Annual Report, Oak Ridge National Laboratory, Rept. ORNL-3017 (1960), pp. 3-6.
92. D. O. Thompson and V. K. Paré, "Temperature Dependence of the Effect of Fast-Neutron-Induced Defects on the Internal Friction and Young's Modulus of Copper," in Solid State Division Annual Report, Oak Ridge National Laboratory, Rept. ORNL-3017 (1960), pp. 36-39.
93. Reference 76, p. 505 et seq.
94. A. D. Brailsford, J. Appl. Phys. 43, 1380 (1972).
95. G. Leibfried, Z. Phyz. 127, 344 (1950).
96. V. K. Paré and H. D. Guberman, J. Appl. Phys. 44, 32 (1973).
97. J. L. Routbort and H. S. Sack, J. Appl. Phys. 37, 4803 (1966).
98. C. R. Heiple and H. K. Birnbaum, J. Appl. Phys. 38, 3294 (1967).
99. R. den Buurman and D. Weiner, Scripta Met. 5, 573 (1971).
100. D. O. Thompson and V. K. Paré, J. Appl. Phys. 31, 528 (1960).
101. R. L. Nielson, PhD. thesis, University of Pittsburgh (1968) (unpublished).
102. H. M. Simpson, A. Sosin, G. R. Edwards, and S. L. Seiffert, Phys. Rev. Lett. 26, 897 (1971).
103. H. M. Simpson, A. Sosin, and D. F. Johnson, Phys. Rev. B5, 1393 (1972).
104. H. M. Simpson and A. Sosin, Phys. Rev. B5, 1382 (1972).
105. M. W. Guinan, PhD. Thesis, University of California, Berkeley (1965); and Lawrence Berkeley Laboratory, Rept. UCRL-11420 (1965).
106. D. O. Thompson and F. M. Glass, Rev. Sci. Instr. 29, 1034 (1958).
107. R. Cabaret, Comp. Rend. 217, 529 (1943).
108. P. G. Bordoni, Nuovo Cimento 4, 177 (1947).
109. Private communication with Ronald M. Finnila, Lawrence Livermore Laboratory (1967).
110. S. G. Gorbics, W. E. Kunz, and A. E. Nash, Nucleonics 21, 63 (1963).
111. P. Morse, Vibration and Sound (McGraw-Hill, New York, 1948).
112. F. E. Terman, Radio Engineers' Handbook (McGraw-Hill, New York, 1943), p. 112.

113. J. D. Jackson, Classical Electrodynamics (Wiley, New York, 1962), p. 23.
114. H. M. Simpson and A. Sosin, Phys. Rev. B5, 1382 (1972).
115. P. G. Bordoni, Ricerca Sci. 19, 851 (1949).
116. D. H. Niblett, "Bordoni Peak in Face-Centered Cubic Metals," in Physical Acoustics, Vol. III, Part A, W. P. Mason, Ed. (Academic Press, New York, 1966), p. 77.
117. P. G. Bordoni, M. Nuovo, and L. Verdini, Nuovo Cimento Supp. 18, 55 (1960).
118. J. L. Routbort and H. S. Sack. Phys. Stat. Solidi 22, 203 (1967).
119. D. H. Niblett and J. Wilkes, Phil. Mag. 2 (8), 1427 (1957).
120. D. O. Thompson and D. K. Holmes, J. Appl. Phys. 30, 525 (1959).
121. K. Chountas, W. Dönitz, K. Papathanassopoulos, and G. Vogl, Phys. Stat. Solidi (b) 53, 219 (1972).
122. D. W. Keefer and J. C. Robinson, Annual Technical Progress Report, AEC Unclassified Programs, GFY 1969, Atomics International, North American Rockwell, Rept. AI-AEC-12860 (n.d.), p. 61.
123. R. C. Fornerod, Mem. Sci. Rev. Metallurg. 66 (2), 157 (1969).
124. D. Keefer, J. C. Robinson, and A. Sosin, Acta Met. 13, 1135 (1965); and 14, 1409 (1966).
125. D. O. Thompson and O. Buck, Phys. Stat. Solidi 37, 53 (1970).
126. G. Roth, G. Sokolowski, and K. Lücke, Phys. Stat. Solidi 40, K77 (1970).
127. G. Roth, G. Sokolowski, and K. Lücke, J. Phys. 32, C2-145 (1971).
128. G. A. Alers and D. O. Thompson, J. Appl. Phys. 32, 283 (1961).
129. R. Stern and A. Granato, Acta Met. 10, 92, 358 (1962); J. Appl. Phys. 33, 458 (1962).
130. P. L. Gruzin and Yu. D. Zharov, Dokl. Akad. Nauk SSSR 164, 1280 (1965).
131. D. Y. F. Lai, Lawrence Livermore Laboratory, Internal Memorandum, Chemistry Dept. Tech. Note CDTN 73-3 (Feb. 5, 1973).
132. R. E. von Holdt, Lawrence Livermore Laboratory, Internal Memorandum, C.I.C. Rept. R3-001 (1969).
133. G. Leibfried, Z. Physik 127, 344 (1950).
134. A. Seeger and P. Schiller, Acta Met. 10, 348 (1962).
135. R. Stuart, Lawrence Livermore Laboratory, personal communication (1973).
136. H. I. Dawson, Thesis, Delft (1964); and Acta Met. 13, 453 (1965).
137. M. Doyama and J. S. Koehler, Phys. Rev. 127, 21 (1962).
138. A. Gordon, Stage III Annealing of Electron-Irradiated Silver, Department of Physics and Materials Research Laboratory, University of

Illinois, Urbana, Illinois, Rept. COO-1198-626 (June 1969); based on Ph.D. thesis, University of Illinois, Urbana (1969).
139. F. Ramsteiner, W. Schüle, and A. Seeger, Phys. Stat. Solidi 2, 1005 (1962).
140. J. A. Manintveld, Thesis, Delft (1954); and Nature 169, 623 (1952).
141. F. Dworschak, K. Herschbach, and J. S. Koehler, Phys. Rev. A133, 292 (1964).
142. R. Kamel and E. A. Attia, Acta Met. 9, 1047 (1961).
143. W. B. Pearson, Handbook of Lattice Spacings and Structures of Metals, Vol. 2 (Pergamon, New York, 1967), p. 80.
144. R. M. Thomson and R. W. Balluffi, J. Appl. Phys. 33, 803 (1962).
145. G. Pound, W. Bitler, and H. Paxton, Phil. Mag. 6, 473 (1961).
146. J. W. Corbett, R. B. Smith, and R. M. Walker, Phys. Rev. 114, 1452 (1959).
147. J. E. Bailey and P. B. Hirsch, Phil. Mag. 5, 485 (1960).
148. D. M. Moon and W. H. Robinson, Can. J. Phys. 45, 1017 (1967).
149. H. J. Levinstein and W. H. Robinson, J. Appl. Phys. 33, 3149 (1962).
150. F. J. Worzala and W. H. Robinson, Phil. Mag. 15, 939 (1967).
151. G. P. Sabol and W. H. Robinson, Work Hardening (Gordon and Breach, New York, 1968), p. 195.
152. C. C. Chen and A. A. Hendrickson, J. Appl. Phys. 42, 2208 (1971).
153. Y. Quéré, J. Phys. Soc. Japan 18, Supp. III, 91 (1963).
154. M. Doyama and J. S. Koehler, Phys. Rev. 127, 21 (1962).
155. S. O. Gertsriken and N. N. Novikov, Soviet Phys.-Phys. Met. Met. 9, 54 (1960).
156. F. Ramsteiner, W. Schüle, and A. Seeger, Phys. Stat. Solidi 2, 1005 (1962).
157. H. Mehrer and A. Seeger, Phys. Stat. Solidi 39, 647 (1970).